New Constraints on Ω_M, Ω_Λ, and w from an Independent Set of Eleven High-Redshift Supernovae Observed with HST[1]

R. A. Knop[2,3,4], G. Aldering[5,4], R. Amanullah[6], P. Astier[7], G. Blanc[5,7], M. S. Burns[8],
A. Conley[5,9], S. E. Deustua[5,10], M. Doi[11], R. Ellis[12], S. Fabbro[13,4], G. Folatelli[6],
A. S. Fruchter[14], G. Garavini[6], S. Garmond[5,9], K. Garton[8], R. Gibbons[5], G. Goldhaber[5,9],
A. Goobar[6], D. E. Groom[5,4], D. Hardin[7], I. Hook[15], D. A. Howell[5], A. G. Kim[5,4],
B. C. Lee[5], C. Lidman[17], J. Mendez[18,19], S. Nobili[6], P. E. Nugent[5,4], R. Pain[7],
N. Panagia[14], C. R. Pennypacker[5], S. Perlmutter[5], R. Quimby[5], J. Raux[7], N. Regnault[5,23],
P. Ruiz-Lapuente[19], G. Sainton[7], B. Schaefer[20], K. Schahmaneche[7], E. Smith[2],
A. L. Spadafora[5], V. Stanishev[6], M. Sullivan[21,12], N. A. Walton[16], L. Wang[5],
W. M. Wood-Vasey[5,9], and N. Yasuda[22]
(THE SUPERNOVA COSMOLOGY PROJECT)

ABSTRACT

We report measurements of Ω_M, Ω_Λ, and w from eleven supernovae at $z = 0.36$–0.86 with high-quality lightcurves measured using WFPC2 on the HST. This is an independent set of high-redshift supernovae that confirms previous supernova evidence for an accelerating Universe. The high-quality lightcurves available from photometry on WFPC2 make it possible for these eleven supernovae alone to provide measurements of the cosmological parameters comparable in statistical weight to the previous results. Combined with earlier Supernova Cosmology Project data, the new supernovae yield a measurement of the mass density $\Omega_\mathrm{M} = 0.25^{+0.07}_{-0.06}$ (statistical) ± 0.04 (identified systematics), or equivalently, a cosmological constant of $\Omega_\Lambda = 0.75^{+0.06}_{-0.07}$ (statistical) ± 0.04 (identified systematics), under the assumptions of a flat universe and that the dark energy equation of state parameter has a constant value $w = -1$. When the supernova results are combined with independent flat-universe measurements of Ω_M from CMB and galaxy redshift distortion data, they provide a measurement of $w = -1.05^{+0.15}_{-0.20}$ (statistical) ± 0.09 (identified systematic), if w is assumed to be constant in time. In addition to high-precision lightcurve measurements, the new data offer greatly improved color measurements of the high-redshift supernovae, and hence improved host-galaxy extinction estimates. These extinction measurements show no anomalous negative $E(B\text{-}V)$ at high redshift. The precision of the measurements is such that it is possible to perform a host-galaxy extinction correction directly for individual supernovae without any assumptions or priors on the parent $E(B\text{-}V)$ distribution. Our cosmological fits using full extinction corrections confirm that dark energy is required with $P(\Omega_\Lambda > 0) > 0.99$, a result consistent with previous and current supernova analyses which rely upon the identification of a low-extinction subset or prior assumptions concerning the intrinsic extinction distribution.

[2]Department of Physics and Astronomy, Vanderbilt University, Nashville, TN 37240, USA

[3]Visiting Astronomer, Kitt Peak National Observatory, National Optical Astronomy Observatory, which is operated by the Association of Universities for Research in Astronomy, Inc. (AURA) under cooperative agreement with the National Science Foundation.

[4]Visiting Astronomer, Cerro Tololo Interamerican Observatory, National Optical Astronomy Observatory, which is operated by the Association of Universities for Research in Astronomy, Inc. (AURA) under cooperative agreement with the National Science Foundation.

[5]E. O. Lawrence Berkeley National Laboratory, 1 Cyclotron Rd., Berkeley, CA 94720, USA

[6]Department of Physics, Stockholm University, SCFAB, S-106 91 Stockholm, Sweden

[7]LPNHE, CNRS-IN2P3, University of Paris VI & VII, Paris, France

[8]Colorado College 14 East Cache La Poudre St., Colorado Springs, CO 80903

[9]Department of Physics, University of California Berkeley, Berkeley, 94720-7300 CA, USA

[10]American Astronomical Society, 2000 Florida Ave, NW, Suite 400, Washington, DC, 20009 USA.

[11]Department of Astronomy and Research Center for the Early Universe, School of Science, University of Tokyo, Tokyo 113-0033, Japan

[12]California Institute of Technology, E. California Blvd, Pasadena, CA 91125, USA

[13]Centro, Multidisiplinar de Astrofísica, Instituo, Superior Técnico, Lisbo

[14]Space Telescope Science Institute, 3700 San Martin Drive, Baltimore, MD 21218, USA

[15]Department of Physics, University of Oxford, Nuclear & Astrophysics Laboratory Keble Road, Oxford, OX1 3RH, UK

[16]Institute of Astronomy, Madingley Road, Cambridge CB3 0HA, UK

[17]European Southern Observatory, Alonso de C ordova 3107, Vitacura, Casilla 19001, Santiago 19, Chile

[18]Isaac Newton Group, Apartado de Correos 321, 38780 Santa Cruz de La Palma, Islas Canarias, Spain

[19]Department of Astronomy, University of Barcelona, Barcelona, Spain

1. Introduction

Five years ago, the Supernova Cosmology Project (SCP) and the High-Z Supernova Search Team both presented studies of distant Type Ia supernovae (SNe Ia) in a series of reports, which gave strong evidence for an acceleration of the Universe's expansion, and hence for a non-zero cosmological constant, or dark energy density (Perlmutter et al. 1998; Garnavich et al. 1998a; Schmidt et al. 1998; Riess et al. 1998; Perlmutter et al. 1999; for a review, see Perlmutter & Schmidt 2003). These results ruled out a flat, matter-dominated ($\Omega_{\rm M} = 1$, $\Omega_\Lambda = 0$) universe. For a flat universe, motivated by inflation theory, these studies yielded a value for the cosmological constant of $\Omega_\Lambda \simeq 0.7$. Even in the absence of assumptions about the geometry of the Universe, the supernova measurements indicate the existence of dark energy with greater than 99% confidence.

The supernova results combined with observations of the power spectrum of the Cosmic Microwave Background (CMB) (e.g., Jaffe et al. 2001; Bennett et al. 2003; Spergel et al. 2003), the properties of massive clusters (e.g., Turner 2001; Allen, Schmidt, & Fabian 2002; Bahcall et al. 2003), and dynamical redshift-space distortions (Hawkins et al. 2002) yield a consistent picture of a flat universe with $\Omega_{\rm M} \simeq 0.3$ and $\Omega_\Lambda \simeq 0.7$ (Bahcall et al. 1999). Each of these measurements is sensitive to different combinations of the parameters, and hence they complement each other. Moreover, because there are three different measurements of two parameters, the combination provides an important consistency check. While the current observations of galaxy clusters and dynamics, and of high-redshift supernovae, primarily probe the "recent" Universe at redshifts of $z < 1$, the CMB measurements probe the early Universe at $z \sim 1100$. That consistent results are obtained by measurements of vastly different epochs of the Universe's history suggests a vindication of the

[20]University of Texas, Department of Astronomy, C-1400, Austin, TX,78712, U.S.A.

[21]Department of Physics, University of Durham, South Road, Durham, DH1 3LE, UK

[22]National Astronomical Observatory, Mitaka, Tokyo 181-8588, Japan

[23]Now at LLR, CNRS-IN2P3, Ecole Polytechnique, Palaiseau, France

standard model of the expanding Universe.

In the redshift range around $z = 0.4$–0.7, the supernova results are most sensitive to a linear combination of Ω_M and Ω_Λ close to $\Omega_M - \Omega_\Lambda$. In contrast, galaxy clustering and dynamics are sensitive primarily to Ω_M alone, while the CMB is most sensitive to $\Omega_M + \Omega_\Lambda$. Although combinations of other measurements lead to a separate confirmation of the Universe's acceleration (e.g., Efstathiou *et al.* 2002), taken alone it is the supernovae that provide the best *direct* evidence for dark energy. Therefore, it is of importance to improve the precision of the supernova result, to confirm the result with additional independent high-redshift supernovae, and also to limit the possible effects of systematic errors.

Perlmutter *et al.* (1997, 1999) and Riess *et al.* (1998) presented extensive accounts of, and bounds for, possible systematic uncertainties in the supernova measurements. One obvious possible source of systematic uncertainty is the effect of host-galaxy dust. For a given mass density, the effect of a cosmological constant on the magnitudes of high-redshift supernovae is to make their observed brightnesses *dimmer* than would have been the case with $\Omega_\Lambda = 0$. Dust extinction from within the host galaxy of the high-redshift supernovae could have a similar effect; however, normal dust will also redden the colors of the supernovae. Therefore, a measurement of the color of the high-redshift supernovae, compared to the known colors of low-redshift SNe Ia, has been used to provide an upper limit on the effect of host-galaxy dust extinction, or a direct measurement of that extinction which may then be corrected. Uncertainties on extinction corrections based on these color measurements usually dominate the statistical error of photometric measurements. Previous analyses have either selected a low-extinction subset of both low- and high-redshift supernovae and not applied corrections directly ("Fit C," the primary analysis of P99), or have used an asymmetric Bayesian prior on the intrinsic extinction distribution to limit the propagated uncertainties from errors in color measurements (Riess *et al.* 1998; "Fit E" of P99).

In Sullivan *et al.* (2003), we set stronger limits on the effects of host-galaxy extinction by comparing the extinction, cosmological parameters, and supernova peak magnitude dispersion for sub-

sets of the SCP supernovae observed in different types of host galaxies, as identified from both HST imaging and Keck spectroscopy of the hosts. We found that supernovae in early-type (E and S0) galaxies show a smaller dispersion in peak magnitude at high redshift, as had previously been seen at low redshift (e.g. Wang, Hoeflich, & Wheeler 1997). This subset of the P99 sample—in hosts unlikely to be strongly affected by extinction—independently provided evidence at the 5σ level that $\Omega_\Lambda > 0$ in a flat Universe and confirmed that host-galaxy dust extinction was unlikely to be a significant systematic in the results of P99, as had been suggested previously (e.g., Rowan-Robinson 2002). The natural next step following the work of Sullivan *et al.* (2003)—presented in the current paper—is to provide high-quality individual unbiased $E(B\text{-}V)$ measurements that allow us to directly measure the effect of host-galaxy extinction on each supernova event without resorting to a prior on the color excess distribution.

The current paper presents eleven new supernovae discovered and observed by the SCP at redshifts $0.36 < z < 0.86$, a range very similar to that of the 42 high-redshift supernovae reported in Perlmutter *et al.* (1999; hereafter P99). The supernovae of that paper, with one exception, were observed entirely with ground-based telescopes; 11 of the 14 new supernovae reported by Riess *et al.* (1998) were also observed from the ground. The eleven supernovae of this work have lightcurves in both the R and I bands measured with the Wide-Field/Planetary Camera (WFPC2) on the Hubble Space Telescope (HST), and represent the largest sample to date of HST-measured SNe Ia at high redshift.

The HST provides two primary advantages for photometry of point sources such as supernovae. First the sky background is much lower, allowing a much higher signal-to-noise ratio in a single exposure. Second, because the telescope is not limited by atmospheric seeing, it has very high spatial resolution. This helps the signal-to-noise ratio by greatly reducing the area of background emission which contributes to the noise of the source measurement, and moreover simplifies the task of separating the variable supernova signal from the host galaxy. With these advantages, the precision of the lightcurve and color measurements is much greater for the eleven supernovae in this pa-

per than was possible for previous ground-based observations. These eleven supernovae themselves provide a high-precision *new* set of high-redshift supernovae to test the accelerating universe results. Moreover, the higher precision lightcurve measurements in both *R*- and *I*-bands allow us to make high-quality, unbiased, individual host-galaxy extinction corrections to each supernova event.

We first describe the PSF-fit photometry method used for extracting the lightcurves from the WFPC2 images (§ 2.1). Next, in § 2.2, we describe the lightcurve fitting procedure, including the methods used for calculating accurate K-corrections. So that all supernovae may be treated consistently, in § 2.3 we apply the slightly updated K-correction procedure to all of the supernovae used in P99. In § 2.4, the cosmological fit methodology we use is described. In § 3, we discuss the evidence for host-galaxy extinction (only significant for three of the eleven new supernovae) from the *R-I* lightcurve colors. In § 4.1, we present the measurements of the cosmological parameters Ω_M and Ω_Λ from the new dataset alone as well as combining this set with the data of P99. In § 4.2, we perform a combined fit with our data and the high-redshift SNe of Riess *et al.* (1998). Finally, in § 4.3 we present measurements of w, the dark energy equation of state parameter, from these data, and from these data combined with recent CMB and galaxy redshift distortion measurements. These discussions of our primary results are followed by updated analyses of systematic uncertainties for these measurements in § 5.

2. Observations, Data Reduction, and Analysis

2.1. WFPC2 Photometry

The supernovae discussed in this paper are listed in Table 1. They were discovered during three different supernova searches, following the techniques described in Perlmutter *et al.* (1995, 1997, 1999). Two of the searches were conducted with the 4m Blanco telescope at the Cerro Tololo Inter-American Observatory (CTIO), in November/December 1997 and March/April 1998. The final search was conducted at the Canada-France-Hawaii Telescope (CFHT) on Mauna Kea in Hawaii in April/May 2000. In each case, 2–3

nights of reference images were followed 3–4 weeks later by 2–3 nights of search images. The two images of each search field were seeing-matched and subtracted, and were searched for residuals indicating a supernova candidate. Weather conditions limited the depth and hence the redshift range of the March/April 1998 search. Out of the three searches, eleven of the resulting supernova discoveries were followed with extensive HST photometry. These supernovae are spaced approximately evenly in the redshift range $0.3 < z < 0.9$. Nine out of the eleven supernovae were discovered very close to maximum light; two were discovered several days before maximum light.

Spectra were obtained with the red side of LRIS on the Keck 10m telescope (Oke *et al.* 1995), with FORS1 on Antu (VLT-UT1) (Appenzeller *et al.* 1998), and with EFOSC2[24] on the ESO 3.6m telescope. These spectra were used to confirm the identification of the candidates as SNe Ia, and to measure the redshift of each candidate. Nine of the eleven supernovae in the set have strong confirmation as Type Ia through the presence of Si II λ6150, Si II λ4190, or Fe II features that match those of a Type Ia observed at a similar epoch. SNe 1998ay and 1998be have spectra which are consistent with SNe Ia spectra, although this identification is less secure for those two. However, we note that the colors (measured at multiple epochs with the HST lightcurves) are inconsistent with other non-Ia types. (We explore the systematic effect of removing those two supernovae from the set in § 5.2.)

Where possible, the redshift, z, of each candidate was measured by matching narrow features in the host galaxy of the supernovae; the precision of these measurements in z is typically 0.001. In cases where there were not sufficient host-galaxy features (SNe 1998aw and 1998ba), redshifts were measured from the supernova itself; in these cases, z is measured with a (conservative) precision of 0.01 (Branch & van den Bergh 1993). Even in the latter case, redshift measurements do not contribute significantly to the uncertainties in the final cosmological measurements since these are dominated by the photometric uncertainties.

Each of these supernovae was imaged with two broadband filters using the Planetary Cam-

---

[24]http://www.ls.eso.org/lasilla/sciops/efosc/

4

Table 1: WFPC2 Supernova Observations

SN Name	z	F675W Observations	F814W Observations
1997ek	0.863	1998-01-05 (400s,400s)	1998-01-05 (500s,700s)
		1998-01-11 (400s,400s)	1998-01-11 (500s,700s)
			1998-02-02 (1100s,1200s)
			1998-02-14 (1100s,1200s)
			1998-02-27 (1100s,1200s)
			1998-11-09 (1100s,1300s)
			1998-11-16 (1100s,1300s)
1997eq	0.538	1998-01-06 (300s,300s)	1998-01-06 (300s,300s)
		1998-01-21 (400s,400s)	1998-01-11 (300s,300s)
			1998-02-02 (500s,700s)
		1998-02-11 (400s,400s)	1998-02-11 (500s,700s)
		1998-02-19 (400s,400s)	1998-02-19 (500s,700s)
1997ez	0.778	1998-01-05 (400s,400s)	1998-01-05 (500s,700s)
		1998-01-11 (400s,400s)	1998-01-11 (500s,700s)
			1998-02-02 (1100s,1200s)
			1998-02-14 (1100s,1200s)
			1998-02-27 (100s,1200s,1100s,1200s)
1998as	0.355	1998-04-08 (400s,400s)	1998-04-08 (500s,700s)
		1998-04-20 (400s,400s)	1998-04-20 (500s,700s)
		1998-05-11 (400s,400s)	1998-05-11 (500s,700s)
		1998-05-15 (400s,400s)	1998-05-15 (500s,700s)
		1998-05-29 (400s,400s)	1998-05-29 (500s,700s)
1998aw	0.440	1998-04-08 (300s,300s)	1998-04-08 (300s,300s)
		1998-04-18 (300s,300s)	1998-04-18 (300s,300s)
		1998-04-29 (400s,400s)	1998-04-29 (500s,700s)
		1998-05-14 (400s,400s)	1998-05-14 (500s,700s)
		1998-05-28 (400s,400s)	1998-05-28 (500s,700s)
1998ax	0.497	1998-04-08 (300s,300s)	1998-04-08 (300s,300s)
		1998-04-18 (300s,300s)	1998-04-18 (300s,300s)
		1998-04-29 (300s,300s)	1998-04-29 (500s,700s)
		1998-05-14 (300s,300s)	1998-05-14 (500s,700s)
		1998-05-27 (300s,300s)	1998-05-27 (500s,700s)
1998ay	0.638	1998-04-08 (400s,400s)	1998-04-08 (500s,700s)
		1998-04-20 (400s,400s)	1998-04-20 (500s,700s)
			1998-05-11 (1100s,1200s)
			1998-05-15 (1100s,1200s)
			1998-06-03 (1100s,1200s)
1998ba	0.430	1998-04-08 (300s,300s)	1998-04-08 (300s,300s)
		1998-04-19 (300s,300s)	1998-04-19 (300s,300s)
		1998-04-29 (400s,400s)	1998-04-29 (500s,700s)
		1998-05-13 (400s,400s)	1998-05-13 (500s,700s)
		1998-05-28 (400s,400s)	1998-05-28 (500s,700s)
1998be	0.644	1998-04-08 (300s,300s)	1998-04-08 (300s,300s)
		1998-04-19 (300s,300s)	1998-04-19 (300s,300s)
		1998-04-30 (400s,400s)	1998-04-30 (500s,700s)
		1998-05-15 (400s,400s)	1998-05-15 (500s,700s)
		1998-05-28 (400s,400s)	1998-05-28 (500s,700s)
1998bi	0.740	1998-04-06 (400s,400s)	1998-04-06 (500s,700s)
		1998-04-18 (400s,400s)	1998-04-18 (500s,700s)
			1998-04-28 (1100s,1200s)
			1998-05-12 (1100s,1200s)
			1998-06-02 (1100s,1200s)
2000fr	0.543		2000-05-08 (2200s)
		2000-05-15 (600s,600s)	2000-05-15 (1100s,1100s)
		2000-05-28 (600s,600s)	2000-05-28 (600s,600s)
		2000-06-10 (500s,500s)	2000-06-10 (600s,600s)
		2000-06-22 (1100s,1300s)	2000-06-22 (1100s,1200s)
		2000-07-08 (1100s,1300s)	2000-07-08 (110s,1200s)

era (PC) CCD of the WFPC2 on the HST, which has a scale of $0.046''$/pixel. Table 1 lists the dates of these observations. The F675W and F814W broadband filters were chosen to have maximum sensitivity to these faint objects, while being as close a match as practical to the rest-frame B and V filters at the targeted redshifts. (Note that all of our WFPC2 observing parameters except the exact target coordinates were fixed prior to the supernova discoveries.) The effective system transmission curves provided by STScI indicate that, when used with WFPC2, F675W is most similar to ground-based R band while F814W is most similar to ground-based I band. These filters roughly correspond to redshifted B- and V-band filters for the supernovae at $z < 0.7$, and redshifted U- and B- band filters for the supernovae at $z > 0.7$.

The HST images were reduced through the standard HST "On-The-Fly Reprocessing" data reduction pipeline provided by the Space Telescope Science Institute. Images were then background subtracted, and images taken in the same orbit were combined to reject cosmic rays using the "crrej" procedure (a part of the STSDAS IRAF package). Photometric fluxes were extracted from the final images using a PSF-fitting procedure. Traditional PSF fitting procedures assume a single isolated point source above a constant background. In this case, the point source was superimposed on the image of the host galaxy. In all cases, the supernova image was separated from the core of the host galaxy; however, in most cases the separation was not enough that an annular measurement of the background would be accurate. Because the host-galaxy flux is the same in all of the images, we used a PSF fitting procedure that fits a PSF *simultaneously* to every image of a given supernova observed through a given photometric filter. The model we fit was:

$$f_i(x, y) = f_{0i} \times \text{psf}(x - x_{0i}, y - y_{0i}) + \text{bg}(x - x_{0i}, y - y_{0i}; a_j) + p_i \quad (1)$$

where $f_i(x, y)$ is the measured flux in pixel (x, y) of the ith image, (x_{0i}, y_{0i}) is the position of the supernova on the ith image, f_{0i} is the total flux in the supernova in the ith image, $\text{psf}(u, v)$ is a normalized point spread function, $\text{bg}(u, v; a)$ is a temporally constant background parametrized by a_j, and p_i is a pedestal offset for the ith image.

There are $4n + m - 1$ parameters in this model, where n is the number of images (typically 2, 5, or 6 previously summed images) and m is the number of parameters a_j that specify the background model (typically 3 or 6). (The -1 is due to the fact that a zeroth-order term in the background is degenerate with one of the p_i terms.) Parameters varied include f_i, x_{0i}, y_{0i}, p_i, and a_j.

Due to the scarcity of objects in our PC images, geometric transformations between the images at different epochs using other objects on the four chips of WFPC2 together allowed an *a priori* determination of (x_{0i}, y_{0i}) good to ~ 1 pixel. Allowing those parameters to vary in the fit (effectively, using the point source signature of the supernova to determine the offset of the image) provided position measurements a factor of ~ 10 better.[25] The model was fit to 13×13 pixel patches extracted from all of the images of a time sequence of a single supernova in a single filter (except for SN 1998ay, which is close enough to the host galaxy that a 7×7 pixel patch was used to avoid having to fit the core of the galaxy with the background model). In four out of the 99 patches used in the fits to the 22 lightcurves, a single bad pixel was masked from the fit. The series of f_{0i} values, corrected as described in the rest of this section, provided the data used in the lightcurve fits described in § 2.2. For one supernova (SN 1997ek at $z = 0.86$), the F814W background was further constrained by a supernova-free "final reference" image taken 11 months after the supernova explosion.[26]

A single Tiny Tim PSF was used as $\text{psf}(u, v)$ for all images of a given filter. The Tiny Tim PSF used was subsampled to 10×10 subpixels; in the fit procedure, it was shifted and integrated (properly summing fractional subpixels). After shifting and resampling to the PC pixel scale, it was con-

---

[25] Note that this may introduce a bias towards higher flux, as the fit will seek out positive fluctuations on which to center the PSF. However, the covariance between the peak flux and position is typically less than $\sim 4\%$ of the product of the positional uncertainty and the flux uncertainty, so the effects of this bias will be very small in comparison to our photometric errors.

[26] Although obtaining final references to subtract the galaxy background is standard procedure for ground-based photometry of high-redshift supernovae, the higher resolution of WFPC2 provides sufficient separation between the supernova and host galaxy that such images are not always necessary, particularly in this redshift range.

volved with an empirical 3×3 electron diffusion kernel with 75% of the flux in the central element (Fruchter 2000).[27] The PSF was normalized in a $0.5''$-radius aperture, chosen to match the standard zeropoint calibration (Holtzman, *et al.* 1995; Dolphin 2000). Although the use of a single PSF for every image is an approximation—the PSF of WFPC2 depends on the epoch of the observation as well as the position on the CCD—this approximation should be valid, especially given that for all of the observations the supernova was positioned close to the center of the PC. To verify that this approximation is valid, we reran the PSF fitting procedure with individually generated PSFs for most supernovae; we also explored using a supernova spectrum instead of a standard star spectrum in generating the PSF. The measured fluxes were not significantly different, showing differences in both directions generally within 1–2% of the supernova peak flux value—much less than our photometric uncertainties on individual data points.

Although one of the great advantages of the Hubble Space Telescope is its low background, CCD photometry of faint objects over a low background suffer from an imperfect charge transfer efficiency (CTE) effect, which can lead to a systematic underestimate of the flux of point sources (Whitemore, Heyer, & Casertano 1999; Dolphin 2000, 2003). On the PC, these effects can be as large as $\sim 15\%$. The measured flux values (f_{0i} above) were corrected for the CTE of WFPC2 following the standard procedure of Dolphin (2000).[28] Uncertainties on the CTE corrections were propagated into the corrected supernova fluxes, although in all cases these uncertainties were smaller than the uncertainties in the raw measured flux values. Because the host galaxy is a smooth background underneath the point source, it was considered as a contribution to the background in the CTE correction. For an image which was a combination of several separate exposures within the same orbit or orbits, the CTE calculation was performed assuming that each SN image had a measured SN flux whose fraction of the total flux was equal to the fraction of that individual im-

age's exposure time to the summed image's total exposure time. This assumption is correct most of the time, with the exception of the few instances where Earthshine affects part of an orbit.

In addition to the HST data, there exists ground-based photometry for each of these supernovae. This includes the images from the search itself, as well as a limited amount of follow-up. The details of which supernovae were observed with which telescopes are given with the lightcurves in Appendix A. Ground-based photometric fluxes were extracted from images using the same aperture photometry procedure of P99. A complete lightcurve in a given filter (R or I) combined the HST data with the ground-based data (using the color-correction procedure described below in § 2.3), using measured zeropoints for the ground-based data and the Vega zeropoints of Dolphin (2000) for the HST data. The uncertainties on those zeropoints (0.003 for F814W or 0.006 for F675W) were added as correlated errors between all HST data points when combining with the ground-based lightcurve. Similarly, the measured uncertainty in the ground-based zeropoint was added as a correlated error to all ground-based fluxes. Ground-based photometric calibrations were based on observations of Landolt (1992) standard stars observed on the same photometric night as a supernova observation; each calibration is confirmed over two or more nights. Ground-based zeropoint uncertainties are generally $\lesssim 0.02$–0.03; the R-band ground based zeropoint for SN 1998ay is only good to ± 0.05. We have compared our ground-based aperture photometry with our HST PSF-fitting photometry using the limited number of sufficiently bright stars present in the PC across the eleven SNe fields. We find the difference between the HST and ground-based photometry to be 0.02 ± 0.02 in both the R- and I-bands, consistent with no offset. The correlated uncertainties between different supernovae arising from ground-based zeropoints based on the same calibration data, and between the HST supernovae (which all share the same zeropoint), were included in the covariance matrix used in all cosmological fits (see § 2.4).

2.2. Lightcurve Fits

It is the magnitude of the supernova at its lightcurve peak that serves as a "calibrated can-

---

[27] See also http://www.stsci.edu/software/tinytim/tinytim_faq.html

[28] These CTE corrections used updated coefficients posted on Dolphin's web page (http://www.noao.edu/staff/dolphin/wfpc2_calib/) in September, 2002.

dle" in estimating the cosmological parameters from the luminosity distance relationship. To estimate this peak magnitude, we performed template fits to the time series of photometric data for each supernova. In addition to the eleven supernovae described here, lightcurve fits were also performed to the supernovae from P99, including 18 supernovae from Hamuy *et al.* (1996a; hereafter H96), and eight from Riess *et al.* (1999a; hereafter R99) which match the same selection criteria used for the H96 supernovae (having data within six days of maximum light and located at $cz > 4000$ km/s, limiting distance modulus error due to peculiar velocities to less than 0.15 magnitudes). Because of new templates and K-corrections (see below), lightcurve fits to the supernovae from H96 and P99 used in the analyses below were redone for consistency. The results of these fits are slightly different from those quoted in P99 for the same supernovae as a result of the change in the lightcurve template, the new K-corrections, and the different fit procedure, all discussed below. For example, because the measured $E(B\text{-}V)$ value was considered in the K-corrections (§ 2.3), whereas it was not in P99, one should expect to see randomly distributed differences in fit supernova lightcurve parameters due to scatter in the color measurements.

Lightcurve fits were performed using a χ^2-minimization procedure based on MINUIT (James & Roos 1975). For both high- and low-redshift supernovae, color corrections and K-corrections are applied (see § 2.3) to the photometric data. These data were then fit to lightcurve templates. Fits were performed to the combined R- and I-band data for each high-redshift supernova. For low-redshift supernovae, fits were performed using only the B- and V-band data (which correspond to de-redshifted R- and I-bands for most of the high-redshift supernovae). The lightcurve model fit to the supernova has four parameters to modify the lightcurve templates: time of rest-frame B-band maximum light, peak flux in R, R-I color at the epoch of rest-frame maximum B-band light, and timescale stretch s. Stretch is a parameter which linearly scales the time axis, so that a supernova with a high stretch has a relatively slow decay from maximum, and a supernova with a low stretch has a relatively fast decay from maximum (Perlmutter *et al.* 1997; Goldhaber *et al.* 2001). For supernovae in the redshift range $z = 0.3$–0.7,

a B template was fit to the R-band lightcurve and a V template was fit to the I-band lightcurve. For supernovae at $z > 0.7$, a U template was fit to the R-band lightcurve and a B template to the I-band lightcurve. Two of the high-redshift supernovae from P99 fall at $z \sim 0.18$ (SN 1997I and SN 1997N); for these supernovae, V and R templates were fit to the R- and I-band data. (The peak B-band magnitude was extracted by adding the intrinsic SN Ia B-V color to the fit V-band magnitude at the epoch of B maximum.)

The B template used in the lightcurve fits was that of Goldhaber *et al.* (2001). For this paper, new V-band and R-band templates were generated following a procedure similar to that of Goldhaber *et al.* (2001), by fitting a smooth parametrized curve through the low-redshift supernova data of H96 and R99. A new U-band template was generated with data from Hamuy *et al.* (1991), Lira *et al.* (1998), Richmond *et al.* (1995), Suntzeff *et al.* (1999), and Wells *et al.* (1994); comparison of our U-band template shows good agreement with the new U-band photometry from Jha (2002) at the relevant epochs. New templates were generated by fitting a smooth curve, $f(t')$, to the low-redshift lightcurve data, where $t' = t/(1+z)/s$; t is the number of observer-frame days relative to the epoch of the B-band maximum of each supernova, z is the redshift of each supernova, and s is the stretch of each supernova as measured from the B-band lightcurves. Lightcurve templates had an initial parabola with a 20-day rise time (Aldering, Knop, & Nugent 2000), joined to a smooth spline section to describe the main part of the lightcurve, then joined to an exponential decay to describe the final tail at $> \sim 70$ days past maximum light. The first 100 days of each of the three templates is listed in Table 2.

Due to a secondary "hump" or "shoulder" ~ 20 days after maximum, the R-band lightcurve does not vary strictly according to the simple time-axis scaling parametrized by stretch which is so successful in describing the different U-, B-, and V-band lightcurves. However, for the two $z \sim 0.18$ supernova to which we fit an R-band template, the peak R- and I- band magnitudes are well constrained, and the stretch is also well measured from the rest-frame V-band lightcurve.

Some of the high-redshift supernovae from P99 lack a supernova-free host-galaxy image. These

Table 2: U, V, and R Lightcurve Templates Used

Day[a]	U flux[b]	V flux[b]	R flux[b]	Day[1]	U flux[b]	V flux[b]	R flux[b]
-19	6.712e-03	4.960e-03	5.779e-03	31	4.790e-02	2.627e-01	3.437e-01
-18	2.685e-02	1.984e-02	2.312e-02	32	4.524e-02	2.481e-01	3.238e-01
-17	6.041e-02	4.464e-02	5.201e-02	33	4.300e-02	2.345e-01	3.054e-01
-16	1.074e-01	7.935e-02	9.246e-02	34	4.112e-02	2.218e-01	2.887e-01
-15	1.678e-01	1.240e-01	1.445e-01	35	3.956e-02	2.099e-01	2.733e-01
-14	2.416e-01	1.785e-01	2.080e-01	36	3.827e-02	1.990e-01	2.592e-01
-13	3.289e-01	2.430e-01	2.832e-01	37	3.722e-02	1.891e-01	2.463e-01
-12	4.296e-01	3.174e-01	3.698e-01	38	3.636e-02	1.802e-01	2.345e-01
-11	5.437e-01	4.017e-01	4.681e-01	39	3.565e-02	1.721e-01	2.237e-01
-10	6.712e-01	4.960e-01	5.779e-01	40	3.506e-02	1.649e-01	2.137e-01
-9	7.486e-01	5.889e-01	6.500e-01	41	3.456e-02	1.583e-01	2.046e-01
-8	8.151e-01	6.726e-01	7.148e-01	42	3.410e-02	1.524e-01	1.962e-01
-7	8.711e-01	7.469e-01	7.725e-01	43	3.365e-02	1.471e-01	1.884e-01
-6	9.168e-01	8.115e-01	8.236e-01	44	3.318e-02	1.423e-01	1.813e-01
-5	9.524e-01	8.660e-01	8.681e-01	45	3.266e-02	1.378e-01	1.747e-01
-4	9.781e-01	9.103e-01	9.062e-01	46	3.205e-02	1.337e-01	1.687e-01
-3	9.940e-01	9.449e-01	9.382e-01	47	3.139e-02	1.299e-01	1.630e-01
-2	1.000e+00	9.706e-01	9.639e-01	48	3.072e-02	1.263e-01	1.578e-01
-1	9.960e-01	9.880e-01	9.834e-01	49	3.005e-02	1.229e-01	1.529e-01
0	9.817e-01	9.976e-01	9.957e-01	50	2.945e-02	1.195e-01	1.483e-01
1	9.569e-01	1.000e+00	1.000e+00	51	2.893e-02	1.161e-01	1.440e-01
2	9.213e-01	9.958e-01	9.952e-01	52	2.853e-02	1.128e-01	1.398e-01
3	8.742e-01	9.856e-01	9.803e-01	53	2.830e-02	1.096e-01	1.359e-01
4	8.172e-01	9.702e-01	9.545e-01	54	2.827e-02	1.064e-01	1.320e-01
5	7.575e-01	9.502e-01	9.196e-01	55	2.849e-02	1.033e-01	1.282e-01
6	6.974e-01	9.263e-01	8.778e-01	56	2.793e-02	1.003e-01	1.244e-01
7	6.375e-01	8.991e-01	8.313e-01	57	2.738e-02	9.743e-02	1.207e-01
8	5.783e-01	8.691e-01	7.821e-01	58	2.684e-02	9.467e-02	1.170e-01
9	5.205e-01	8.369e-01	7.324e-01	59	2.630e-02	9.207e-02	1.133e-01
10	4.646e-01	8.031e-01	6.842e-01	60	2.578e-02	8.964e-02	1.097e-01
11	4.113e-01	7.683e-01	6.396e-01	61	2.527e-02	8.741e-02	1.061e-01
12	3.610e-01	7.330e-01	6.007e-01	62	2.477e-02	8.538e-02	1.026e-01
13	3.145e-01	6.977e-01	5.691e-01	63	2.428e-02	8.359e-02	9.910e-02
14	2.725e-01	6.629e-01	5.444e-01	64	2.380e-02	8.207e-02	9.568e-02
15	2.356e-01	6.293e-01	5.254e-01	65	2.333e-02	8.083e-02	9.232e-02
16	2.044e-01	5.972e-01	5.113e-01	66	2.287e-02	7.927e-02	8.902e-02
17	1.783e-01	5.667e-01	5.011e-01	67	2.242e-02	7.774e-02	8.579e-02
18	1.567e-01	5.376e-01	4.938e-01	68	2.197e-02	7.624e-02	8.264e-02
19	1.388e-01	5.099e-01	4.887e-01	69	2.154e-02	7.476e-02	7.958e-02
20	1.239e-01	4.835e-01	4.848e-01	70	2.111e-02	7.332e-02	7.660e-02
21	1.115e-01	4.583e-01	4.814e-01	71	2.070e-02	7.191e-02	7.373e-02
22	1.008e-01	4.342e-01	4.776e-01	72	2.029e-02	7.052e-02	7.096e-02
23	9.144e-02	4.113e-01	4.725e-01	73	1.989e-02	6.916e-02	6.832e-02
24	8.314e-02	3.894e-01	4.653e-01	74	1.949e-02	6.782e-02	6.581e-02
25	7.583e-02	3.685e-01	4.552e-01	75	1.911e-02	6.651e-02	6.344e-02
26	6.941e-02	3.486e-01	4.414e-01	76	1.873e-02	6.523e-02	6.199e-02
27	6.380e-02	3.296e-01	4.247e-01	77	1.836e-02	6.397e-02	6.057e-02
28	5.891e-02	3.115e-01	4.058e-01	78	1.799e-02	6.274e-02	5.918e-02
29	5.467e-02	2.943e-01	3.855e-01	79	1.764e-02	6.153e-02	5.783e-02
30	5.102e-02	2.781e-01	3.645e-01	80	1.729e-02	6.034e-02	5.650e-02

a: Day is relative to the epoch of the maximum of the B-band lightcurve. The B-band template may be found in Goldhaber et $al.$ (2001).
b: Relative fluxes.

supernovae were fit with an additional variable parameter: the zero-level of the I-band lightcurve. The supernovae treated in this manner include SNe 1997O, 1997Q, 1997R, and 1997am.

The late-time lightcurve behavior may bias the result of a lightcurve fit (Aldering, Knop, & Nugent 2000); it is therefore important that the low- and high-redshift supernovae are treated in as consistent a manner as possible. Few or none of the high-redshift supernovae have high-precision measurements more than ∼40–50 rest-frame days after maximum light, so as in Perlmutter *et al.* (1997) and P99 these late-time points were eliminated from the low-redshift lightcurve data before the template-fit procedure. Additionally, to allow for systematic offset uncertainties on the host-galaxy subtraction, an "error floor" of 0.007 times the maximum lightcurve flux was applied; any lightcurve point with an uncertainty below the error floor had its uncertainty replaced by that value (Goldhaber *et al.* 2001).

The final results of the lightcurve fits, including the effect of color corrections and K-corrections, are listed in Table 3 for the eleven supernovae of this paper. Table 4 shows the results of new lightcurve fits to the high-redshift supernovae of P99 used in this paper (see § 2.5), and Table 5 shows the results of lightcurve fits for the low-redshift supernovae from H96 and R99.[29] Appendix A tabulates all of the lightcurve data for the eleven HST supernovae in this paper. The lightcurves for these supernovae (and the F675W WFPC2 image nearest maximum light) are shown in Figures 1 and 2. Note that there are correlated errors between all of the ground-based points for each supernova in these figures, as a single ground-based zeropoint was used to scale each of them together with the HST photometry.

2.3. Color- and K-Corrections

In order to combine data from different telescopes, color corrections were applied to remove the differences in the spectral responses of the filters relative to the Bessell system (Bessell 1990). For the ground-based telescopes, the filters are close enough to the standard Bessell filters that a single linear color term (measured at each observa-

tory with standard stars) suffices to put the data onto the Bessell system, with most corrections being smaller than 0.01 magnitudes. The WFPC2 filters are different enough from the ground-based filters, however, that a linear term is not sufficient. Moreover, the differences between a SN Ia and standard star spectral energy distribution are significant. In this case, color corrections were calculated by integrating template SN Ia spectra (described below) through the system response.

In order to perform lightcurve template fitting, a cross-filter K-correction must be applied to transform the data in the observed filter into a rest-frame magnitude in the filter used for the lightcurve template (Kim, Goobar, & Perlmutter 1996). The color correction to the nearest standard Bessell filter followed by a K-correction to a rest-frame filter is equivalent to a direct K-correction from the observed filter to the standard rest-frame filter. In practice, we perform the two steps separately so that all photometry may be combined to provide a lightcurve effectively observed through a standard (e.g. R-band) filter, which may then be fit with a single series of K-corrections. The data tabulated in Appendix A have all been color-corrected to the standard Bessell filters.

Color and K-corrections were performed following the procedure of Nugent, Kim, & Perlmutter (2002). In order to perform these corrections, a template SN Ia spectrum for each epoch of the lightcurve, as described in that paper, is necessary. The spectral template used in this present work began with the template of that paper. To it was applied a smooth multiplicative function at each day such that integration of the spectrum through the standard filters would produce the proper intrinsic colors for a Type Ia supernova (including a mild dependence of those intrinsic colors on stretch).

The proper intrinsic colors for the supernova spectral template were determined in the $BVRI$ spectral range by smooth fits to the low-redshift supernova data of H96 and R99. For each color (B-V, V-R, and R-I), every data point from those papers was K-corrected and corrected for Galactic extinction. These data were plotted together, and then a smooth curve was fit to the plot of color versus date relative to maximum. This curve is given by two parameters, each of which is a func-

---

[29]These three tables are available in electronic form from http://supernova.lbl.gov.
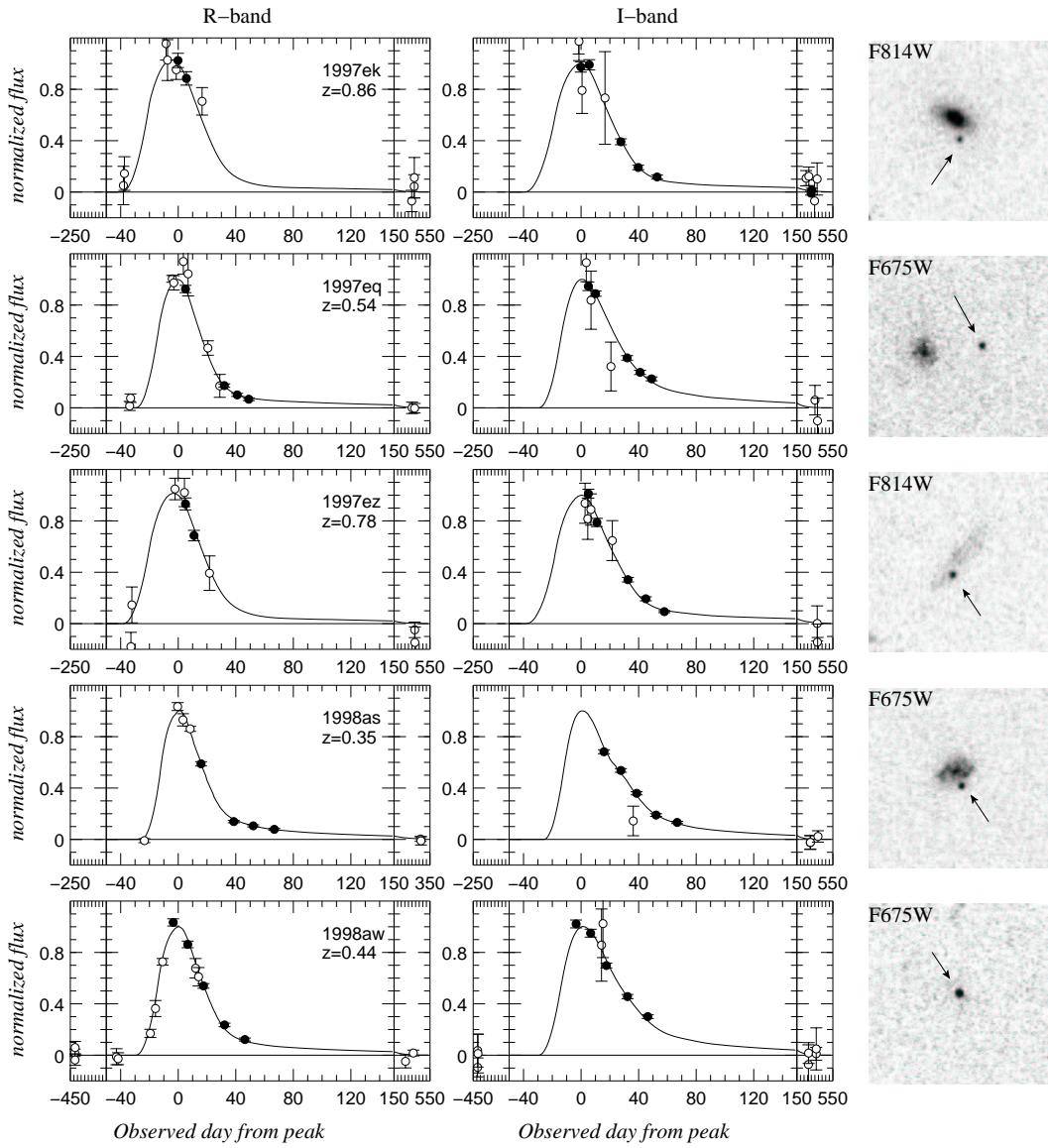
Fig. 1.— Lightcurves and images from the PC CCD on WFPC2 for the HST supernovae reported in this paper. The left column shows the *R*-band (including F675W HST data), and the middle column shows *I*-band lightcurves (including F814W HST data). Open circles represent ground-based data points, and filled circles represent WFPC2 data points. Note that there are correlated errors between all of the ground-based points for each supernova in these figures, as a single ground-based zeropoint was used to scale each of them together with the HST photometry. The right column shows $6'' \times 6''$ images, summed from all HST images of the supernova in the indicated filter.
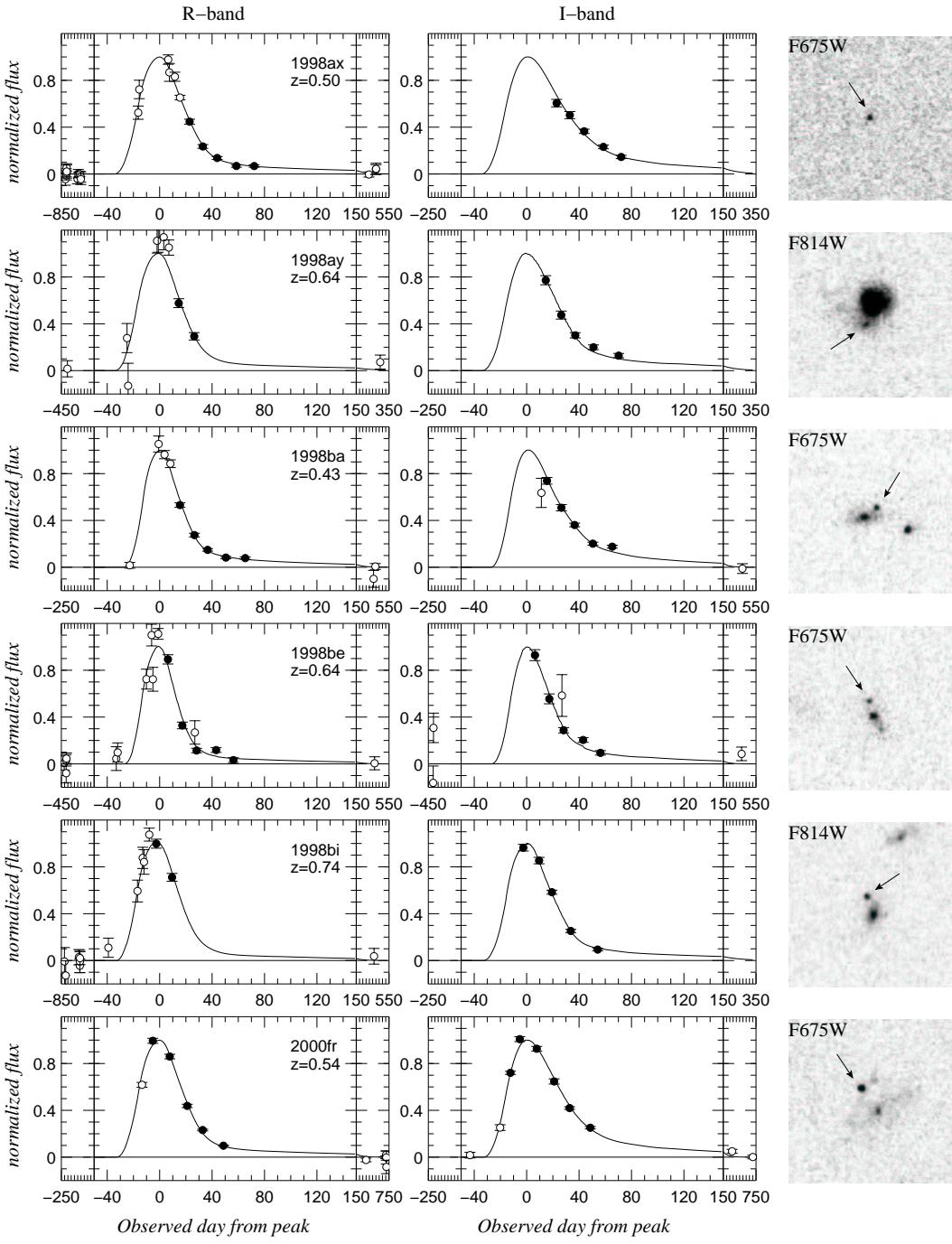
Fig. 2.— Lightcurves and images from the PC CCD on WFPC2 for the HST supernovae reported in this paper (continued). The left column shows the *R*-band (including F675W HST data), and the middle column shows *I*-band lightcurves (including F814W HST data). Open circles represent ground-based data points, and filled circles represent WFPC2 data points. Note that there are correlated errors between all of the ground-based points for each supernova in these figures, as a single ground-based zeropoint was used to scale each of them together with the HST photometry. The right column shows $6'' \times 6''$ images, summed from all HST images of the supernova in the indicated filter.

12

Table 3: Supernova Lightcurve Fits: HST Supernovae from this paper

| SN	z	m_X (a)	m_B (b)	m_B^{eff} (c)	m_B^{eff} Ext. Corr. (d)	Stretch (s)	$R\text{-}I$ (e)	$E(B\text{-}V)$ Gal. (f)	$E(B\text{-}V)_{\text{host}}$ (g)	Excluded from Subsets (h)
1997ek	0.863	23.32	24.51 ± 0.03	24.59 ± 0.19	24.95 ± 0.44	1.056 ± 0.058	0.838 ± 0.054	0.042	-0.091 ± 0.075	
1997eq	0.538	22.63	23.21 ± 0.02	23.15 ± 0.18	23.02 ± 0.17	0.960 ± 0.027	0.202 ± 0.030	0.044	0.035 ± 0.034	
1997ez	0.778	23.17	24.29 ± 0.03	24.41 ± 0.18	24.00 ± 0.42	1.078 ± 0.030	0.701 ± 0.048	0.026	0.095 ± 0.068	
1998as	0.355	22.18	22.72 ± 0.03	22.66 ± 0.17	22.02 ± 0.15	0.956 ± 0.012	0.226 ± 0.027	0.037	0.158 ± 0.030	2,3
1998aw	0.440	22.56	23.22 ± 0.02	23.26 ± 0.17	—	1.026 ± 0.019	0.300 ± 0.024	0.026	0.259 ± 0.026	1–3
1998ax	0.497	22.63	23.25 ± 0.05	23.47 ± 0.17	22.96 ± 0.20	1.150 ± 0.032	0.212 ± 0.041	0.035	0.113 ± 0.044	2,3
1998ay	0.638	23.26	23.86 ± 0.08	23.92 ± 0.19	23.85 ± 0.33	1.040 ± 0.041	0.339 ± 0.067	0.035	0.015 ± 0.084	3
1998ba	0.430	22.34	22.97 ± 0.05	22.90 ± 0.18	22.75 ± 0.18	0.954 ± 0.020	0.094 ± 0.036	0.024	0.040 ± 0.038	
1998be	0.644	23.33	23.91 ± 0.04	23.64 ± 0.18	23.26 ± 0.27	0.816 ± 0.028	0.436 ± 0.051	0.029	0.106 ± 0.065	3
1998bi	0.740	22.86	23.92 ± 0.02	23.85 ± 0.17	23.75 ± 0.37	0.950 ± 0.027	0.552 ± 0.037	0.026	0.026 ± 0.050	
2000fr	0.543	22.44	23.07 ± 0.02	23.16 ± 0.17	23.27 ± 0.14	1.064 ± 0.011	0.135 ± 0.022	0.030	-0.031 ± 0.025	

a: Magnitude in the observed filter at the peak of the rest-frame B-band lightcurve. X=R for $z < 0.7$, X=I for $z > 0.7$.

b: This value has been K-corrected and corrected for Galactic extinction: $m_B \equiv m_X - K_{BX} - A_X$, where K_{BX} is the cross-filter K-correction and A_X is the Galactic extinction correction. These were the values used in the cosmological fits. The quoted error bar is the uncertainty on the peak magnitude from the lightcurve fit.

c: This value includes the stretch correction: $m_B^{eff} \equiv m_B + \alpha(s - 1)$. α is the best-fit value of the stretch-luminosity slope from the fit to the primary low-extinction subset (Fit 3 in § 4). The quoted error bar includes all uncertainties for non-extinction-corrected fits described in § 2.4. Note that these values are only provided for convenience; they were not used directly in any cosmological fits, since α is also a fit parameter.

d: Similar to column c, only with the host-galaxy extinction correction applied. The stretch/luminosity slope used for this value is that from the fit to the primary subset (Fit 6 in § 4). The quoted error bar includes all uncertainties for extinction-corrected fits described in § 2.4. A line indicates a supernova which did not appear in the primary subset (see § 2.5.)

e: This is the observed R-I color at the epoch of the rest-frame B-band lightcurve peak.

f: Schlegel, Finkbeiner, & Davis (1998); this extinction is already included in the quoted values of m_B.

g: Measurement uncertainty only; no intrinsic color dispersion included.

h: These supernovae are excluded from the indicated subsets; see § 2.5.

Table 4: Supernova Lightcurve Fits: New Fits to Perlmutter (1999) SNe

SN	z	m_X (a)	m_B (b)	m_B^{eff} (c)	m_B^{eff} Ext. Corr. (d)	Stretch (s)	R-I (e)	E(B-V) Gal. (f)	E(B-V)$_{\rm host}$ (g)	Excluded from Subsets (h)
1995ar	0.465	22.80	23.48 ± 0.08	23.35 ± 0.22	21.54 ± 0.97	0.909 ± 0.104	0.509 ± 0.222	0.022	0.448 ± 0.242	
1995as	0.498	23.03	23.69 ± 0.07	23.74 ± 0.23	23.52 ± 0.87	1.035 ± 0.090	0.155 ± 0.197	0.021	0.051 ± 0.212	3
1995aw	0.400	21.78	22.28 ± 0.03	22.57 ± 0.18	23.17 ± 0.45	1.194 ± 0.037	-0.127 ± 0.103	0.040	-0.160 ± 0.107	
1995ax	0.615	22.56	23.21 ± 0.06	23.38 ± 0.22	23.98 ± 1.02	1.112 ± 0.073	0.152 ± 0.204	0.033	-0.153 ± 0.249	
1995ay	0.480	22.64	23.07 ± 0.04	22.90 ± 0.19	22.74 ± 0.70	0.880 ± 0.064	0.209 ± 0.158	0.114	0.047 ± 0.170	
1995az	0.450	22.46	22.70 ± 0.07	22.66 ± 0.20	23.04 ± 0.58	0.973 ± 0.064	0.087 ± 0.135	0.181	-0.089 ± 0.144	
1995ba	0.388	22.07	22.64 ± 0.06	22.60 ± 0.18	22.74 ± 0.45	0.971 ± 0.047	0.006 ± 0.105	0.018	-0.033 ± 0.110	
1996cf	0.570	22.71	23.31 ± 0.03	23.30 ± 0.18	23.53 ± 0.45	0.996 ± 0.045	0.162 ± 0.091	0.040	-0.054 ± 0.107	3
1996cg	0.490	22.46	23.09 ± 0.03	23.11 ± 0.18	22.26 ± 0.45	1.011 ± 0.040	0.300 ± 0.099	0.035	0.205 ± 0.107	3
1996ci	0.495	22.19	22.83 ± 0.02	22.78 ± 0.18	22.92 ± 0.32	0.964 ± 0.040	0.083 ± 0.070	0.028	-0.033 ± 0.075	
1996cl	0.828	23.37	24.53 ± 0.17	24.49 ± 0.46	25.92 ± 0.97	0.974 ± 0.239	0.549 ± 0.184	0.035	-0.344 ± 0.251	
1996cm	0.450	22.67	23.26 ± 0.07	23.11 ± 0.18	22.63 ± 0.77	0.899 ± 0.061	0.214 ± 0.174	0.049	0.124 ± 0.185	3
1996cn	0.430	22.58	23.25 ± 0.03	23.09 ± 0.19	—	0.890 ± 0.066	0.379 ± 0.090	0.025	0.332 ± 0.097	1–3
1997F	0.580	22.93	23.51 ± 0.06	23.57 ± 0.20	23.30 ± 0.95	1.041 ± 0.066	0.275 ± 0.197	0.040	0.063 ± 0.232	
1997H	0.526	22.70	23.26 ± 0.04	23.09 ± 0.19	22.51 ± 0.80	0.882 ± 0.043	0.303 ± 0.174	0.051	0.150 ± 0.194	
1997I	0.172	20.18	20.34 ± 0.01	20.29 ± 0.17	20.19 ± 0.28	0.967 ± 0.009	0.065 ± 0.047	0.051	0.026 ± 0.064	
1997N	0.180	20.39	20.38 ± 0.02	20.48 ± 0.17	21.28 ± 0.52	1.067 ± 0.015	-0.141 ± 0.093	0.031	-0.200 ± 0.123	
1997O	0.374	22.99	23.53 ± 0.06	23.60 ± 0.18	—	1.048 ± 0.054	0.087 ± 0.152	0.029	0.049 ± 0.162	1–3
1997P	0.472	22.53	23.16 ± 0.04	22.99 ± 0.18	23.24 ± 0.91	0.888 ± 0.034	0.058 ± 0.207	0.033	-0.052 ± 0.219	
1997Q	0.430	22.01	22.61 ± 0.02	22.52 ± 0.17	22.55 ± 0.62	0.935 ± 0.024	0.061 ± 0.140	0.030	-0.002 ± 0.148	
1997R	0.657	23.29	23.89 ± 0.05	23.80 ± 0.19	23.68 ± 0.90	0.940 ± 0.059	0.393 ± 0.175	0.030	0.032 ± 0.222	
1997ac	0.320	21.42	21.87 ± 0.02	21.96 ± 0.17	21.95 ± 0.33	1.061 ± 0.015	0.063 ± 0.065	0.027	0.001 ± 0.072	
1997af	0.579	22.94	23.60 ± 0.07	23.38 ± 0.18	24.31 ± 1.09	0.850 ± 0.045	0.045 ± 0.226	0.028	-0.215 ± 0.265	
1997ai	0.450	22.34	22.94 ± 0.05	22.63 ± 0.22	22.58 ± 0.59	0.788 ± 0.084	0.143 ± 0.133	0.045	0.026 ± 0.142	
1997aj	0.581	22.58	23.24 ± 0.07	23.16 ± 0.18	24.05 ± 0.79	0.947 ± 0.045	0.045 ± 0.164	0.033	-0.213 ± 0.193	
1997am	0.416	22.01	22.58 ± 0.08	22.63 ± 0.18	22.65 ± 0.46	1.032 ± 0.060	0.037 ± 0.113	0.036	-0.008 ± 0.119	
1997ap	0.830	23.16	24.35 ± 0.07	24.38 ± 0.18	23.74 ± 0.50	1.023 ± 0.045	0.903 ± 0.082	0.026	0.155 ± 0.118	

a: X=R for $z < 0.7$, X=I for $z > 0.7$

b: This value has been K-corrected and corrected for Galactic extinction: $m_B \equiv m_X - K_{BX} - A_X$, where K_{BX} is the cross-filter K-correction and A_X is the Galactic extinction correction. These were the values used in the cosmological fits. The quoted error bar is the uncertainty on the peak magnitude from the lightcurve fit.

c: This value includes the stretch correction: $m_B^{eff} \equiv m_B + \alpha(s - 1)$. α is the best-fit value of the stretch-luminosity slope from the fit to the primary low-extinction subset (Fit 3 in § 4). The quoted error bar includes all uncertainties for non-extinction-corrected fits described in § 2.4. Note that these values are only provided for convenience; they were not used directly in any cosmological fits, since α is also a fit parameter.

d: Similar to column c, only with the host-galaxy extinction correction applied. The stretch/luminosity slope used for this value is that from the fit to the primary subset (Fit 6 in § 4). The quoted error bar includes all uncertainties for extinction-corrected fits described in § 2.4. A line indicates a supernova which did not appear in the primary subset (see § 2.5.)

e: This is the observed R-I color at the epoch of the rest-frame B-band lightcurve peak.

f: Schlegel, Finkbeiner, & Davis (1998); this extinction is already included in the quoted values of m_B.

g: Measurement uncertainty only; no intrinsic color dispersion included.

h: These supernovae are excluded from the indicated subsets; see § 2.5.

Table 5: Supernova Lightcurve Fits: Low-z SNe from Hamuy (1996) and Riess (1999)

SN (a)	z	m_B^{meas} (b)	m_B (c)	m_B^{eff} (d)	m_B^{eff} Ext. corr. (e)	Stretch (s)	R-I (f)	E(B-V) Gal. (g)	E(B-V)$_{host}$ (h)	Excluded from Subsets (i)
1990O	0.030	16.58	16.18 ± 0.03	16.33 ± 0.20	16.30 ± 0.17	1.106 ± 0.026	0.043 ± 0.025	0.098	0.001 ± 0.026	
1990af	0.050	17.92	17.76 ± 0.01	17.39 ± 0.18	17.42 ± 0.13	0.749 ± 0.010	0.077 ± 0.011	0.035	0.011 ± 0.011	
1992P	0.026	16.12	16.05 ± 0.02	16.14 ± 0.19	16.16 ± 0.16	1.061 ± 0.027	-0.045 ± 0.018	0.020	-0.008 ± 0.019	
1992ae	0.075	18.59	18.42 ± 0.04	18.35 ± 0.18	18.35 ± 0.15	0.957 ± 0.018	0.098 ± 0.028	0.036	0.003 ± 0.031	
1992ag	0.026	16.67	16.26 ± 0.02	16.34 ± 0.20	15.55 ± 0.16	1.053 ± 0.015	0.220 ± 0.020	0.097	0.189 ± 0.021	2,3
1992al	0.014	14.61	14.48 ± 0.01	14.42 ± 0.23	14.53 ± 0.20	0.959 ± 0.011	-0.054 ± 0.012	0.034	-0.025 ± 0.013	
1992aq	0.101	19.38	19.30 ± 0.02	19.12 ± 0.17	19.24 ± 0.15	0.878 ± 0.017	0.142 ± 0.023	0.012	-0.019 ± 0.026	
1992bc	0.020	15.18	15.10 ± 0.01	15.18 ± 0.20	15.36 ± 0.16	1.053 ± 0.006	-0.087 ± 0.009	0.022	-0.046 ± 0.009	
1992bg	0.036	17.41	16.66 ± 0.04	16.66 ± 0.20	16.68 ± 0.16	1.003 ± 0.014	0.128 ± 0.025	0.181	-0.006 ± 0.026	
1992bh	0.045	17.71	17.60 ± 0.02	17.64 ± 0.18	17.22 ± 0.14	1.027 ± 0.016	0.101 ± 0.018	0.022	0.100 ± 0.019	
1992bl	0.043	17.37	17.31 ± 0.03	17.03 ± 0.18	17.10 ± 0.14	0.812 ± 0.012	0.017 ± 0.023	0.012	-0.002 ± 0.024	
1992bo	0.018	15.89	15.78 ± 0.01	15.42 ± 0.21	15.31 ± 0.17	0.756 ± 0.005	0.048 ± 0.012	0.027	0.043 ± 0.012	
1992bp	0.079	18.59	18.29 ± 0.01	18.16 ± 0.18	18.41 ± 0.13	0.906 ± 0.014	0.088 ± 0.015	0.068	-0.056 ± 0.017	
1992br	0.088	19.52	19.37 ± 0.08	18.93 ± 0.20	—	0.700 ± 0.021	0.186 ± 0.047	0.027	0.030 ± 0.052	1–3
1992bs	0.063	18.26	18.20 ± 0.04	18.26 ± 0.18	18.37 ± 0.14	1.038 ± 0.016	0.011 ± 0.022	0.013	-0.031 ± 0.024	
1993B	0.071	18.74	18.37 ± 0.04	18.40 ± 0.18	18.10 ± 0.15	1.021 ± 0.019	0.181 ± 0.027	0.080	0.071 ± 0.029	
1993O	0.052	17.87	17.64 ± 0.01	17.53 ± 0.18	17.61 ± 0.13	0.926 ± 0.007	0.042 ± 0.012	0.053	-0.014 ± 0.012	
1993ag	0.050	18.32	17.83 ± 0.02	17.73 ± 0.18	17.26 ± 0.15	0.936 ± 0.015	0.217 ± 0.020	0.111	0.120 ± 0.021	2,3
1994M	0.024	16.34	16.24 ± 0.03	16.07 ± 0.20	15.84 ± 0.16	0.882 ± 0.015	0.043 ± 0.022	0.023	0.063 ± 0.022	
1994S	0.016	14.85	14.78 ± 0.02	14.83 ± 0.22	14.86 ± 0.19	1.033 ± 0.026	-0.061 ± 0.019	0.018	-0.010 ± 0.019	
1995ac	0.049	17.23	17.05 ± 0.01	17.17 ± 0.18	17.17 ± 0.13	1.083 ± 0.012	0.026 ± 0.011	0.042	-0.005 ± 0.011	
1995bd	0.016	17.34	15.32 ± 0.01	15.37 ± 0.30	—	1.039 ± 0.008	0.735 ± 0.008	0.490	0.348 ± 0.009	1–3
1996C	0.030	16.62	16.57 ± 0.04	16.74 ± 0.19	16.50 ± 0.16	1.120 ± 0.020	0.012 ± 0.026	0.014	0.051 ± 0.027	
1996ab	0.125	19.72	19.57 ± 0.04	19.47 ± 0.19	19.82 ± 0.16	0.934 ± 0.032	0.174 ± 0.025	0.032	-0.082 ± 0.029	
1996bl	0.035	17.08	16.66 ± 0.01	16.71 ± 0.19	16.55 ± 0.14	1.031 ± 0.015	0.093 ± 0.012	0.099	0.036 ± 0.012	
1996bo	0.016	16.18	15.85 ± 0.01	15.65 ± 0.22	—	0.862 ± 0.006	0.406 ± 0.008	0.077	0.383 ± 0.008	1–3

a: Supernovae through 1993ag are from H96, later ones from R99.
b: This is the measured peak magnitude of the B-band lightcurve.
c: This includes the Galactic extinction correction and a K-correction: $M - B \equiv m_B^{meas} - K_B - A_B$, where K_B is the K-correction and A_B is the Galactic extinction correction. The quoted error bar is the uncertainty on the peak magnitude from the lightcurve fit.
d: This value includes the stretch correction: $m_B^{eff} \equiv m_B^{meas} - K_B - A_B + \alpha(s - 1)$. α is the best-fit value of the stretch/luminosity slope from the fit to the primary low-extinction subset (Fit 3 in § 4). The quoted error bar includes all uncertainties for non-extinction corrected fits described in § 2.4. Note that these values are only provided for convenience; they were not used directly in any cosmological fits, since the α is also a fit parameter.
e: Similar to column d, only with the host-galaxy extinction correction applied. The stretch/luminosity slope used for this value is that from the fit to the primary subset (Fit 6 in § 4). The quoted error bar includes all uncertainties for extinction-corrected fits described in § 2.4. A line indicates a supernova which did not appear in the primary subset (see § 2.5.)
f: This value has been K-corrected and corrected for Galactic extinction.
g: This is the measured B-V color at the epoch of rest-frame B-band lightcurve maximum.
h: Schlegel, Finkbeiner, & Davis (1998); this extinction is already included in the quoted values of m_B in column c.
i: These supernovae are excluded from the indicated subsets; § 2.5.

tion of time and is described by a spline under tension: an "intercept" $b(t)$ and a "slope" $m(t)$. At any given date the intrinsic color is

$$color(t') = b(t') + m(t') \times (1/s^3 - 1) \quad (2)$$

where $t' = t/(s(1+z))$, z is the redshift of the supernova, and s is the timescale stretch of the supernova from a simultaneous fit to the B and V lightcurves (matching the procedure used for most of the high-redshift supernovae). This arbitrary functional form was chosen to match the stretch vs. color distribution.

As the goal was to determine intrinsic colors without making any assumptions about reddening, no host-galaxy extinction corrections were applied to the literature data at this stage of the analysis. Instead, host-galaxy extinction was handled by performing a robust blue-side ridge-line fit to the supernova color curves, so as to extract the unreddened intrinsic color. Individual color points that were outliers were prevented from having too much weight in the fit with a small added dispersion on each point. The blue ridge-line was selected by allowing any point more than 1σ to the red side of the fit model only to contribute to the χ^2 as if it were 1σ away. Additionally, those supernovae which were most reddened were omitted. The resulting fit procedure provided B-V, V-R, and R-I as a function of epoch and stretch; those colors were used to correct the template spectrum as described above.

Some of our data extend into the rest-frame U-band range of the spectrum. This is obvious for supernovae at $z > 0.7$ where a U-band template is fit to the R-band data. However, even for supernovae at $z \gtrsim 0.55$, the de-redshifted R-band filter begins to overlap the U-band range of the rest-frame spectrum. Thus, it is also important to know the intrinsic U-B color so as to generate a proper spectral template. We used data from the literature, as given in Table 6. Here, there is an insufficient number of supernova lightcurves to reasonably use the sort of ridge-line analysis used above to eliminate the effects of host-galaxy extinction in determining the intrinsic $BVRI$ colors. Instead, for U-B, we perform extinction corrections using the $E(B$-$V)$ values from Phillips $et\ al.$ (1999). Based on Table 6, we adopt a U-B color of -0.4 at the epoch of rest-B maximum. This value is also consistent with the data shown in

Jha (2002) for supernovae with timescale stretch of $s \sim 1$, although the data are not determinative. In contrast to the other colors, U-B was not considered to be a function of stretch. Even though Jha (2002) does show U-B depending on lightcurve stretch, the supernovae in this work that would be most affected (those at $z > 0.7$ where $E(B$-$V)$ is estimated from the rest-frame U-B color) cover a small range in stretch; current low-redshift U-B data do not show a significant slope within that range. See § 5.4 for the effect of systematic error in the assumed intrinsic U-B colors.

Any intrinsic uncertainty in B-V is already subsumed within the assumed intrinsic dispersion of extinction-corrected peak magnitudes (see § 2.4); however, we might expect a larger dispersion in intrinsic U-B due to e.g., metallicity effects (Hoeflich, Wheeler, & Thielemann 1998; Lentz $et\ al.$ 2000). The low-redshift U-band photometry may also have unmodeled scatter e.g., related to the lack of extensive UV supernova spectrophotometry for K-corrections. The effect on extinction-corrected magnitudes will be further increased by the greater effect of dust extinction on the bluer U-band light. The scatter of our extinction-corrected magnitudes about the best-fit cosmology suggests an intrinsic uncertainty in U-B of 0.04 magnitudes. This is also consistent with the U-B data of Jha (2002) over the range of timescale stretch of our $z > 0.7$ SNe Ia, after two extreme color outliers from Jha (2002) are removed; there is no evidence of such extreme color objects in our dataset. Note that this intrinsic U-B dispersion is in addition to the intrinsic magnitude dispersion assumed after extinction correction.

The template spectrum which has been constructed may be used to perform color- and K-corrections on both the low- and high-redshift supernovae to be used for cosmology. However, it must be further modified to account for the reddening effects of dust extinction in the supernova host galaxy, and extinction of the redshifted spectrum due to Galactic dust. To calculate the reddening effects of both Galactic and host-galaxy extinction, we used the interstellar extinction law of O'Donnell (1994) with the standard value of the parameter $R_V = 3.1$. Color excess ($E(B$-$V)$) values due to Galactic extinction were obtained from Schlegel, Finkbeiner, & Davis (1998).

The $E(B$-$V)$ values quoted in Tables 3, 4, and 5

Table 6: U-B SN Ia Colors at Epoch of B-band Maximum

SN	Raw U-B^a	Corrected U-B^b	Reference
1980N	-0.21	-0.29	Hamuy *et al.* (1991)
1989B	0.08	-0.33	Wells *et al.* (1994)
1990N	-0.35	-0.45	Lira *et al.* (1998)
1994D	-0.50	-0.52	Wu, Yan, & Zou (1995)
1998bu	-0.23	-0.51	Suntzeff *et al.* (1999)

a: This is the measured U-B value from the cited paper.

b: This U-B value is K-corrected, and corrected for host-galaxy and Galactic extinction.

are the values necessary to reproduce the observed R-I color at the epoch of the maximum of the rest-frame B lightcurve. This reproduction was performed by modifying the spectral template exactly as described above, given the intrinsic color of the supernova from the fit stretch, the Galactic extinction, and the host-galaxy $E(B$-$V)$ parameter. The modified spectrum was integrated through the Bessell R- and I-band filters, and $E(B$-$V)$ was varied until the R-I value matched the peak color from the lightcurve fit.

For each supernova, this finally modified spectral template was integrated through the Bessell and WFPC2 filter transmission functions to provide color and K-corrections. The exact spectral template needed for a given data point on a given supernova is dependent on parameters of the fit: the stretch, the time of each point relative to the epoch of rest-B maximum, and the host-galaxy $E(B$-$V)$ (measured as described above). Thus, color and K-corrections were performed iteratively with lightcurve fitting in order to generate the final corrections used in the fits described in § 2.2. An initial date of maximum, stretch, and host-galaxy extinction was assumed in order to generate K-corrections for the first iteration of the fit. The parameters resulting from that fit were used to generate new color and K-corrections, and the whole procedure was repeated until the results of the fit converged. Generally, the fit converged within 2–3 iterations.

2.4. Cosmological Fit Methodology

Cosmological fits to the luminosity distance modulus equation from the Friedmann-Robertson-Walker metric followed the procedure of P99. The set of supernova redshifts (z) and K-corrected peak B-magnitudes (m_B) were fit to the equation

$$m_B = \mathcal{M} + 5 \log \mathcal{D}_\mathcal{L}(z; \Omega_\mathrm{M}, \Omega_\Lambda) - \alpha(s - 1) \quad (3)$$

where s is the stretch value for the supernova, $\mathcal{D}_\mathcal{L} \equiv H_0 d_L$ is the "Hubble-constant-free" luminosity distance (Perlmutter *et al.* 1997), and $\mathcal{M} \equiv M_B - 5 \log H_0 + 25$ is the "Hubble-constant-free" B-band peak absolute magnitude of a $s = 1$ SN Ia with true absolute peak magnitude M_B. With this procedure, neither H_0 nor M_B need be known independently. The peak magnitude of a SN Ia is mildly dependent on the lightcurve decay time scale, such that supernovae with a slow decay (high stretch) tend to be over-luminous, while supernovae with a fast decay (low stretch) tend to be under-luminous (Phillips *et al.* 1993); α is a slope that parameterizes this relationship.

There are four parameters in the fit: the mass density Ω_M and cosmological constant Ω_Λ, as well as the two nuisance parameters, $\mathcal{M}$ and α. The four-dimensional $(\Omega_\mathrm{M}, \Omega_\Lambda, \mathcal{M}, \alpha)$ space is divided into a grid, and at each grid point a χ^2 value is calculated by fitting the luminosity distance equation to the peak B-band magnitudes and redshifts of the supernovae. The range of parameter space explored included $\Omega_\mathrm{M} = [0, 3)$, $\Omega_\Lambda = [-1, 3)$ (for fits where host-galaxy extinction corrections are not directly applied) or $\Omega_\mathrm{M} = [0, 4]$, $\Omega_\Lambda = [-1, 4)$ (for fits with host-galaxy extinction corrections). The two nuisance parameters are fit in the ranges $\alpha = [-1, 4)$ and $\mathcal{M} = [-3.9, 3.2)$. No further constraints are placed on the parameters. (These ranges for the four fit parameters contain $> 99.99\%$ of the probability.) At each point on the 4-dimensional grid, a χ^2 is calculated, and a

probability is determined from $P \propto e^{-\chi^2/2}$. The probability of the whole 4-dimensional grid is normalized, and then integrated over the two dimensions corresponding to the "nuisance" parameters.

For each fit, all peak m_B values were corrected for Galactic extinction using $E(B\text{-}V)$ values from Schlegel, Finkbeiner, & Davis (1998), using the extinction law of O'Donnell (1994) integrated through the *observed* filter.[30] For our primary fits, the total effective statistical uncertainty on each value of m_B included the following contributions:

- the uncertainty on m_B from the lightcurve fits;
- the uncertainty on s, multiplied by α
- the covariance between m_B and s;
- a contribution from the uncertainty in the redshift due to peculiar velocity (assumed to have a dispersion of 300 km s^{-1} along the line of site);
- 10% of the Galactic extinction correction; and
- 0.17 magnitudes of intrinsic dispersion (H96).

Fits where host-galaxy extinction corrections are explicitly applied use the first five items above plus:

- the uncertainty on $E(B\text{-}V)$ multiplied by R_B;
- the covariance between $E(B\text{-}V)$ and m_B;
- 0.11 magnitudes of intrinsic dispersion (Phillips *et al.* 1999); and
- an additional 0.04 magnitudes of intrinsic U-B dispersion for $z > 0.7$.

Host-galaxy extinction corrections used a value $R_B \equiv A_B/E(B\text{-}V) = 4.1$, which results from passing a SN Ia spectrum through the standard O'Donnell (1994) extinction law. Except where explicitly noted below, the $E(B\text{-}V)$ uncertainties are *not* reduced by any prior assumptions on the intrinsic color excess distribution. Although there is almost certainly some intrinsic dispersion either in R_B, or in the true B-V color of a SN Ia (Nobili *et al.* 2003), we do not explicitly include such a

term. The effect of such a dispersion is included, in principle, in the 0.11 magnitudes of intrinsic magnitude dispersion which Phillips *et al.* (1999) found after applying extinction corrections.

As discussed in § 2.3, the intrinsic U-B dispersion is likely to be greater than the intrinsic B-V dispersion. For those supernovae most affected by this (i.e. those at $z > 0.7$), we included an additional uncertainty corresponding to 0.04 magnitudes of intrinsic U-B dispersion, converted into a magnitude error using the O'Donnell extinction law.

This set of statistical uncertainties is slightly different from that used in P99. For these fits, the test value of α was used to propagate the stretch errors into the corrected B-band magnitude errors; in contrast, P99 used a single value of α for purposes of error propagation.

2.5. Supernova Subsets

In P99, separate analyses were performed and compared for the supernova sample before and after removing supernovae with less secure identification as Type Ia. The results were shown to be consistent, providing a cross-check of the cosmological conclusions. For the analyses of this paper, adding and comparing eleven very-well-measured SNe Ia, we only consider from P99 the more securely spectrally identified SNe Ia with reasonable color measurements (i.e. $\sigma_{R-I} < 0.25$); those supernovae are listed in Table 4. Following P99, we omit one supernova which is an outlier in the stretch distribution, with $s < 0.7$ (SN 1992br), and one SN which is a $> 6\sigma$ outlier from the best-fit cosmology (SN 1997O). We also omit those supernovae which are most seriously reddened, with $E(B\text{-}V) > 0.25$ and $> 3\sigma$ above zero; host-galaxy extinction corrections have been found in studies of low-redshift supernovae to overcorrect these reddest objects (Phillips *et al.* 1999). This cut removes two SNe at low redshift (SNe 1995bd and 1996bo), one from P99 (SN 1996cn), and one of the eleven HST supernovae from this paper (SN 1998aw). The resulting "full primary subset" of SNe Ia is identified as Subset 1 in the tables.

For the analyses of a "low-extinction primary subset," Subset 2, we further cull out four supernovae with host-galaxy $E(B\text{-}V) > 0.1$ and $> 2\sigma$ above zero, including two of the HST supernovae

---

[30]This supersedes P99, where an incorrect dependence on z of the effective R_R for Galactic extinction was applied. The corrected procedure decreases the flat-universe value of $\Omega_{\rm M}$ by 0.03.

from this paper (SNe 1992ag, 1993ag, 1998as, and 1998ax). The low-extinction primary subset includes eight of the eleven new HST supernovae presented in this paper.

Subset 3, the "low-extinction strict Ia subset," makes an even more stringent cut on spectral confirmation, including only those supernovae whose confirmations as Type Ia SNe are unquestionable. This subset is used in § 5.2 to estimate any possible systematic bias resulting from type contamination. An additional six supernovae, including two of the HST supernovae from this paper, are omitted from Subset 3 beyond those omitted from Subset 2; these are SNe 1995as, 1996cf, 1996cg, 1996cm, 1998ay, and 1998be.

3. Colors and Extinction

In this section, we discuss the limits on host-galaxy extinction we can set based on the measured colors of our supernovae. For the primary fit of our P99 analysis, extinction was estimated by comparing the mean host-galaxy $E(B\text{-}V)$ values from the low- and high-redshift samples. Although the uncertainties on individual $E(B\text{-}V)$ values for high-redshift supernovae were large, the uncertainty on the mean of the distribution was only 0.02 magnitudes. P99 showed that there was no significant difference in the mean host-galaxy reddening between the low and high-redshift samples of supernovae of the primary analysis (Fit C). This tightly constrained the systematic uncertainty on the cosmological results due to differences in extinction. The models of Hatano, Branch, & Deaton (1998) suggest that most SNe Ia should be found with little or no host galaxy extinction. By making a cut to include only those objects which have small $E(B\text{-}V)$ values (and then verifying the consistency of low- and high-redshift mean reddening), we are creating a subsample likely to have quite low extinction. The strength of this method is that it does not depend on the exact shape of the intrinsic extinction distribution, but only requires that most supernovae show low extinction. Figure 3 (discussed below) demonstrates that most supernovae indeed have low-extinction, as expected from the Hatano, Branch, & Deaton (1998) models. Monte Carlo simulations of our data using the Hatano, Branch, & Deaton (1998) extinction distribution function

and our low-extinction $E(B\text{-}V)$ cuts confirm the robustness of this approach, and further, demonstrate that similarly low extinction subsamples are obtained for both low- and high-redshift datasets despite the larger color uncertainties for some of the P99 supernovae.

Riess *et al.* (1998) used the work of Hatano, Branch, & Deaton (1998) differently, by applying a one-sided Bayesian prior to their measured $E(B\text{-}V)$ values and uncertainties. A prior formed from the Hatano, Branch, & Deaton (1998) extinction distribution function would have zero probability for negative values of $E(B\text{-}V)$, a peak at $E(B\text{-}V) \sim 0$ with roughly 50% of the probability, and an exponential tail to higher extinctions. As discussed in P99 (see the "Fit E" discussion, where P99 apply the same method), when uncertainties on high- and low-redshift supernova colors differ, use of an asymmetric prior may introduce bias into the cosmological results, depending on the details of the prior. While a prior with a tight enough peak at low extinction values introduces little bias (especially when low- and high-redshift supernovae have comparable uncertainties), it does reduce the apparent $E(B\text{-}V)$ error bars on all but the most reddened supernovae. As we will show in Figure 10 (§ 4.1) the use of this prior almost completely eliminates the contribution of color uncertainties to the size of the cosmological confidence regions, meaning that an extinction correction using a sharp enough prior is much more akin to simply selecting a low-extinction subset than to performing an assumption-free extinction correction using the $E(B\text{-}V)$ measurement uncertainties.

The high precision measurements of the $R\text{-}I$ color afforded by the WFPC2 lightcurves for the new supernovae in this work allow a direct estimation of the host-galaxy $E(B\text{-}V)$ color excess without any need to resort to any prior assumptions concerning the intrinsic extinction distribution.

Figure 3 shows histograms of the host-galaxy $E(B\text{-}V)$ values from different samples of the supernovae used in this paper. For the bottom two panels, a line is over-plotted that treats the H96 low-extinction subset's $E(B\text{-}V)$ values as a parent distribution, and shows the expected distribution for the other samples given their measurement uncertainties. The low-extinction subset of each sample (the grey histogram) has a
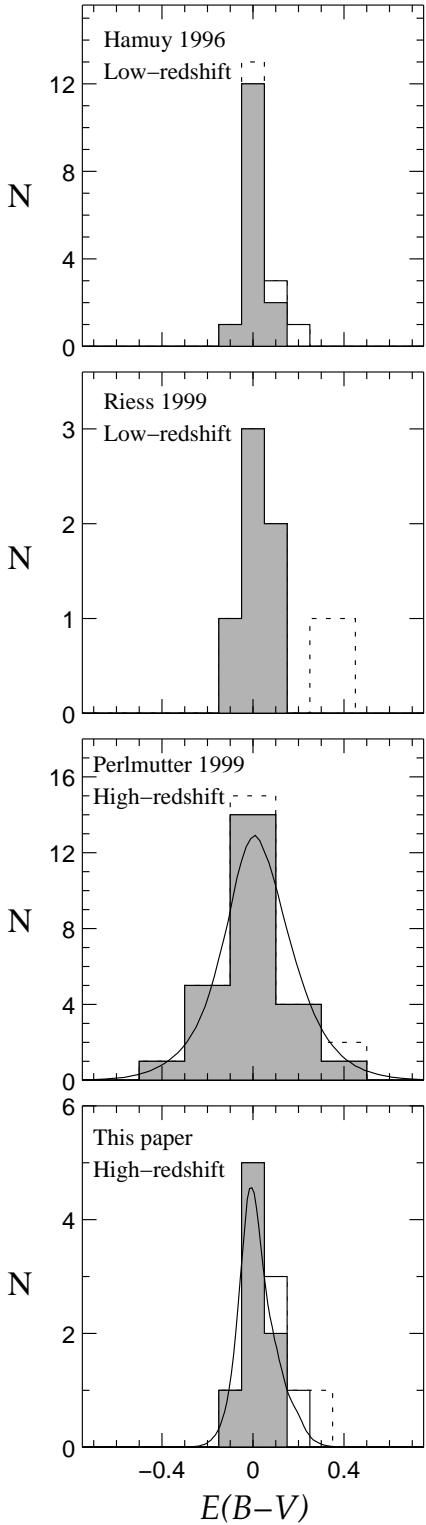
Fig. 3.— Histograms of $E(B\text{-}V)$ for the four samples of supernovae used in this paper. The filled grey histogram represents just the low-extinction subset (Subset 2). The open boxes on top of that represent supernovae which are in the primary subset (Subset 1) but excluded from the low-extinction subset. Finally, the dotted histogram represents those supernovae which are in the full sample but omitted from the primary subset. The solid lines drawn over the bottom two panels is a simulation of the distribution expected if the low-extinction subset of the H96 sample represented the true distribution of SN colors, given the error bars of the low-extinction subset of each high-redshift sample.

Table 7: Mean $E(B\text{-}V)$ Values

Sample	Complete Set	Low-extinction Primary Subset SNe[a]
Low z	$+0.095 \pm 0.003$	-0.001 ± 0.003
P99	$+0.018 \pm 0.024$	-0.004 ± 0.025
HST	$+0.090 \pm 0.012$	$+0.012 \pm 0.015$

a: SNe omitted from our low-extinction primary subset, Subset 2, (§ 2.5) have been omitted from these means. This excludes outliers, as well as supernovae with both $E(B\text{-}V) > 0.1$ and $E(B\text{-}V) > 2\sigma$ above zero.


Fig. 4.— A plot of $E(B\text{-}V)$ as a function of redshift for the 11 HST-observed supernovae of this paper shows that the blue edge of the distribution shows no significant evolution with redshift. (The larger dispersion at lower redshifts is expected for a flux-limited sample.) Error bars include only measurement errors, and no assumed intrinsic color dispersion. Filled circles are those supernovae in the low-extinction subset (Subset 2).

color excess distribution which is consistent with that of the low-extinction subset of H96. Table 7 lists the variance-weighted mean $E(B\text{-}V)$ values for the low-redshift supernovae and for each sample of high-redshift supernovae. Although varying amounts of extinction are detectable in the mean colors of each full sample, the supernovae in the low-extinction primary subset (§ 2.5) of each sample are consistent with $E(B\text{-}V) = 0$. This subset is consistent with the models of Hatano, Branch, & Deaton (1998), discussed above, in which most SNe Ia are observed in regions of very low extinction. We will consider cosmological fits both to this low-extinction subset and to the primary subset with host-galaxy reddening corrections applied.

Figure 4 shows $E(B\text{-}V)$ vs. redshift for the eleven supernovae of this paper. Three of the lowest redshift SNe are likely to be significantly reddened: SN 1998as at $z = 0.36$, SN 1998aw at $z = 0.44$, and SN 1998ax at $z = 0.50$. This higher incidence of extincted SNe at the low-redshift end of our sample is consistent with expectations for a flux-limited survey, where extincted supernovae will be preferentially detected at lower redshifts. Indeed, the distribution of $E(B\text{-}V)$ values versus redshift shown in Figure 4 is consistent with the results of a Monte Carlo simulation similar to that of Hatano, Branch, & Deaton (1998), but including the effects of the survey flux limit. Several authors (including Leibundgut (2001) and Falco *et al.* (1999)) have suggested that there is evidence from the $E(B\text{-}V)$ values in Riess *et al.* (1998) that high-redshift supernovae are bluer statistically than their low-redshift counterparts. Our

data show no such effect (nor did our P99 SNe).

The mean host-galaxy color excess calculated for the highest redshift supernovae is critically dependent on the assumed intrinsic $U\text{-}B$ color (see § 2.3). An offset in this assumed $U\text{-}B$ will affect the high-redshift supernovae much more than the low-redshift supernovae (whose measurements are primarily of the rest frame B- and V-band lightcurves). The K-corrected, rest-frame B-band magnitudes are also dependent on the assumed supernova colors that went into deriving the K-corrections. If the assumed $U\text{-}B$ color is too red, it will affect the cross-filter K-correction applied to R-band data at $z \gtrsim 0.5$, thereby changing derived rest frame colors. In § 5, we consider the effect of changing the reference $U\text{-}B$ color.

4. Cosmological Results

4.1. Ω_{M} and Ω_{Λ}

Figures 5 through 7 show Hubble Diagrams which effective B-band peak magnitudes and redshifts for the new supernovae of this paper; these magnitudes have been K- and stretch corrected, and have been corrected for Galactic extinction. Figure 5 shows all of the data in the low-extinction
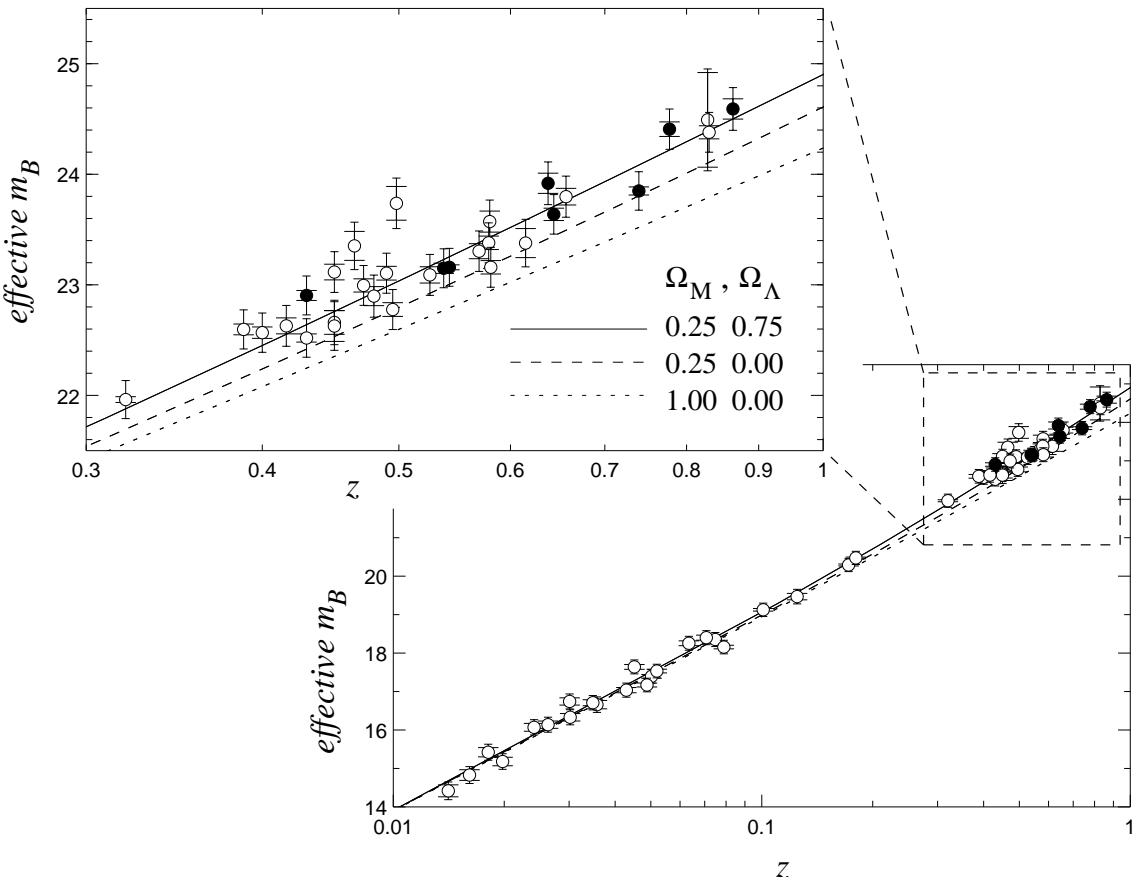
Fig. 5.— Hubble diagram of effective K- and stretch-corrected m_B vs. redshift for the supernovae in the primary low-extinction subset. Filled circles represent the HST supernovae of this paper. Inner error bars show just the measurement uncertainties; outer error bars include 0.17 magnitudes of intrinsic dispersion. The solid line is the best-fit flat-universe cosmology from the low-extinction subset; the dashed and dotted lines represent the indicated cosmologies.
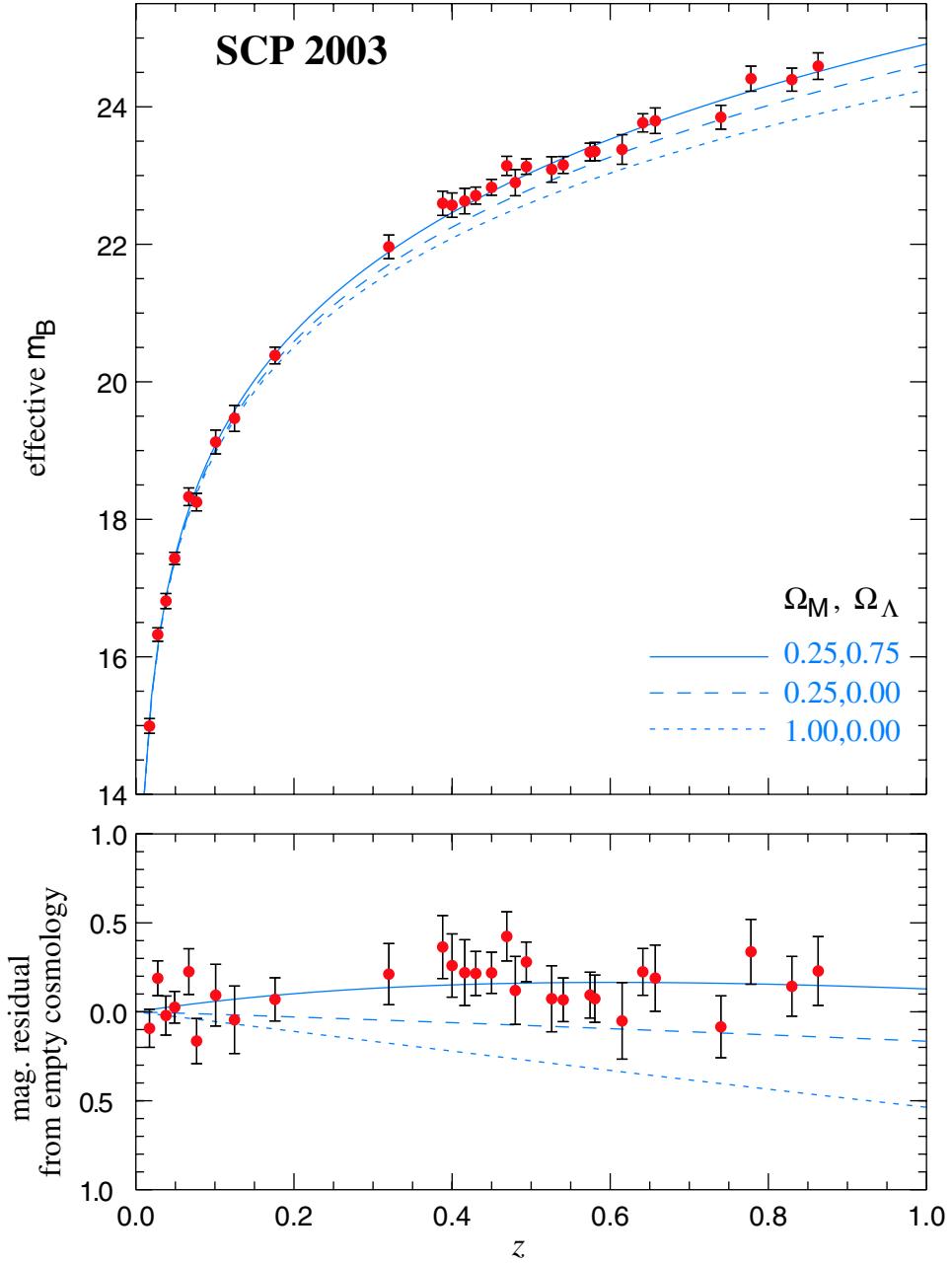
Fig. 6.— Upper panel: Averaged Hubble diagram with a linear redshift scale for all supernovae from our low-extinction subsample. Here supernovae within $\Delta z < 0.01$ of each other have been combined using a weighted average in order to more clearly show the quality and behavior of the dataset. (Note that these averaged points are for display only, and have not been used for any quantitative analyses.) The solid curve overlaid on the data represents our best-fit flat-universe model, $(\Omega_M, \Omega_\Lambda) = (0.25, 0.75)$ (Fit 3 of Table 8). Two other cosmological models are shown for comparison: $(\Omega_M, \Omega_\Lambda) = (0.25, 0)$ and $(\Omega_M, \Omega_\Lambda) = (1, 0)$. Lower panel: Residuals of the averaged data relative to an empty universe, illustrating the strength with which dark energy has been detected. Also shown are the suite of models from the upper panel, including a solid curve for our best-fit flat-universe model.

23
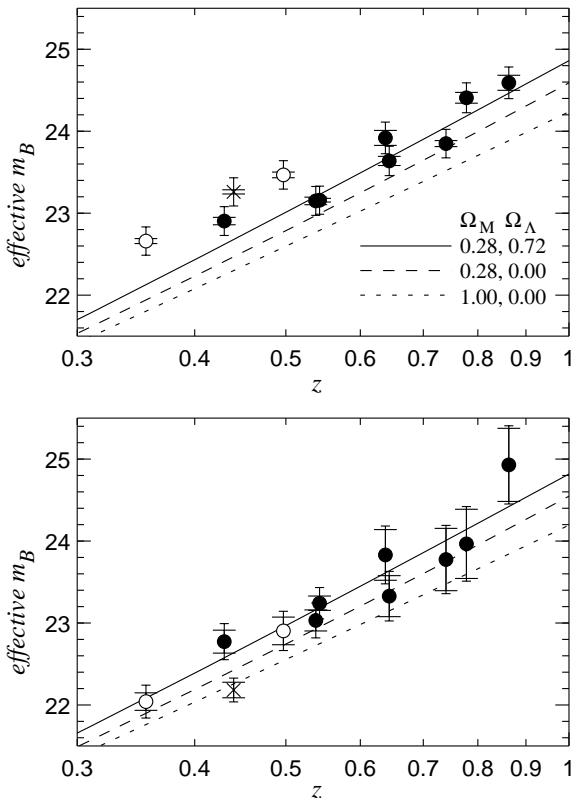
Fig. 7.— Hubble diagram of effective K- and stretch-corrected m_B vs. redshift for the 11 supernovae observed with WFPC2 and reported in this paper. Circles represent supernovae in the primary subset (Subset 1); the one point plotted as a cross (the very reddened supernova SN 1998aw) is omitted from that subset. Open circles represent reddened supernovae omitted from the low-extinction primary subset (Subset 2), while filled circles are in both Subsets 1 and 2. **Upper plot:** no host-galaxy $E(B\text{-}V)$ extinction corrections have been applied. Inner error bars only include the measurement error. Outer error bars include 0.17 magnitudes of intrinsic dispersion. **Lower plot:** extinction corrections have been applied using the standard interstellar extinction law. Error bars have been increased by the uncertainty in this extinction correction. Again, inner error bars represent only measurement uncertainties, while outer error bars include 0.11 magnitudes of intrinsic dispersion. Lines are for three example cosmologies with the indicated values of Ω_M and Ω_Λ; the solid line is the best-fit flat-universe cosmology to our full primary subset with extinction corrections applied.

24
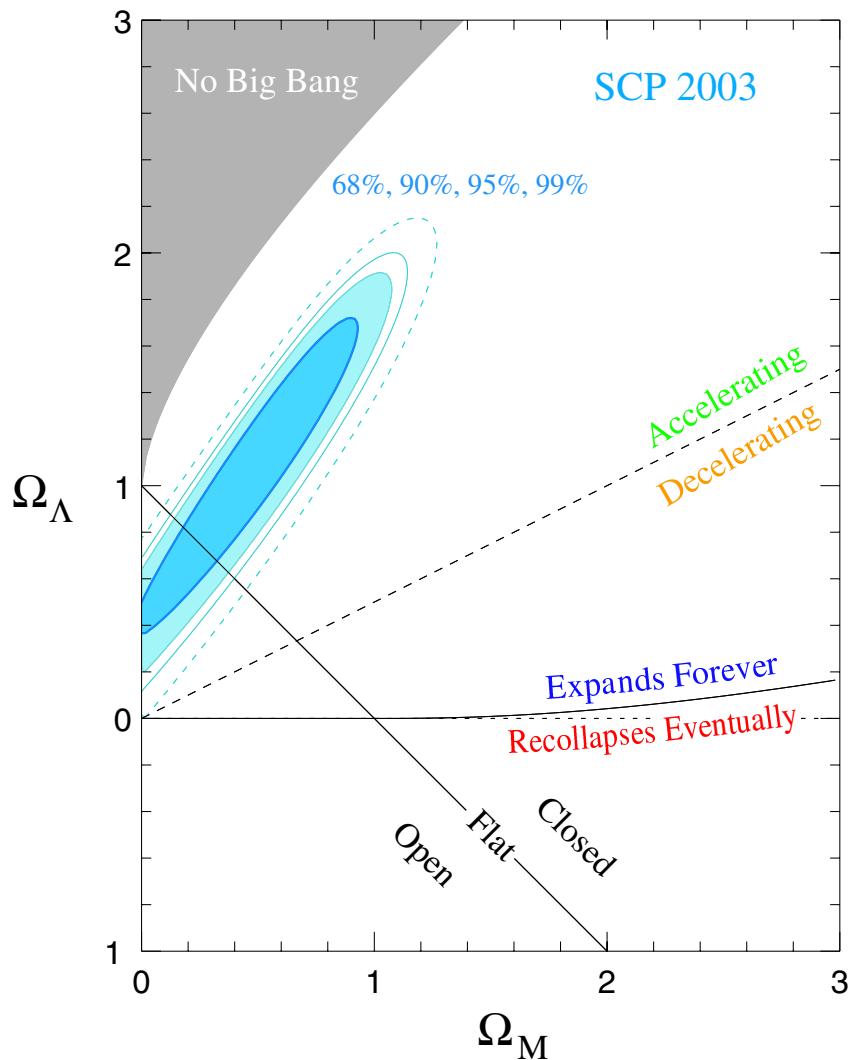
Fig. 8.— 68%, 90%, 95%, and 99% confidence regions for Ω_M and Ω_Λ from this paper's primary analysis, the fit to the low-extinction primary subset (Fit 3).

subset of supernovae. For the sake of clarity, Figure 6 shows the same subset, but for this figure supernovae with redshifts within 0.01 of each other have been combined in a variance-weighted average. The lower panel of Figure 6 shows the residuals from an empty universe ($\Omega_M = 0$, $\Omega_\Lambda = 0$), illustrating the strength with which dark energy has been detected. In both Figures 5 and 6, the solid line represents the flat-universe cosmology resulting from our fits to the low-extinction subset. Figure 7 shows just the eleven HST supernovae from this paper. In the upper panel of this latter figure, the stretch- and K-corrected effective m_B values and uncertainties are plotted. In the lower panel, effective m_B values have also been corrected for host-galaxy extinction based on measured $E(B\text{-}V)$ values. The solid line in this figure represents the best-fit flat-universe cosmology to the full primary subset with extinction corrections applied.

Table 8 lists results from fits to both of our primary subsets of supernovae. Supernovae from both the H96 and R99 low-redshift samples were included in all fits. The first three lines show fits to the low-extinction primary subset. So that the new sample of high-redshift supernovae may be compared to those from P99, each high-redshift sample was fit separately (Fits 1 and 2). Fit 3 combines all of the current SCP high-redshift supernovae from the low-extinction subsets, and represents the primary result on Ω_M and Ω_Λ for this paper; Figure 8 shows the confidence regions for Ω_M vs. Ω_Λ from this fit. Figure 9 shows the comparison of the confidence regions when each high-redshift sample is treated separately. Note that Fit 2 provides comparable and consistent measurements of Ω_M and Ω_Λ to Fit 1. Additionally, the sizes of the confidence regions from the 8 HST SNe in Fit 2 is similar to those in Fit 1, which includes 25 high-redshift supernovae from P99.

Fits 4–6 in Table 8 show the results for the primary subset when host-galaxy extinction corrections have been applied. Figure 10 compares these results to those of the primary low-extinction fit. The primary fits of Figure 9 are reproduced in the top row of Figure 10. The second row has host-galaxy extinction corrections applied using the one-sided prior used by Fit E of P99 and Riess *et al.* (1998) discussed in § 3. The third row has full extinction corrections applied without any prior assumptions on the intrinsic $E(B\text{-}V)$
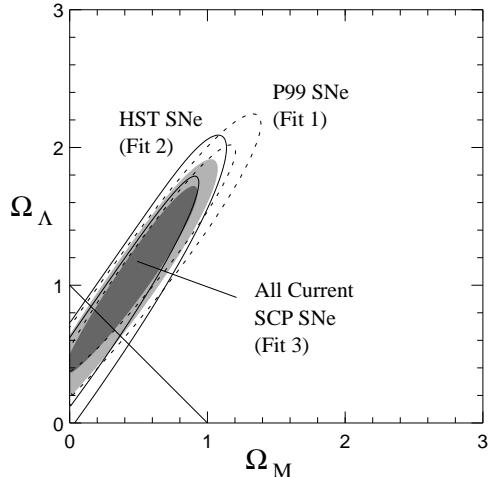

Fig. 9.— Contours indicate 68% and 90% confidence regions for fits to supernovae from the low-extinction primary subset, including just the high-redshift SNe from P99 (dotted lines), just the new HST high-redshift SNe (solid lines), and all SCP high-redshift SNe (filled contours). The low-redshift SNe from the primary subset are included in all fits. The new, independent sample of high-redshift supernovae provide measurements of Ω_M and Ω_Λ consistent with those from the P99 sample.

distribution. Three conclusions are apparent from this plot. First, using a strongly peaked prior on extinction prevents the $E(B\text{-}V)$ error bars from being fully propagated into the cosmological confidence regions, and hence apparently tightens the constraints. However, for a peaked prior, this is very similar to assuming no extinction and not performing an extinction correction (but without testing the assumption), while for a wider prior there is a danger of introducing bias. Second, the current set of supernovae provide much smaller confidence regions on the Ω_Λ versus Ω_M plane than do the SNe Ia from previous high-redshift samples when unbiased extinction corrections are applied. Whereas Figure 9 shows that the current set of supernovae give comparable measurements of Ω_M and Ω_Λ when the low-extinction subsample is used with no host-galaxy extinction corrections, Figure 10 shows that the much higher precision

Table 8: Cosmological fits

Fit #	High-Redshift SNe Included in Fit[a]	N_{SNe}	Min. χ^2	Ω_M for Flat[b]	Ω_Λ for Flat[b]	$P(\Omega_\Lambda > 0)$	$\mathcal{M}$	α
Fits to the Low-Extinction Primary Subset								
1	SNe from P99	46	52	$0.25^{+0.08}_{-0.07}$	$0.75^{+0.07}_{-0.07}$	0.9995	-3.49 ± 0.05	1.58 ± 0.31
2	New HST SNe from this paper	29	30	$0.25^{+0.09}_{-0.08}$	$0.75^{+0.08}_{-0.09}$	0.9947	-3.47 ± 0.05	1.06 ± 0.37
3	**All SCP SNe**	**54**	**60**	$\mathbf{0.25^{+0.07}_{-0.06}}$	$\mathbf{0.75^{+0.06}_{-0.07}}$	**0.9997**	$\mathbf{-3.48 \pm 0.05}$	$\mathbf{1.47 \pm 0.29}$
Fits to Full Primary Subset, with Extinction Correction								
4	SNe from P99	48	56	$0.21^{+0.18}_{-0.15}$	$0.79^{+0.15}_{-0.18}$	0.9967	-3.55 ± 0.05	1.30 ± 0.30
5	New HST SNe from this paper	33	39	$0.27^{+0.12}_{-0.10}$	$0.73^{+0.10}_{-0.12}$	0.9953	-3.54 ± 0.05	1.29 ± 0.28
6	All SCP SNe	58	65	$0.28^{+0.11}_{-0.10}$	$0.72^{+0.10}_{-0.11}$	0.9974	-3.53 ± 0.05	1.18 ± 0.30

a: All fits include the low-redshift SNe from H96 and R99. See § 2.5 for the definitions of the supernova subsets.
b: This is the intersection of the fit probability distribution with the line $\Omega_M + \Omega_\Lambda = 1$.

color measurements from the WFPC2 data allow us directly to set much better limits on the effects of host-galaxy extinction on the cosmological results. Finally, the cosmology which results from the extinction-corrected fits is consistent with the fits to our low-extinction primary subset. Contrary to the assertion of Rowan-Robinson (2002), even when host-galaxy extinction is directly and fully accounted for, dark energy is required with $P(\Omega_\Lambda > 0) > 0.99$.

4.2. Combined High-Redshift Supernova Measurements

Figure 11 shows measurements of Ω_M and Ω_Λ which combine the high-redshift supernova data of Riess *et al.* (1998) together with the SCP data presented in this paper and in P99. The contours show confidence intervals from the 54 supernovae of the low-extinction primary Subset 2 (used in Fit 3 of Table 8), plus the nine well-observed confirmed Type Ia supernovae from Riess *et al.* (1998) (using the lightcurve parameters resulting from their template-fitting analysis); following the criteria of Subset 2, SN 1997ck from that paper has been omitted, as that supernova

was not confirmed spectrally. We also omit from Riess *et al.* (1998) the supernovae they measured using the "snapshot" method (due to the very sparsely sampled lightcurve), and two SCP supernovae that Riess *et al.* (1998) used from the P99 data set which are redundant with our sample. This fit has a minimum χ^2 of 65 with 63 supernovae. Under the assumption of a flat universe, it yields a measurement of the mass density of $\Omega_M = 0.26^{+0.07}_{-0.06}$, or equivalently a cosmological constant of $\Omega_\Lambda = 0.74^{+0.06}_{-0.07}$. Recent ground-based data on eight new high-redshift supernovae from Tonry *et al.* (2003) (not included in this fit) are consistent with these results. Note that in this fit, the nine supernovae from Riess *et al.* (1998) were not treated in exactly the same manner as the others. The details of the template fitting will naturally have been different, which can introduce small differences (see § 5.1). More importantly, the K-corrections applied by Riess *et al.* (1998) to derive distance moduli were almost certainly different from those used in this paper.
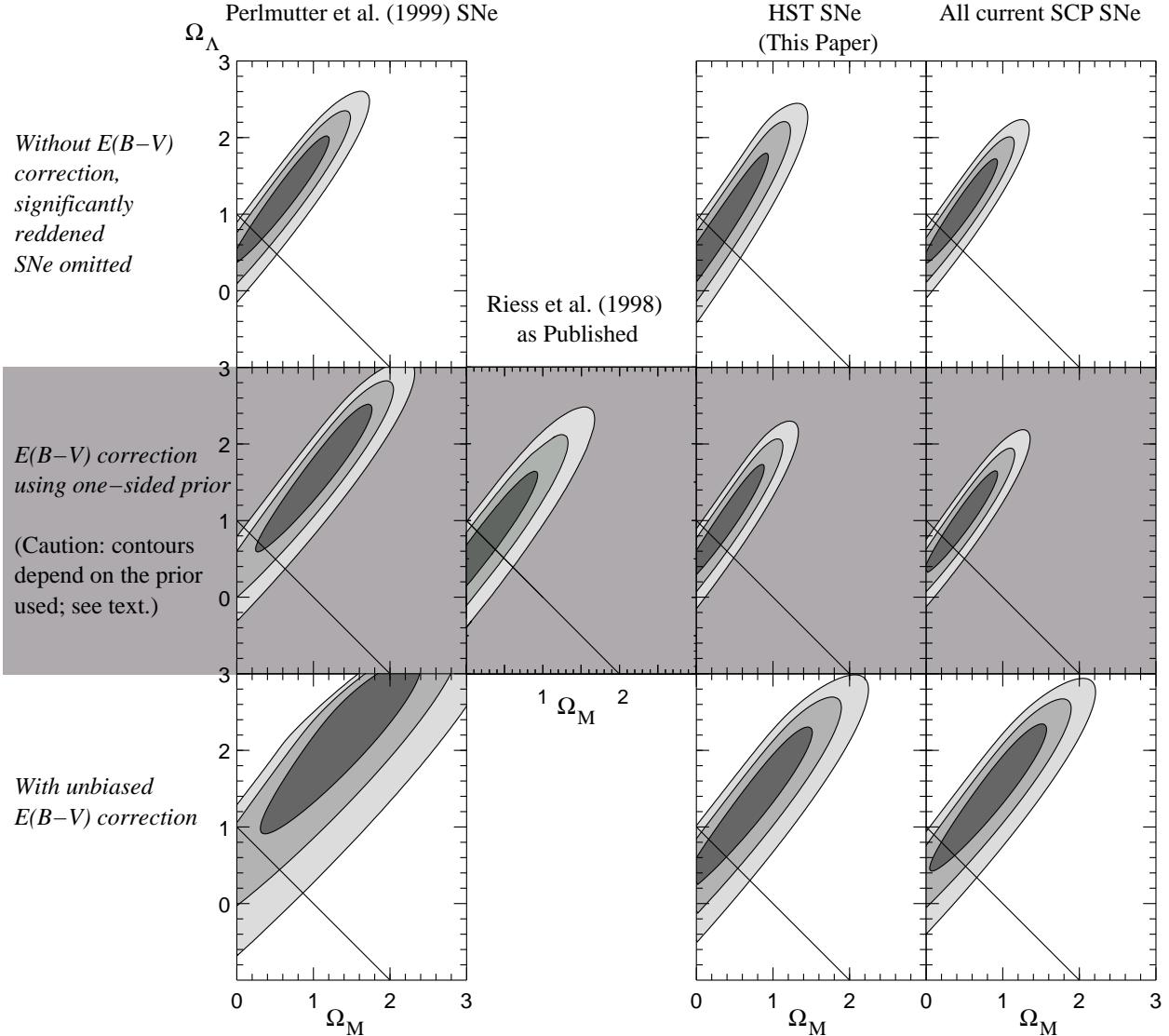
Fig. 10.— 68.3%, 95.4%, and 99.7% confidence regions for Ω_M and Ω_Λ using different data subsets and methods for treating host-galaxy extinction corrections. The top row represents our fits to the low-extinction primary subset, where significantly reddened supernovae have been omitted and host-galaxy extinction corrections are not applied. The second row shows fits where extinction corrections have been applied using a one-sided extinction prior. These fits are sensitive to the choice of prior, and can either yield results equivalent to analyses assuming low extinction (but without testing the assumption), or yield biased results (see text). Note that the published contours from Riess *et al.* (1998; their Fig. 6, solid contours) presented results from fits that included nine well-observed supernovae (that are comparable to the primary subsets used in the other panels), but also four supernovae with very sparsely sampled lightcurves, one supernova at $z = 0.97$ without a spectral confirmation, as well as two supernovae from the P99 set. The third row shows fits with unbiased extinction corrections applied to our primary subset. The HST SNe presented in this paper show a marked improvement in the precision of the color measurements, and hence in the precision of the Ω_M and Ω_Λ measurements when a full extinction correction is applied. With full and unbiased extinction corrections, dark energy is still required with $P(\Omega_\Lambda > 0) = 0.99$.

28
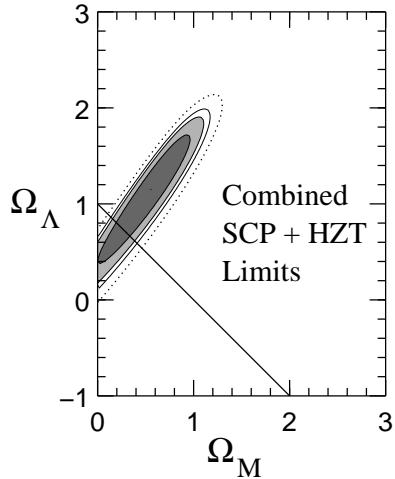
Fig. 11.— 68%, 90%, 95%, and 99% confidence regions for Ω_M and Ω_Λ, combining the high-redshift data of the SCP (this paper and P99) and Riess *et al.* (1998). The fit includes Subset 2 supernovae from the SCP plus the nine well-observed confirmed SNe Ia from Riess *et al.* (1998).

4.3. Dark Energy Equation of State

The fits of the previous section used a traditional constrained cosmology where Ω_M is the energy density of non-relativistic matter (i.e. pressure $p = 0$), and Ω_Λ is the energy density in a cosmological constant (i.e. pressure $p = -\rho$, where ρ is the energy density). In Einstein's field equations, the gravitational effect enters in terms of $\rho + 3p$. If $w \equiv p/\rho$ is the equation of state parameter, then for matter $w = 0$, while for vacuum energy (i.e. a cosmological constant) $w = -1$. In fact, it is possible to achieve an accelerating Universe so long as there is a component with $w <\sim -1/2$. (If there were no contribution from Ω_M, only $w < -1/3$ dark energy is necessary for acceleration; however, for plausible mass densities $\Omega_M \gtrsim 0.2$, the dark energy must have a more negative value of w.) The Hubble diagram for high-redshift supernovae provides a measurement of w (P99, Garnavich *et al.* 1998b). Panels (a) and (b) of Figure 12 show the joint confidence regions for Ω_M versus w from the SCP supernovae, including

the new HST supernovae, under the assumptions that w is constant with time, and that the Universe is flat, i.e. $\Omega_M + \Omega_X = 1$ (where Ω_X is the energy density in the component with equation of state w, in units of the critical density). The supernova alone data set a 99% confidence limit of $w < -0.64$ for any positive value of Ω_M, without any prior assumptions on w.

A fit with extinction corrections applied to the full primary subset (Fit 6, shown in Figure 12b) gives a 99% confidence limit of $w < -1.00$. However, this latter limit should be approached with caution, because w is not well bounded from below with the supernova data alone. Although Figure 12 only shows confidence intervals down to $w = -2$, the 68% confidence interval from Fit 3 extends to $w < -4$, and the 99% confidence interval extends to $w < -10$; these confidence intervals extend to even further negative w in Fit 6. The weight of probability at very low (and probably implausible) w pulls the 68% confidence interval in Fit 6 (Figure 12b) downward. A fit which used a prior to restrict w to more reasonable values (say $w > -2$) would show similar outer confidence intervals, but a 68% confidence interval more similar to that of the low-extinction subset in Figure 12a.

Other methods provide measurements of Ω_M and w which are complementary to the supernova results. Two of these measurements are plotted in the middle row of Figure 12, compared with the supernova measurements (in dotted contours). In filled contours are results from the redshift-distortion parameter and bias-factor measurement of the 2dF Galaxy Redshift Survey (2dFGRS) (Hawkins *et al.* 2002; Verde *et al.* 2002). These provide a measurement of the growth parameter, $f = 0.51 \pm 0.11$, at the survey redshift $z = 0.15$. We have used the method of Linder & Jenkins (2003) to directly solve for $f(\Omega_M, w, z)$ rather than convert f to Ω_M, as the conversion formula given in Hawkins *et al.* (2002) is valid only for $w = -1$. Comparison of the 2dFGRS value of f with the calculated values of $f(\Omega_M, w, z)$ yields the joint confidence region for Ω_M and w.[31]

In solid lines in panels (c) and (d) of Figure 12 are contours representing confidence re-

---

[31] Note that we have not used the independent 2dFGRS power spectrum constraint on $\Omega_M h$ because it has not yet been generalized for different values of w.
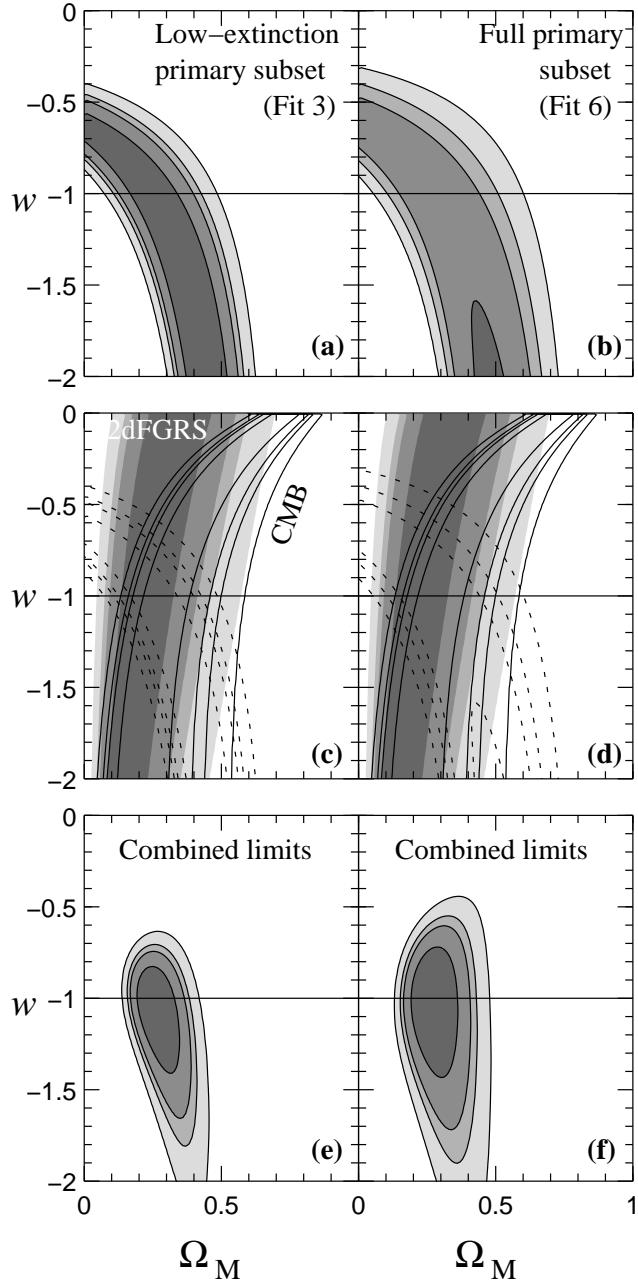
Fig. 12.— Joint measurements of Ω_M and w assuming $\Omega_M + \Omega_X = 1$ and that w is not time-varying. Confidence regions plotted are 68%, 90%, 95%, and 99%. The left column (panels a, c, and e) shows fits to the low-extinction primary subset; the right column (panels b, d, and f) shows fits to the primary subset with unbiased individual host-galaxy extinction corrections applied to each supernova. The upper panels (a and b) show the confidence intervals from the SCP supernovae alone. The middle panels (c and d) overlay this (dotted lines) with measurements from 2dFGRS (filled contours) (Hawkins *et al.* 2002) and combined CMB measurements (solid contours) (Bennett *et al.* 2003; Spergel *et al.* 2003). The bottom panels (e and f) combine the three confidence regions to provide a combined measurement of Ω_M and w.

gions based on the distance to the surface of last scattering at $z = 1089$ from the Wilkinson Microwave Anisotropy Probe (WMAP) and other CMB measurements (Bennett *et al.* 2003; Spergel *et al.* 2003). For a given Ω_M and w, this reduced distance to the surface of last scattering, I, is given by:

$$I = \int_0^{1089} [((1-\Omega_M)/\Omega_M)(1+z)^{3(1+w)}+(1+z)^3]^{-1/2} \, dz \tag{4}$$

The plotted CMB constraints come from the "WMAPext" sample, which includes other CMB experiments in addition to WMAP. They yield a measurement of $I_0 = 1.76 \pm 0.058$, corresponding to $\Omega_M = 0.29$ at $w = -1$. Confidence intervals are generated by calculating a probability using $\chi^2 = [(I - I_0)/\sigma_{I_0}]^2$, where I is calculated for each Ω_M, w.

As both of these measurements show mild correlations between Ω_M and w in a different sense from that of the supernova measurement, the combined measurements provide much tighter overall constraints on both parameters. The confidence regions which combine these three measurements are shown in panels (e) and (f) of Figure 12. When the resulting probability distribution is marginalized over Ω_M, we obtain a measurement of $w = -1.05^{+0.15}_{-0.20}$ (for the low-extinction subset), or $w = -1.02^{+0.19}_{-0.24}$ (for the full primary subset with host-galaxy extinction corrections applied). When the probability distribution is marginalized over w, we obtain a flat-universe measurement of $\Omega_M = 0.27^{+0.06}_{-0.05}$ (for the low-extinction subset), or $\Omega_M = 0.28^{+0.06}_{-0.05}$ (for the primary subset with host-galaxy extinction corrections applied). The 95% confidence limits on w when our data are combined with CMB and 2dFGRS are $-1.61 < w < -0.78$ for the low-extinction primary subset, or $-1.67 < w < -0.62$ for the full extinction-corrected primary subset. If we add an additional prior that $w \geq -1$, we obtain a 95% upper confidence limit of $w < -0.78$ for the low-extinction primary subset, or $w < -0.67$ for the extinction-corrected full primary subset. These values may be compared with the limit in Spergel *et al.* (2003) which combines the CMB, 2dFGRS power spectrum, and HST key project H_0 measurements to yield a 95% upper limit of $w < -0.78$ assuming $w \geq -1$. Although both our

measurement and that of Spergel *et al.* (2003) include CMB data, they are complementary in that our limit does not include the H_0 prior, nor does it include any of the same external constraints, such as those from large scale structure.

These combined measurements remain consistent with a low density universe dominated by vacuum energy (constant $w = -1$), but are also consistent with a wide range of other both time-varying-w and constant-w dark energy models.

5. Systematic Errors

The effect of most systematic errors in the Ω_M vs. Ω_Λ plane is asymmetric in a manner similar to the asymmetry of our statistical errors. For the effects listed below, a systematic difference will tend to move the confidence ellipses primarily along their major axis. In other words, these systematic effects produce a larger uncertainty in $\Omega_M + \Omega_\Lambda$ than in $\Omega_M - \Omega_\Lambda$ (or, equivalently, in a measurement of Ω_M or Ω_Λ alone under the assumption of a flat universe). This means that systematic effects do not currently hamper the cosmological measurements from supernovae where they have the greatest weight relative to other techniques, nor do they significantly diminish the direct evidence from supernovae for the presence of dark energy. However, they do limit the ability of supernovae to measure the spatial curvature ("geometry") of the Universe. (Note that the semi-major axis is not precisely in the direction of $\Omega_M + \Omega_\Lambda$, nor is the semi-minor axis precisely aligned with $\Omega_M - \Omega_\Lambda$, but since these are useful constraints we will quantify the systematic uncertainties along these two directions.) Figure 13 shows the effects of some of the systematics discussed in the following subsections.

Systematic effects on flat-universe measurements of w are smaller than the current statistical uncertainties. The right column of Figure 13 shows the effect of the systematics on the Ω_M versus w confidence regions derived from our supernova data alone. To quantify the effect of identified systematics in the following subsections, we determine the shift in the maximum-likelihood value of w when the supernova data is combined with the Ω_M versus w confidence regions from 2dF-GRS and the CMB (See § 4.3.)

(a) Type Contamination

(b) Malmquist Bias

(c) Intrinsic U–B: K–corrections

Systematics: Fits 4–6

(d) Intrinsic U–B: Extinction Corrections

(e) Changing R_B
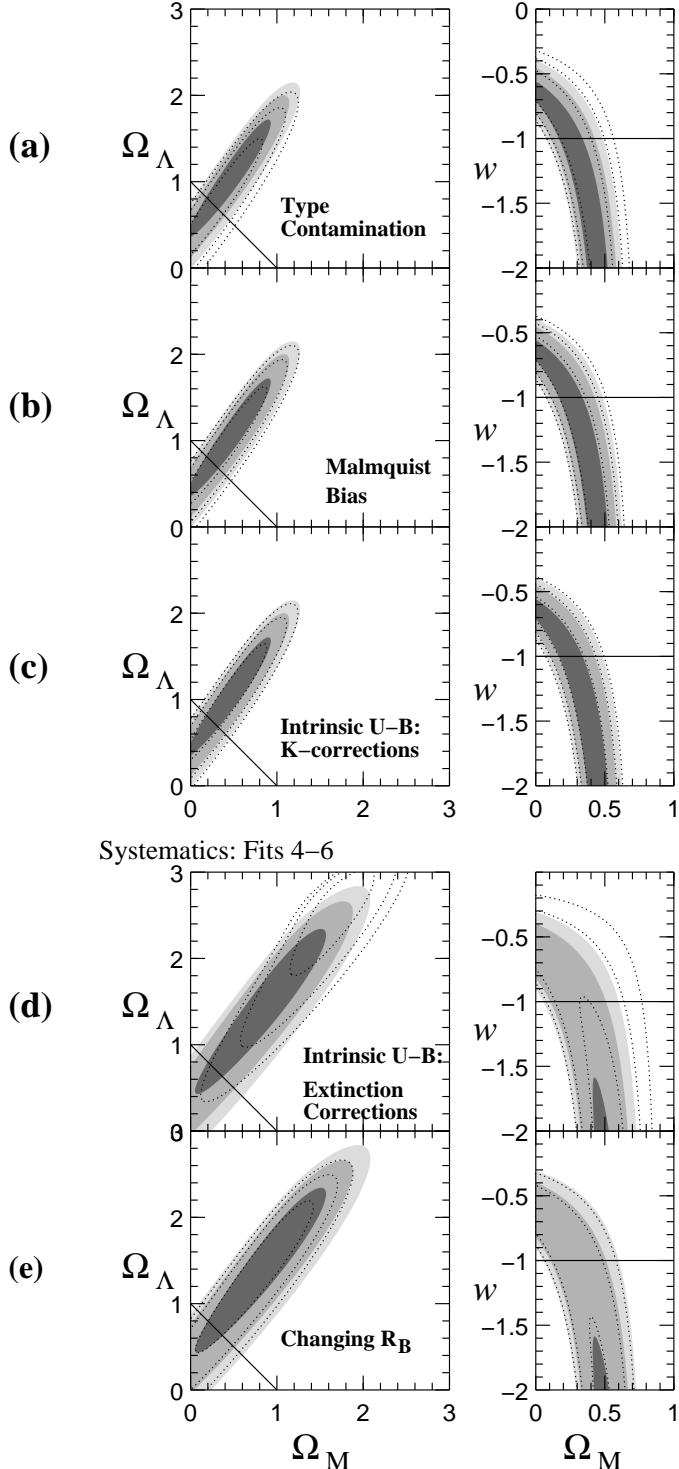
Fig. 13.— Simulated effects of identified systematic errors on the cosmological parameters, estimated by applying the systematic effect to the supernova parameters used in the cosmological fits. The left column shows fits to Ω_M and Ω_Λ, and the right column to Ω_M and the dark energy equation of state parameter w. Rows (a)–(c) show our primary fit (Fit 3) in filled contours. (a) The dotted contours show the results of a fit to Subset 3, only those supernovae with the most secure spectral identifications as Type Ia SNe. (b) The dotted contours show a fit to Subset 1 where the supernova magnitudes have been dimmed to correct for Malmquist bias. (c) The dotted contours show a fit to Subset 2, where K-corrections have been applied using a template spectrum with an intrinsic value of U-$B=-0.5$ at the epoch of B-maximum. (d) The filled contours is Fit 6, the fit to the full primary subset with host-galaxy extinction corrections applied; the dotted contours show a fit to the same Subset, but using a template spectrum with an intrinsic value of U-$B=-0.5$ for estimating both K-corrections and color excesses. (e) The dotted contours apply extinction corrections to Subset 1 using a value of $R_B = 3.5$ rather than the standard $R_B = 4.1$ which was used for Fit 6 (filled contours).

5.1. Fit Method, Subset Selection, and Choice of α

There are multiple reasonable choices for lightcurve fitting methods which yield slightly different results for the lightcurve parameters. For the supernovae in P99, the R-band data on high-redshift supernovae provided much stronger limits on the stretch (the shape of the lightcurve) than did more sparse I-band lightcurves. For consistency, in P99 the stretch values for the low-redshift supernovae were therefore measured using only the B-band lightcurves.

In this paper, there are high-quality photometric measurements from WFPC2 in both R and I bands. Thus, data in both colors contribute significantly to the constraints on stretch. Additionally, photometry is extracted from HST and ground-based images in very different apertures, meaning that different amounts of host galaxy light will be included; this background must be subtracted from each before the two are combined. As such, it is more appropriate to fit these supernovae with fixed rather than floating lightcurve zero offsets. As this is the most appropriate fit method for the HST supernovae, the low-redshift supernovae should be treated consistently. These procedures which are most appropriate for the HST supernovae were used for all new fits performed in this paper, and listed in Tables 3 through 5.

To estimate the size of the effect due to these differences in fitting method, cosmological confidence intervals were generated from the "Case C" subset of P99 using the new fits presented in this paper and compared to the results quoted in P99 and other variations on the fitting method. Differences in the fit method can change the flat-universe value of Ω_{M} by ~0.03, and the value of $\Omega_{\mathrm{M}} + \Omega_{\Lambda}$ by up to ~0.8. (This is still much less than the major-axis extent of the statistical confidence ellipse in this direction.) We use these values as the "fit-method" systematic uncertainties. We similarly performed joint fits to Ω_{M}, w in the flat-universe, constant-w case to the supernovae from P99 with different lightcurve fit methodologies, and from these fits we adopt a fit-method systematic uncertainty of 0.02 on constant w (once combined with measurements from 2dFGRS and the CMB).

We have also performed a fit without any stretch correction at all, i.e. using fixed $\alpha = 0$. Although the quality of the fit is worse ($\chi^2 = 82$ with 54 supernovae, in comparison to $\chi^2 = 60$ from Fit 3), it yields consistent cosmological results, with shifts ($\Delta\Omega_{\mathrm{M}}^{\mathrm{flat}} < 0.01$) much smaller than the already-adopted "fit method" systematic. We have likewise performed a fit to the complete set of supernovae (including all from P99 with measured colors). The fit cosmological values are similarly consistent with the primary low-extinction fit. We therefore conclude that the effects of these choices are subsumed in the "fit method" systematic.

5.2. Non-Type Ia Supernova Contamination

All subsets of supernovae used for cosmological fits in this paper omit supernovae for which there is not a spectral confirmation of the supernova type. Nonetheless, it is possible in some cases where that confirmation is weak that we may have contamination from non-Type Ia supernovae. To estimate such an effect, we performed fits using only those supernovae which have a firm identification as Type Ia; this is the "strict-Ia subset" from § 2.5. The comparison between our primary fit (Fit 3) and this fit with a more stringent type cut is shown in row (a) of Figure 13. This fit has a value of Ω_{M} in a flat universe which is 0.03 higher than that of Fit 3. The value of $\Omega_{\mathrm{M}} + \Omega_{\Lambda}$ is 0.48 lower than that of Fit 3. We adopt these values as our "type contamination" systematic error.

The size of this systematic for w is shown in the right panel of Figure 13a. Combined with CMB and 2dFGRS measurements, the best-fit value of w is larger by 0.07; we adopt this as our type contamination systematic error on w.

5.3. Malmquist Bias

As most of our supernovae are from flux-limited samples, they will suffer Malmquist bias (Malmquist 1924, 1936). This effect was discussed extensively in P99, and here we update that discussion to include our new HST SNe Ia. For the measurement of the cosmological parameters, it is the difference between the Malmquist bias of the low-redshift and high-redshift samples which matters. In particular, the apparent probability of $\Omega_{\Lambda} > 0$ is enhanced only if the low-redshift supernovae suffer more Malmquist bias than the

high-redshift supernovae, as this makes the high-redshift SNe Ia seem fainter.

The P99 high-redshift dataset was estimated to have little Malmquist bias (0.01 mag) because the SN discovery magnitudes were decorrelated with the measured peak magnitudes. However, for the new HST sample, nine of the eleven SNe Ia (selected from larger samples of supernovae found in the searches) were found almost exactly at maximum light. This may reflect a spectroscopic flux limit superimposed on the original search flux limit since only spectroscopically confirmed SNe Ia were considered, and of those, generally the higher redshift SNe Ia from a given search were chosen for HST for follow-up. In particular, the SNe Ia selected for follow-up from the fall 1997 search were all found at maximum light, while all but SN 1998aw from the spring 1998 search were found at maximum light. SN 2000fr was found well before maximum. Thus, the new high-redshift dataset is likely to suffer more Malmquist bias than the P99 dataset. Further complicating the interpretation for the high-redshift supernovae is the fact that our new HST supernovae are spread over a wide range in redshift, such that a single brightness correction for Malmquist bias causes a more complicated change in the fitted cosmological parameters. This is unlike the situation in P99 in which most supernovae were at $z \sim 0.5$. Following the calculation in P99 for a high-redshift flux-limited SN sample we estimate that the maximum Malmquist bias for the ensemble of HST supernovae is ~ 0.03 mag. However, we caution that it is supernovae near the flux limit which are most strongly biased, and therefore, that a subsample comprised of the highest-redshift members drawn from a larger flux-limited sample will be more biased. When combined with the P99 high-redshift supernovae, the bias is likely to be ~ 0.02 mag since both samples have roughly the same statistical weight.

As for the low-redshift SNe Ia, in P99 we established that since most of the SNe Ia from the H96 flux-limited search were found near maximum, that sample suffered about 0.04 mag of Malmquist bias. On the other hand, some of the R99 SNe Ia were discovered using a galaxy-targeted technique, which therefore is not limited by the SN flux and may be more akin to a volume-limited sample (Li, Filippenko, & Riess 2001). Thus, the addition of the R99 SNe Ia could slightly reduce the overall Malmquist bias of the low-redshift sample. If we were to assume no Malmquist bias for the R99 SNe Ia, and allowing for the fact that they contribute only $\sim 1/4$ the statistical weight of the H96 supernovae, we estimate that the Malmquist bias in the current low-redshift sample is roughly 0.03 mag.

Since Malmquist bias results in the selection of overly-bright supernovae at the limits of a flux-limited survey, and since the flux-limit can be strongly correlated with redshift[32], this bias can result in an apparent distortion of the shape of the Hubble diagram. This may affect estimates of the dark energy equation of state. The selection effects for the current high-redshift supernovae are not sufficiently well-defined to warrant a more detailed modeling of this effect than is presented here. However, for future work, much better control of the selection criteria for SNe Ia at both low- and high-redshift will be required in order to properly estimate the impact of this small bias.

For the current study, however, we simply note that since the *differences* in the Malmquist biases of the high- and low-redshift subsets of SN are likely to be *smaller* in this work than in P99, the current results are less likely to be affected by Malmquist bias. Given the above estimates of 0.03 mag of bias in the low-redshift sample, and 0.02 mag of bias in the high-redshift sample, the *difference* in the biases is only 0.01 mag. To perform a quantitative estimate of the effects of Malmquist bias, we have performed a fit by applying the mean offsets described above to each member of a sample in our primary subset. This fit is plotted in Figure 13b. The H96 supernovae have their magnitudes increased (made dimmer) by 0.04, the P99 supernovae by 0.01, and six of the eight HST supernovae in our primary subset have their magnitudes increased by 0.04. The two HST supernovae (SNe 1998bi, and 2000fr) which were found before maximum light are assumed not to be biased, and the other nine are offset by 0.04, yielding the above estimated 0.03 magnitudes for the sample. A fit with these changed values to the supernova peak magnitudes yields a flat-universe value which is different from our pri-

---

[32] They are 100% correlated for a single field, but this correlation can be diluted by combining fields of different depths.

mary fit by $\Omega_M = 0.01$, and a value of $\Omega_M + \Omega_\Lambda$ which is different by 0.18. The best-fit value of w, when combined with the other cosmological measurements, is 0.03 larger. We adopt these values— all much less than our statistical uncertainties—as our Malmquist bias systematic error.

5.4. K-corrections and Supernova Colors

The generation of the spectral template used for calculating K-corrections is described in § 2.3. The degree to which uncertainties in the K-correction introduce systematic uncertainties into the cosmological parameters depends on whether or not extinction corrections are being individually applied to supernovae. In particular, our K-corrections are most uncertain in the rest-frame U-band range of the supernova spectrum, due to limited published spectrophotometry. As discussed in § 2.2, our primary fits use a spectral template which has a color U-B=-0.4 at the epoch of B-maximum. We have investigated the effects on our cosmology of replacing the spectral template used both for K-corrections and for determining color excesses with a template that has U-B=-0.5 at the epoch of maximum B light.

Figure 13c shows the effect on the fitted cosmology caused by using the different template for calculating K-corrections when individual host-galaxy extinction corrections are not applied. These effects are very mild, indicating that our K-corrections are robust with respect to the intrinsic U-B color of a supernova. Based on the comparison of these fits, we adopt a K-correction systematic uncertainty of 0.13 on $\Omega_M + \Omega_\Lambda$ and of 0.01 in w; the systematic uncertainty on the flat-universe value of Ω_M due to this effect is negligible.

Although the effects of a different intrinsic U-B color on the K-corrections are mild, the effects on calculated color excesses are much greater. Figure 13d shows the difference between Fit 6, where host-galaxy extinction corrections have been applied using our standard color-excess values, and a fit where color-excess values have been determined assuming the intrinsic U-B color of a supernova is -0.5 at maximum light. As with other systematics, the primary effect is to move the confidence intervals along their major axis. In this case, the large shift in $\Omega_M + \Omega_\Lambda$ is mainly due to the fact that with this bluer reference U-B color, we would believe that all of our $z > 0.7$ supernovae are suf-

fering from an amount of host-galaxy extinction which is greater than that suffered by supernovae at lower redshift. Given that the more distant supernovae are dimmer and thus closer to our detection limits than the moderate redshift supernovae, this scenario is implausible. If anything, one would expect the higher redshift supernovae to be *less* subject to host-galaxy extinction due to selection effects. Nonetheless, a value of U-B=-0.5 at the epoch of B-band maximum is currently possible given the U-band information available. Only for those fits where extinction corrections are applied, we have an additional intrinsic U-B systematic error of 0.07 on the flat-universe value of Ω_M, and a systematic error of 1.78 on $\Omega_M + \Omega_\Lambda$. The systematic uncertainty on w is 0.10. It is likely that these values represent an overestimate of this systematic.

5.5. Dust Properties

As discussed in § 3, Phillips *et al.* (1999) found that some of the reddest supernovae at low redshift appear to be overcorrected for extinction given the standard reddening law. As shown in the lower panel of Figure 7, our most reddened high-redshift supernova (SN 1998as, which is omitted from the primary subset) is similarly overcorrected. One possible explanation is that a lower value of R_B is appropriate for SN Ia host galaxies. If we use a value of $R_B = 3.5$ (Phillips *et al.* 1999) rather than the standard value of $R_B = 4.1$ to perform extinction corrections, it slightly changes the best-fit cosmological values for fits where extinction correction are applied (Fit 6); this change is shown in Figure 13e. The best-fit value of $\Omega_M + \Omega_\Lambda$ changes by 0.18, and the best-fit value of w when combined with the other cosmological measurements changes by 0.01; this systematic has a negligible effect on the flat-universe value of Ω_M.

A related source of systematic error is possible evolution in the properties of the host-galaxy dust. To examine the scale of the effect, we consider a situation where dust in $z < 0.3$ spiral galaxies has a Cardelli, Clayton, & Mathas (1989) $R_V = 3.1$ law whereas higher-redshift galaxy dust has a ratio of selective-to-total extinction that is half as large, i.e. $R_V = 1.6$. We use the Monte Carlo code described in Kim *et al.* (2003) to study the bias induced when an $R_V = 3.1$ extinction correction is inappropriately applied to all supernovae.

We incorporate the redshift and $E(B\text{-}V)$ distributions of the supernovae considered in this paper and an $E(B\text{-}V) < 0.1$ cut is applied. For an input cosmology of $\Omega_M = 0.21$ and $\Omega_\Lambda = 0.79$, we find a modest shift in the cosmological parameters to $\Omega_M = 0.25$ and $\Omega_\Lambda = 0.77$ without assuming a flat universe.

This bias moves almost exactly along the line $\Omega_M + \Omega_\Lambda = 1$, increasing uncertainty along the thin axis of the error contour. However, the extreme difference in dust properties considered in the Monte Carlo contributes a shift in the cosmological parameters that is less than 1 σ of our quoted statistical error bars. We adopt 0.04 as the "dust evolution" systematic uncertainty on Ω_M in a flat universe for those fits where host-galaxy extinction corrections are applied; this particular systematic is insignificant along the major axis of the confidence ellipses.

The flat-universe value of w, when combined with the 2dFGRS and CMB results, increases by 0.06 under this simple model of dust evolution. We adopt this as the dust evolution systematic on w for those fits where host-galaxy extinction corrections are applied.

5.6. Gravitational Lensing

Gravitational lensing decreases the modal brightness and causes increased dispersion and positive skewness in the Hubble diagram for high-redshift supernovae. The size of the effect depends on the fraction of compact objects of the total mass density of the universe, Ω_M. This has been discussed in some detail in the literature (Wambsganss *et al.* 1997; Frieman 1997; Holz 1998; Kantowski 1998; Seljak & Holz 1999; Metcalf & Silk 1999; Metcalf 1999; Holz 2001; Wang, Holz, & Munshi 2002; Minty, Heavens, & Hawkins 2002; Amanullah, Mörtsell & Goobar 2003; Dalal *et al.* 2003; Oguri, Suto, & Turner 2003), especially in relation to the P99 and Riess *et al.* (1998) SN datasets. A very conservative assumption of an "empty beam" model in a universe filled with compact objects allowed P99 to demonstrate that gravitational lensing does not alter the case for dark energy.

Gravitational lensing may result in a biased determination of the cosmological parameter determination, as discussed in Amanullah, Mörtsell &

Goobar (2003). The potential bias increases with the redshift of the supernovae in the sample. For example, for the most distant known Type Ia SN, SN1997ff at z=1.7, there is evidence for significant magnification, $\Delta m \sim -0.3$ (Lewis & Ibata 2001; Mörtsell, Gunnarsson & Goobar 2001; Benitez *et al.* 2002).

As the SN sample considered in this paper does not reach as far, the (de)magnification distortions are expected to be small, in general below 0.05 magnitudes, and less than 1% for the cases considered in P99. To estimate the systematic uncertainties in the cosmological parameters we have used the SNOC package (Goobar *et al.* 2001) to simulate 100 realizations of our data sets assuming a 20% universal fraction of Ω_M in compact objects, i.e. of the same order as the halo fraction deduced for the Milky Way from microlensing along the line of sight to the Large Magellanic Cloud (Alcock *et al.* 2000). The light beams are otherwise assumed to travel through space randomly filled with galaxy halos with mass density equally divided into SIS and NFW profiles, as described in Bergström *et al.* (2000). According to our simulations we find that (for a flat universe) the fitted value of Ω_M is systematically shifted by 0.01 on the average, with a statistical dispersion $\sigma_{\Delta\Omega_M} = 0.01$. We adopt 0.01 as our gravitational lensing systematic error in the flat-universe value of Ω_M. The effect on $\Omega_M + \Omega_\Lambda$ is very small compared to other systematics, biasing the sum by only 0.04.

The simulated offsets due to gravitational lensing, when combined with CMB and galaxy redshift distortion measurements, increase the value of w by 0.05; we adopt this as a gravitational lensing systematic on w.

5.7. Supernova Population Drift

In P99 we discussed in detail whether the high-redshift SNe Ia could have systematically different properties than low-redshift SNe Ia, and in particular, whether intrinsic differences might remain after correction for stretch. One might imagine this to occur if the range of the physical parameters controlling SN Ia brightnesses have little overlap between low- and high-redshift such that corrections applied to low-redshift are inappropriate or incomplete for high-redshift SNe Ia. Since P99, considerable additional work has been done to ad-

dress this issue.

In addition to comparisons of stretch range (P99), as well as spectral (Perlmutter *et al.* 1998; Coil *et al.* 2000) and lightcurve (Goldhaber *et al.* 2001) features, several tests performed directly with the P99 high-redshift SNe Ia have shown excellent consistency with low-redshift SNe Ia. Most recently, in Sullivan *et al.* (2003) we have presented results on the Hubble diagram of distant Type Ia supernovae from P99 that have been morphologically-typed with HST. We found no difference in the cosmological results from their morphologically-segregated subsamples. In particular, E/S0 galaxies—for which one expects the tightest possible correlation between progenitor mass and redshift—not only agree with the cosmological fits using only spiral galaxies, but by themselves confirm the results of P99. This is strong evidence that, while age or metallicity could in principle affect the brightnesses of SNe Ia, stretch correction eliminates these differences. Likewise, the lightcurve rise-time—a possible indicator of the energetics of the SN explosion (see Nugent *et al.* 1995; Hoeflich, Wheeler, & Thielemann 1998)— while initially suggested to be different between high- and low-redshift SNe Ia (Riess *et al.* 1999b), has been demonstrated to agree very well (within 1.8 ± 1.2 days, Aldering, Knop, & Nugent 2000).

On the theoretical side, the SN formation models of Kobayashi *et al.* (1998) and Nomoto, Nakamura, & Kobayashi (1999) suggest that the progenitor binary system must have [Fe/H]> -1 in order to produce a SN Ia. This would impose a lower limit to the metallicities of all SNe Ia, and thus limit the extent of any metallicity-induced brightness differences between high- and low-redshift SNe Ia. On the empirical side, the lack of a gradient in the intrinsic luminosities of SNe Ia with galactocentric distance, coupled with the fact that metallicity gradients are common in spiral galaxies (Henry & Worthey 1999), lead Ivanov, Hamuy, & Pinto (2000) to suggest that metallicity is not a key parameter in controlling SNe Ia brightnesses at optical wavelengths— though note that Lentz *et al.* (2000) show how it can affect the ultraviolet. In addition, Hamuy *et al.* (2000, 2001) find that lightcurve width is not dependent on host-galaxy metallicity.

Alternatively, population age effects, including pre-explosion cooling undergone by the progenitor

white dwarf and other effects linked to the mass of the primary exploding white dwarf have been suggested (for a review, see Ruiz-Lapuente 2003). As the local sample of SNe Ia represents populations of all ages and metallicities, both effects can be studied locally. Several low-redshift studies have presented data suggesting that SNe Ia intrinsic luminosities (i.e., those prior to stretch correction) may correlate with host-galaxy environment (Hamuy *et al.* 1996b; Branch, Romanishin, & Baron 1996; Wang, Hoeflich, & Wheeler 1997; Hamuy *et al.* 2000; Ivanov, Hamuy, & Pinto 2000; Howell 2001; Wang *et al.* 2003; R99). These findings are actually encouraging, since unlike stretch itself, there is some hope that host-galaxy environment variations can be translated into physical parameters such as age and metallicity. These parameters can help relate any drifts in the SNe Ia population to evolution of the host galaxies.

More importantly for cosmology, R99 used their sample of 22 local SNe Ia to demonstrate that any brightness variations between SNe Ia in different host-galaxy environments disappear after correction for lightcurve width. We have quantified this agreement using a larger local sample of supernovae compiled in Wang *et al.* (2003), 14 of which have E/S0 hosts and 27 of which have spiral hosts. We find that after lightcurve-width correction there can be less than a 0.01 ± 0.05 mag offset between SNe Ia in local spirals and ellipticals. This indicates that lightcurve width is able to correct for age or other differences.

Finally, Wang *et al.* (2003) demonstrate a new method, *CMAGIC*, which is able to standardize the vast majority of local SNe Ia to within 0.08 mag (in contrast to $\sim$ 0.11 mag which lightcurve-width corrections can attain (Phillips *et al.* 1999)). This imposes even more severe limits on the fraction of SNe Ia generated by any alternate progenitor scenario, or requires that variations in the progenitor properties have little effect on whether the resulting SN can be standardized.

The data from the new SNe Ia presented here do offer one new test for consistency between low- and high-redshift SNe Ia. The quality of our HST data provides measurements of the SN peak magnitudes and lightcurve widths rivaling those for nearby SNe Ia. This allows a direct comparison between the stretch-luminosity relations at low- and high-redshifts. Figure 14 shows that the HST high-
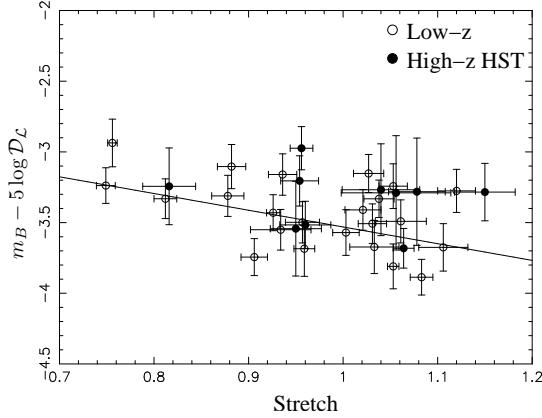
Fig. 14.— Stretch-luminosity relationship for low-redshift SNe (open circles) and high-redshift HST SNe (filled circles). Each point is the K-corrected and extinction-corrected m_B for that supernova, minus $\mathcal{D}_\mathcal{L}$, the "Hubble-constant-free luminosity distance" (see § 2.4), plotted against the stretch of that SN. The line drawn represents the best-fit values of α and $\mathcal{M}$ from Fit 6, the fit to all Subset 1 supernovae with host-galaxy extinction corrections applied. Note in particular that our HST SNe Ia all have low-redshift counterparts.

redshift supernovae are found at similar stretches and luminosities as the low-redshift supernovae. The low- and high-redshift samples are consistent with the same stretch-luminosity relationship, although it is primarily the low-redshift supernovae that require a non-zero slope for this relationship.

5.8. Possible Additional Sources of Systematic Uncertainties

Other potential sources of systematic uncertainties have been suggested. Aguirre (1999a,b) and Aguirre & Zoltan (2000) argued that the presence of "grey" dust, i.e. a homogeneous intergalactic component with weak differential extinction properties over the rest-frame optical wavelength regime could not be ruled out by the P99 data. Since then, measurements of a SN Ia at $z \simeq 1.7$ (Riess et $al.$ 2001) were claimed to rule out the "grey" dust scenario as a non-cosmological alternative explanation to the dimming of high-redshift supernovae; however, there remain some outstanding issues with this interpretation (e.g.,

Goobar, Bergström, & Mörtsell 2002; Blakeslee et $al.$ 2003). A direct test for extinction over a wide wavelength range, rest-frame B-I, have been performed by Riess et $al.$ (2000) on a single supernova at $z = 0.46$, SN 1999Q, which showed no grey dust signature; however, see Nobili et $al.$ (2003). Although the situation remains inconclusive, there is no direct evidence that "grey" dust is a dominant source of uncertainties. It remains an important issue to be addressed by future data sets including near-infrared observations.

More recently, the possibility of axion-photon oscillations making high-redshift supernovae appear dimmer was suggested by Csaki, Kaloper, & Terning (2002). This attenuation would be wavelength dependent, and thus could be explored with spectroscopic studies of high-shift sources (Mörtsell, Bergstrom, & Goobar 2002). Preliminary studies of QSO spectra between $z = 0.15$ and $z = 5.3$ set a very conservative upper limit on the possible dimming of z∼0.8 supernovae to 0.2 magnitudes (Mörtsell & Goobar 2003)

For the current data sample, the above mentioned sources of systematic uncertainties are difficult to quantify at present, but are believed to be subdominant in the total error budget.

5.9. Total Identified Systematic Uncertainty

The identified systematic errors are summarized in Table 9. Adding together these errors in quadrature, we obtain a total systematic error of 0.04 on the flat-universe value of Ω_M (along approximately the minor axis of the confidence ellipses shown in Ω_M vs. Ω_Λ plots); this is smaller than but approaching our statistical uncertainty of 0.06. The total systematic uncertainty on $\Omega_M + \Omega_\Lambda$ is 0.96 (along approximately the major axis of the confidence ellipses). Finally, for the low-extinction subset, we have a systematic uncertainty on constant w of 0.09, less than our high-side statistical uncertainty of 0.15.

For fits with host-galaxy extinction corrections applied, we have to consider the additional systematic effects of an uncertainty in the intrinsic value of U-B on determined color excesses, and of dust properties. In this case, we have a total systematic error of 0.09 on the flat-universe value of Ω_M or Ω_Λ, and a total systematic error of 2.0 on

Table 9: Identified Systematic Uncertainties

Source of	Systematic Uncertainty On:			Notes
Uncertainty	Flat-Universe			
	Ω_{M}or $\Omega_{\Lambda}{}^{a}$	$\Omega_{\mathrm{M}} + \Omega_{\Lambda}$	constant w^{b}	
Fit method	0.03 (0.5σ)	0.80	0.02	
Type contamination	0.03 (0.5σ)	0.48	0.07	
Malmquist Bias	0.01 (0.2σ)	0.18	0.03	
Intrinsic U-B: K-corrections	0.00 (0.0σ)	0.13	0.01	c
Gravitational Lensing	0.01 (0.2σ)	0.04	0.05	
Systematic with host-galaxy extinction corrections:				
Intrinsic U-B: color excess	0.07 (0.7σ)	1.78	0.10	d
Extinction Slope	0.00 (0.0σ)	0.18	0.01	d
Dust Evolution	0.03 (0.3σ)	0.02	0.06	d

a: Each systematic is given as an offset from the flat-universe value of Ω_{M}, and in terms of the smaller side of the statistical error bar (0.06 for Fit 3 to the low-extinction subset, 0.10 for Fit 6 to the full primary subset).
b: This is the offset on the maximum-likelihood value of w when the the fit is combined with the 2dFGRS and CMB measurements.
c: Only used where host-galaxy extinction corrections are not applied.
d: Only used where host-galaxy extinction corrections are applied.

$\Omega_{\mathrm{M}} + \Omega_{\Lambda}$; as discussed in § 5.4, this is likely to be an overestimate of the true systematic error. The total systematic uncertainty on constant w for the extinction-corrected full primary sample is 0.15.

6. Summary and Conclusions

1. We present a new, independent set of eleven high-redshift supernovae ($z = 0.36$–0.86). These supernovae have very high-quality photometry measured with WFPC2 on the HST. The higher quality lightcurve measurements have small enough errors on each $E(B\text{-}V)$ measurement to allow an unbiased correction of host-galaxy reddening. We have performed improved color and K-corrections, necessary to combine WFPC2 photometric filters with ground-based photometric filters.

2. The cosmological fits to Ω_{M} and Ω_{Λ} are consistent with the SCP's previous results (P99), providing strong evidence for a cosmological constant. This is a significant confirmation of the results of P99 and Riess *et al.* (1998), and represents a completely new set of high-redshift supernovae yielding the same results as the earlier supernova work.

Moreover, these results are consistent with a number of other cosmological measurements, and together with other current cosmological observations is pointing towards a consensus $\Omega_{\mathrm{M}} \sim 0.3$, $\Omega_{\Lambda} \sim 0.7$ Universe.

3. Most identified systematic errors on Ω_{M} and Ω_{Λ} affect the cosmological results primarily by moving them along the direction where the statistical uncertainty is largest, that is, along the major axis of the confidence ellipses. Systematics are much smaller along the minor (approximately $\Omega_{\mathrm{M}} - \Omega_{\Lambda}$) axis of the confidence regions, and may be described by giving the systematic error on Ω_{M} or Ω_{Λ} alone in the flat-universe case. Our total identified systematic error for the low-extinction sample analysis is 0.04 on the flat-universe value of Ω_{M} or Ω_{Λ}. For fits with host-galaxy extinction corrections, a conservative estimate of the total identified systematic error is 0.09.

In the more uncertain major axis, our total identified systematic error is 0.96 on $\Omega_{\mathrm{M}}+\Omega_{\Lambda}$ for the low-extinction primary subset, and 2.0 on the extinction-corrected full primary subset. Given the large size of these sys-

tematics in this direction, any conclusions drawn from the positions of supernova confidence ellipses along this direction should be approached with caution.

4. Under the assumption of a flat universe with vacuum energy (constant $w = -1$), we find a value of $\Omega_{\rm M} = 0.25^{+0.07}_{-0.06}$ (statistical) ± 0.04 (identified systematic), or equivalently, a cosmological constant of $\Omega_\Lambda = 0.75^{+0.06}_{-0.07}$ (statistical) ± 0.04 (identified systematic). This result is robust to host-galaxy extinction, and a fit with full, unbiased, individual extinction corrections applied yields a flat-universe cosmological constant of $\Omega_\Lambda = 0.72^{+0.10}_{-0.11}$ (statistical) ± 0.09 (identified systematic). Our best confidence regions for $\Omega_{\rm M}$ versus Ω_Λ are shown in Figure 8.

5. When combined with the 2dFGRS galaxy redshift distortion measurement and recent CMB data, we find a value for the dark energy equation of state parameter $w = -1.05^{+0.15}_{-0.20}$ marginalizing over $\Omega_{\rm M}$ (or a mass density $\Omega_{\rm M} = 0.27^{+0.06}_{-0.05}$ marginalizing over w), under the assumptions that the Universe is spatially flat and that w is constant in time. The identified systematic uncertainty on w is 0.09. The current confidence regions on the flat-universe values of $\Omega_{\rm M}$ and w are shown in Figure 12. The supernovae data are consistent with a low-mass Universe dominated by vacuum energy ($w = -1$), but they are also consistent with a wide range of constant or time-varying dark energy models.

In summary, high-redshift supernovae continue to be the best single tool for directly measuring the density of dark energy. This new set of supernovae observed with the HST confirm and strengthen previous supernova evidence for an accelerating universe, and show that those results are robust even when host-galaxy extinction is fully accounted for. High-redshift supernovae, together with other cosmological measurements, are providing a consistent picture of a low-mass, flat universe filled with dark energy. The next task for cosmologists is to better measure the properties of the dark energy, so as to further our understand-

ing of its nature. Combinations of current cosmological techniques have begun to provide measurements of its most general property (specifically, the equation of state parameter when it is assumed to be constant). Future work will refine these measurements, and in particular reduce the systematic uncertainties that will soon limit the current series of supernova studies. As new instruments become available,[33] it will begin to be possible to relax the condition of a constant equation of state parameter, and to question whether the properties of the dark energy have been changing throughout the history of the Universe.

---

[33]See, e.g., http://snap.lbl.gov/

A. Lightcurve Data

Tabulated below are lightcurve data for the eleven HST supernovae presented in this paper. For each event, there are two lightcurves, one for R-band and one for I-band. All photometry has been color-corrected to the standard Bessel filters as described in § 3, using color corrections which assume the lightcurve parameters in Table 3. These lightcurves, together with a $7'' \times 7''$ thumbnail of the F675W WFPC2 image closest to maximum light, are shown in Figures 1 and 2. Note that there are correlated errors between the data points. For the ground-based data, there is a covariance because for a given supernova the same final reference images were subtracted from all other ground-based points. Similarly, the HST data include a covariance due to a single background model having been used for all points for a given supernova (see § 2.1). In addition to this, the relative photometric zeropoint magnitudes were determined separately for the ground-based and HST photometry; in the former case, standard stars from Landolt (1992) were used to measure magnitudes of secondary standard stars in the supernova field of view. In the latter case, zeropoints from Dolphin (2000) were used. These covariance matrices will be available from the SCP website.[34]

Because uncertainties are flux uncertainties rather than magnitude uncertainties, each lightcurve is presented in arbitrary flux units. For each lightcurve, the zeropoint necessary to convert these to magnitudes is given. The magnitude may be calculated using the standard formula:

$$ m \; = \; -2.5 \log f \; + \; m_{zp} \tag{A1} $$

where m_{zp} is the quoted zeropoint and f is the flux value from the table. (Because we include early-time and late-time lightcurve points when the supernova flux is undetected given our photometry errors, some of the measured fluxes scatter to negative values. Note that it is impossible to formally calculate a magnitude for these points, and also that flux values are the proper way to quote the data as they better reflect the units in which our photometry errors are approximately Gaussian.)

The telescope used for each data point is indicated. BTC = the Big Throughput Camera on the CTIO 4m telescope. CTIO = the prime focus imager on the CTIO 4m telescope. WIYN = the Nasmyth 2k×2k imager on the WIYN 3.5m telescope at Kitt Peak observatory. INT = the WFC (wide-field camera) on the INT 2.5m telescope at La Palma. KECK = the LRIS imager on the Keck 10m telescope. NTT = the SUSI-2 imager on the NTT 3.6m telescope at ESO. CFHT = the CFHT12K multi-chip imager on the 3.6m CFHT telescope on Mauna Kea in Hawaii. Finally, HSTPC indicates data obtained from the Planetary Camera CCD on WFPC2.

---

[34]http://supernova.lbl.gov/

Table 10: SN 1997ek-R

Julian Day -2,400,000	Flux[a]	Telescope
50780.63	0.24 ± 1.27	BTC
50780.69	0.57 ± 0.93	BTC
50781.61	-0.28 ± 1.05	BTC
50781.66	1.22 ± 0.89	BTC
50781.67	0.29 ± 0.89	BTC
50781.72	0.16 ± 1.01	BTC
50810.58	2.71 ± 1.28	BTC
50810.59	4.63 ± 1.29	BTC
50810.60	5.25 ± 1.24	BTC
50810.67	4.85 ± 1.32	BTC
50810.68	5.04 ± 1.24	BTC
50810.69	5.70 ± 1.28	BTC
50811.66	4.34 ± 1.10	BTC
50811.68	4.53 ± 1.07	BTC
50811.69	3.55 ± 1.22	BTC
50817.67	4.92 ± 0.91	BTC
50817.68	5.09 ± 0.84	BTC
50817.69	3.17 ± 0.83	BTC
50817.70	2.65 ± 0.84	BTC
50817.71	3.71 ± 0.85	BTC
50817.72	3.34 ± 1.02	BTC
50817.73	4.45 ± 1.06	BTC
50817.73	4.77 ± 1.04	BTC
50817.74	3.10 ± 1.04	BTC
50818.92	4.18 ± 0.23	HSTPC
50824.77	3.61 ± 0.21	HSTPC
50835.67	2.49 ± 0.87	BTC
50835.68	3.20 ± 0.90	BTC
50835.69	2.56 ± 0.99	BTC
50835.70	3.01 ± 1.05	BTC
50835.70	3.26 ± 1.12	BTC
51165.71	-0.05 ± 0.60	BTC
51165.71	-0.67 ± 0.61	BTC
51165.74	-0.55 ± 0.71	BTC
51166.63	0.44 ± 2.12	BTC
51166.65	1.20 ± 1.28	BTC
51166.66	-0.67 ± 1.49	BTC
51193.59	0.47 ± 0.77	BTC
51193.60	-0.86 ± 0.79	BTC
51193.61	0.76 ± 0.70	BTC
51193.62	0.18 ± 0.73	BTC
51194.65	0.46 ± 0.64	BTC

a: Zeropoint: 25.678

Table 11: SN 1997ek-I

Julian Day -2,400,000	Flux[a]	Telescope
50816.60	5.62 ± 1.45	BTC
50817.56	3.22 ± 1.30	BTC
50817.57	4.27 ± 1.35	BTC
50817.58	4.70 ± 1.40	BTC
50817.58	5.41 ± 1.43	BTC
50817.59	5.82 ± 1.36	BTC
50817.60	4.47 ± 1.66	BTC
50817.61	5.16 ± 1.52	BTC
50817.63	3.68 ± 1.52	BTC
50817.64	4.48 ± 1.48	BTC
50817.64	3.31 ± 1.59	BTC
50817.65	5.89 ± 1.23	BTC
50817.66	4.38 ± 1.44	BTC
50818.93	3.83 ± 0.16	HSTPC
50819.74	2.02 ± 1.70	WIYN
50819.76	3.05 ± 1.65	WIYN
50819.78	4.18 ± 1.90	WIYN
50819.79	1.71 ± 1.60	WIYN
50819.81	4.31 ± 1.57	WIYN
50819.82	3.84 ± 2.09	WIYN
50824.78	3.89 ± 0.16	HSTPC
50835.72	2.72 ± 1.96	BTC
50835.73	3.06 ± 2.05	BTC
50846.74	1.54 ± 0.09	HSTPC
50858.84	0.75 ± 0.07	HSTPC
50871.95	0.46 ± 0.06	HSTPC
51072.07	0.50 ± 0.57	KECK
51072.07	0.35 ± 0.58	KECK
51072.07	0.69 ± 0.58	KECK
51072.11	0.31 ± 0.55	KECK
51072.11	0.94 ± 0.58	KECK
51072.12	-0.23 ± 0.57	KECK
51101.99	-0.37 ± 0.54	KECK
51102.00	0.51 ± 0.58	KECK
51102.00	0.58 ± 0.59	KECK
51102.05	1.20 ± 0.75	KECK
51102.06	1.53 ± 0.90	KECK
51126.93	-0.04 ± 0.06	HSTPC
51134.26	0.06 ± 0.05	HSTPC
51165.70	-0.66 ± 1.15	BTC
51165.72	0.21 ± 1.06	BTC
51165.73	-0.44 ± 1.12	BTC
51193.64	0.01 ± 1.12	BTC
51193.65	-0.28 ± 1.13	BTC
51193.67	-0.46 ± 1.50	BTC
51194.59	0.99 ± 1.17	BTC
51194.60	1.34 ± 1.30	BTC
51194.60	0.73 ± 1.15	BTC

a: Zeropoint: 24.801

Table 12: SN 1997eq-R

Julian Day -2,400,000	Flux[a]	Telescope
50780.60	0.01 ± 0.12	BTC
50780.66	0.21 ± 0.12	BTC
50781.60	-0.08 ± 0.10	BTC
50781.63	0.19 ± 0.10	BTC
50781.68	0.09 ± 0.10	BTC
50781.72	0.14 ± 0.11	BTC
50810.61	1.76 ± 0.12	BTC
50810.62	1.80 ± 0.12	BTC
50810.63	1.88 ± 0.13	BTC
50810.64	1.87 ± 0.11	BTC
50810.70	1.91 ± 0.12	BTC
50810.71	1.82 ± 0.11	BTC
50811.70	1.78 ± 0.10	BTC
50818.34	2.23 ± 0.28	INT
50818.36	1.98 ± 0.24	INT
50819.85	1.69 ± 0.05	HSTPC
50821.66	2.14 ± 0.54	WIYN
50821.67	1.79 ± 0.39	WIYN
50835.41	0.85 ± 0.13	INT
50835.42	0.87 ± 0.18	INT
50835.43	0.85 ± 0.34	INT
50843.68	0.37 ± 0.18	WIYN
50843.70	0.02 ± 0.40	WIYN
50846.81	0.32 ± 0.02	HSTPC
50855.82	0.18 ± 0.02	HSTPC
50863.82	0.12 ± 0.02	HSTPC
51165.56	0.01 ± 0.12	BTC
51165.61	0.01 ± 0.41	BTC
51165.62	-0.61 ± 0.67	BTC
51165.64	0.00 ± 0.12	BTC
51193.58	-0.03 ± 0.10	BTC
51193.63	0.02 ± 0.09	BTC

a: Zeropoint: 23.284

Table 13: SN 1997eq-I

Julian Day -2,400,000	Flux[a]	Telescope
50818.37	1.15 ± 0.50	INT
50818.38	1.05 ± 0.32	INT
50818.39	1.20 ± 0.32	INT
50818.41	0.94 ± 0.49	INT
50818.43	1.20 ± 0.48	INT
50818.46	1.05 ± 0.25	INT
50819.87	0.91 ± 0.03	HSTPC
50821.68	0.93 ± 0.35	WIYN
50821.69	0.83 ± 0.41	WIYN
50821.70	0.65 ± 0.38	WIYN
50824.90	0.86 ± 0.02	HSTPC
50835.54	0.59 ± 0.27	INT
50835.56	0.13 ± 0.29	INT
50835.58	-0.11 ± 0.50	INT
50846.82	0.38 ± 0.02	HSTPC
50855.83	0.27 ± 0.02	HSTPC
50863.83	0.22 ± 0.01	HSTPC
51165.57	0.03 ± 0.29	BTC
51165.60	0.06 ± 0.34	BTC
51165.63	0.07 ± 0.20	BTC
51165.65	0.06 ± 0.17	BTC
51193.58	-0.10 ± 0.17	BTC

a: Zeropoint: 22.388

Table 14: SN 1997ez-R

Julian Day -2,400,000	Flux[a]	Telescope
50780.75	-0.41 ± 1.15	BTC
50780.82	-0.88 ± 0.96	BTC
50781.74	-1.46 ± 1.01	BTC
50781.79	0.29 ± 1.18	BTC
50781.79	1.09 ± 0.96	BTC
50811.77	6.05 ± 1.04	BTC
50811.77	3.90 ± 1.89	WIYN
50811.77	5.82 ± 1.03	BTC
50811.78	5.62 ± 1.02	BTC
50811.78	5.82 ± 2.22	WIYN
50811.79	3.97 ± 4.73	WIYN
50811.81	5.97 ± 1.04	BTC
50811.81	4.83 ± 1.16	BTC
50817.84	5.51 ± 1.22	BTC
50817.85	7.72 ± 1.63	BTC
50817.86	4.58 ± 2.15	BTC
50818.70	4.93 ± 1.13	INT
50818.72	5.04 ± 1.09	INT
50819.06	4.96 ± 0.25	HSTPC
50824.97	3.65 ± 0.22	HSTPC
50835.66	4.69 ± 1.49	INT
50835.67	2.88 ± 1.68	INT
50835.81	1.81 ± 1.49	BTC
50835.82	-0.07 ± 1.66	BTC
50835.83	0.52 ± 1.70	BTC
51193.75	-0.14 ± 0.74	BTC
51193.76	0.37 ± 0.69	BTC
51193.76	0.00 ± 1.08	BTC
51193.77	-1.23 ± 0.85	BTC
51193.78	-0.20 ± 0.83	BTC
51193.79	-0.21 ± 0.78	BTC
51193.80	-1.80 ± 1.63	WIYN
51195.73	-1.37 ± 1.26	WIYN
51195.75	-0.21 ± 1.40	WIYN
51195.77	-0.58 ± 1.18	WIYN
51195.78	-0.92 ± 1.36	WIYN

a: Zeropoint: 25.688

Table 15: SN 1997ez-I

Julian Day -2,400,000	Flux[a]	Telescope
50816.74	2.05 ± 1.90	BTC
50816.76	4.83 ± 2.03	BTC
50816.77	4.64 ± 1.89	BTC
50816.78	6.11 ± 1.90	BTC
50816.78	5.02 ± 2.02	BTC
50816.85	6.84 ± 2.14	BTC
50818.63	4.19 ± 2.23	INT
50818.65	4.24 ± 1.55	INT
50818.66	4.12 ± 1.54	INT
50818.68	4.30 ± 1.54	INT
50819.07	5.23 ± 0.18	HSTPC
50820.79	4.42 ± 1.56	WIYN
50820.81	5.69 ± 1.50	WIYN
50820.83	3.92 ± 1.46	WIYN
50820.84	4.22 ± 1.42	WIYN
50820.86	6.08 ± 1.67	WIYN
50820.87	3.26 ± 1.70	WIYN
50824.99	4.07 ± 0.17	HSTPC
50835.60	5.27 ± 1.77	INT
50835.61	0.53 ± 2.03	INT
50835.63	5.55 ± 1.94	INT
50835.64	5.62 ± 2.52	INT
50835.84	3.39 ± 2.13	BTC
50835.85	1.78 ± 2.23	BTC
50835.86	-0.47 ± 2.56	BTC
50846.55	1.77 ± 0.09	HSTPC
50858.98	1.00 ± 0.08	HSTPC
50871.89	0.48 ± 0.04	HSTPC
51189.97	0.80 ± 1.13	WIYN
51189.98	-0.74 ± 1.22	WIYN
51190.00	-0.20 ± 1.35	WIYN
51191.90	-0.54 ± 1.34	WIYN
51191.92	-1.64 ± 1.16	WIYN
51191.93	0.15 ± 1.28	WIYN
51194.70	-3.19 ± 2.44	BTC
51194.71	-1.06 ± 2.73	BTC
51194.72	-0.60 ± 2.43	BTC
51194.73	-0.52 ± 2.81	BTC
51194.74	-1.26 ± 2.28	BTC
51194.75	-0.84 ± 2.49	BTC
51194.76	-0.27 ± 1.90	BTC
51194.77	-2.00 ± 2.19	BTC
51194.78	-1.89 ± 2.02	BTC
51194.78	-1.58 ± 2.61	BTC
51194.79	-0.68 ± 2.38	BTC

a: Zeropoint: 24.954

Table 16: SN 1998as-R

Julian Day -2,400,000	Flux[a]	Telescope
50872.63	-0.10 ± 0.10	BTC
50872.66	-0.07 ± 0.09	BTC
50872.67	0.06 ± 0.09	BTC
50872.72	-0.07 ± 0.10	BTC
50872.73	-0.06 ± 0.11	BTC
50873.57	0.06 ± 0.11	BTC
50873.58	0.03 ± 0.10	BTC
50895.58	2.33 ± 0.12	BTC
50895.62	2.47 ± 0.15	BTC
50896.58	2.64 ± 0.12	BTC
50899.70	2.24 ± 0.12	BTC
50904.68	2.15 ± 0.11	BTC
50904.69	2.05 ± 0.10	BTC
50904.70	2.20 ± 0.10	BTC
50904.71	1.95 ± 0.11	BTC
50904.72	2.00 ± 0.10	BTC
50912.29	1.42 ± 0.04	HSTPC
50935.01	0.33 ± 0.02	HSTPC
50948.52	0.25 ± 0.02	HSTPC
50963.17	0.19 ± 0.02	HSTPC
51193.83	0.06 ± 0.08	BTC
51193.84	-0.07 ± 0.08	BTC
51193.86	0.04 ± 0.08	BTC
51196.03	0.21 ± 0.13	WIYN
51196.04	-0.19 ± 0.12	WIYN
51196.05	-0.11 ± 0.16	WIYN

a: Zeropoint: 23.139

Table 17: SN 1998as-I

Julian Day -2,400,000	Flux[a]	Telescope
50912.31	9.24 ± 0.21	HSTPC
50924.07	7.27 ± 0.19	HSTPC
50932.65	1.95 ± 1.56	WIYN
50935.02	4.86 ± 0.17	HSTPC
50948.53	2.57 ± 0.14	HSTPC
50963.19	1.79 ± 0.12	HSTPC
51194.86	-1.02 ± 0.98	BTC
51194.87	0.60 ± 1.12	BTC
51196.93	-0.55 ± 1.23	WIYN
51196.94	0.73 ± 1.12	WIYN
51196.96	-1.44 ± 1.28	WIYN
51280.50	0.53 ± 1.60	BTC
51280.51	-2.08 ± 1.50	BTC
51280.51	0.67 ± 1.50	BTC
51280.52	0.60 ± 1.33	BTC
51280.53	1.32 ± 1.45	BTC
51280.54	0.72 ± 1.46	BTC

a: Zeropoint: 24.788

Table 18: SN 1998aw-R

Julian Day -2,400,000	Flux[a]	Telescope
50513.71	0.08 ± 0.14	BTC
50513.73	-0.08 ± 0.16	BTC
50513.75	0.06 ± 0.13	BTC
50514.71	0.08 ± 0.14	BTC
50517.74	-0.19 ± 0.14	BTC
50517.76	0.04 ± 0.16	BTC
50518.79	0.31 ± 0.17	BTC
50518.81	-0.02 ± 0.17	BTC
50872.56	-0.03 ± 0.21	BTC
50872.59	-0.03 ± 0.22	BTC
50873.73	-0.03 ± 0.18	BTC
50873.74	-0.09 ± 0.15	BTC
50895.60	0.02 ± 0.16	BTC
50895.64	0.55 ± 0.16	BTC
50896.58	0.67 ± 0.15	BTC
50896.60	0.39 ± 0.16	BTC
50899.69	0.89 ± 0.15	BTC
50904.63	1.87 ± 0.14	BTC
50904.64	1.66 ± 0.14	BTC
50904.65	1.75 ± 0.13	BTC
50904.66	1.82 ± 0.14	BTC
50904.67	1.82 ± 0.14	BTC
50912.03	2.53 ± 0.07	HSTPC
50922.11	2.11 ± 0.06	HSTPC
50927.56	2.05 ± 0.38	BTC
50927.57	1.80 ± 0.34	BTC
50927.60	1.69 ± 0.36	BTC
50927.61	0.96 ± 0.41	BTC
50929.64	1.48 ± 0.28	WIYN
50929.65	1.06 ± 0.33	WIYN
50929.67	1.90 ± 0.31	WIYN
50933.07	1.32 ± 0.04	HSTPC
50947.71	0.58 ± 0.03	HSTPC
50961.83	0.30 ± 0.03	HSTPC
51192.96	-0.19 ± 0.26	WIYN
51192.98	-0.14 ± 0.39	WIYN
51193.00	0.18 ± 0.28	WIYN
51193.02	-0.14 ± 0.24	WIYN
51193.03	-0.29 ± 0.28	WIYN
51279.60	0.01 ± 0.13	BTC
51279.61	0.04 ± 0.14	BTC
51279.63	-0.04 ± 0.12	BTC
51279.66	0.01 ± 0.13	BTC
51280.56	0.14 ± 0.16	BTC
51280.57	0.17 ± 0.15	BTC

a: Zeropoint: 23.536

Table 19: SN 1998aw-I

Julian Day -2,400,000	Flux[a]	Telescope
50513.76	-0.33 ± 0.25	BTC
50514.74	-0.10 ± 0.22	BTC
50514.76	-0.12 ± 0.21	BTC
50514.78	0.06 ± 0.23	BTC
50518.73	0.18 ± 0.42	BTC
50518.75	-0.08 ± 0.34	BTC
50912.04	1.79 ± 0.05	HSTPC
50922.12	1.67 ± 0.05	HSTPC
50929.70	1.50 ± 0.49	WIYN
50930.71	1.80 ± 0.46	WIYN
50933.08	1.23 ± 0.03	HSTPC
50947.73	0.80 ± 0.03	HSTPC
50961.84	0.53 ± 0.03	HSTPC
51194.03	-0.07 ± 0.32	WIYN
51194.05	-0.26 ± 0.51	WIYN
51195.97	-0.21 ± 0.32	WIYN
51195.98	0.13 ± 0.27	WIYN
51196.00	0.10 ± 0.29	WIYN
51196.02	0.05 ± 0.27	WIYN
51279.59	-0.03 ± 0.21	BTC
51279.62	-0.06 ± 0.25	BTC
51279.64	0.15 ± 0.21	BTC
51279.65	0.01 ± 0.23	BTC
51279.66	0.19 ± 0.25	BTC
51280.55	0.14 ± 0.31	BTC
51280.57	-0.02 ± 0.28	BTC
51280.59	-0.30 ± 0.29	BTC
51280.60	0.09 ± 0.29	BTC

a: Zeropoint: 22.874

Table 20: SN 1998ax-R

Julian Day -2,400,000	Flux[a]	Telescope
50138.65	-0.03 ± 0.09	CTIO
50138.67	-0.09 ± 0.10	CTIO
50159.64	-0.09 ± 0.08	CTIO
50159.66	0.03 ± 0.07	CTIO
50160.67	0.01 ± 0.07	CTIO
50160.68	0.02 ± 0.06	CTIO
50168.59	-0.03 ± 0.07	CTIO
50168.65	0.14 ± 0.06	CTIO
50169.64	0.13 ± 0.15	CTIO
50169.67	-0.01 ± 0.08	CTIO
50432.83	-0.06 ± 0.06	CTIO
50453.84	-0.01 ± 0.08	CTIO
50454.77	0.01 ± 0.06	CTIO
50459.82	-0.02 ± 0.04	CTIO
50459.83	-0.02 ± 0.05	CTIO
50459.84	0.02 ± 0.05	CTIO
50490.79	0.01 ± 0.06	BTC
50490.79	0.07 ± 0.06	BTC
50490.80	-0.04 ± 0.06	BTC
50490.80	-0.04 ± 0.06	BTC
50513.71	-0.03 ± 0.06	BTC
50514.72	-0.06 ± 0.06	BTC
50872.54	0.72 ± 0.12	BTC
50872.57	0.58 ± 0.12	BTC
50873.53	0.84 ± 0.17	BTC
50873.55	0.95 ± 0.10	BTC
50895.52	1.42 ± 0.09	BTC
50895.55	1.06 ± 0.19	BTC
50895.71	1.24 ± 0.07	BTC
50896.53	1.14 ± 0.10	BTC
50900.70	1.14 ± 0.07	BTC
50900.71	1.04 ± 0.07	BTC
50904.59	0.91 ± 0.06	BTC
50904.60	0.84 ± 0.06	BTC
50904.61	0.81 ± 0.06	BTC
50904.62	0.84 ± 0.06	BTC
50904.63	0.89 ± 0.06	BTC
50911.96	0.59 ± 0.03	HSTPC
50922.04	0.31 ± 0.02	HSTPC
50933.00	0.18 ± 0.02	HSTPC
50947.65	0.09 ± 0.01	HSTPC
50961.23	0.09 ± 0.01	HSTPC
51193.80	-0.00 ± 0.05	BTC
51193.81	-0.00 ± 0.05	BTC
51193.82	-0.01 ± 0.06	BTC
51279.52	-0.01 ± 0.08	BTC
51279.57	0.11 ± 0.08	BTC
51280.61	0.06 ± 0.06	BTC

a: Zeropoint: 22.922

Table 21: SN 1998ax-I

Julian Day -2,400,000	Flux[a]	Telescope
50911.97	1.95 ± 0.10	HSTPC
50922.05	1.62 ± 0.10	HSTPC
50933.01	1.18 ± 0.06	HSTPC
50947.66	0.75 ± 0.05	HSTPC
50961.24	0.47 ± 0.04	HSTPC

a: Zeropoint: 23.685

Table 22: SN 1998ay-R

Julian Day -2,400,000	Flux[a]	Telescope
50521.85	0.02 ± 0.50	WIYN
50521.86	0.17 ± 0.56	WIYN
50872.54	2.11 ± 1.08	BTC
50872.57	1.27 ± 0.97	BTC
50873.53	0.57 ± 1.81	BTC
50873.55	-0.70 ± 1.04	BTC
50895.52	5.69 ± 0.90	BTC
50895.55	6.69 ± 1.91	BTC
50895.71	6.10 ± 0.78	BTC
50896.53	6.70 ± 1.24	BTC
50900.70	5.74 ± 0.76	BTC
50900.71	6.74 ± 0.91	BTC
50904.59	5.48 ± 0.78	BTC
50904.60	5.64 ± 0.75	BTC
50904.61	5.61 ± 0.78	BTC
50904.62	5.76 ± 0.82	BTC
50904.63	5.91 ± 0.79	BTC
50912.16	3.11 ± 0.20	HSTPC
50923.99	1.58 ± 0.17	HSTPC
51193.80	-0.09 ± 0.60	BTC
51193.81	0.61 ± 0.48	BTC
51193.82	0.53 ± 0.64	BTC

a: Zeropoint: 25.093

Table 23: SN 1998ay-I

Julian Day -2,400,000	Flux[a]	Telescope
50912.17	1.56 ± 0.08	HSTPC
50924.00	0.96 ± 0.07	HSTPC
50934.68	0.61 ± 0.04	HSTPC
50948.59	0.40 ± 0.04	HSTPC
50967.81	0.26 ± 0.04	HSTPC

a: Zeropoint: 23.685

Table 24: SN 1998ba-R

Julian Day -2,400,000	Flux[a]	Telescope
50873.79	0.03 ± 0.09	BTC
50873.80	0.09 ± 0.09	BTC
50873.81	0.01 ± 0.09	BTC
50873.82	0.03 ± 0.09	BTC
50873.83	0.01 ± 0.08	BTC
50873.84	-0.03 ± 0.09	BTC
50895.78	1.50 ± 0.14	BTC
50895.85	1.64 ± 0.15	BTC
50899.75	1.52 ± 0.11	BTC
50899.84	1.43 ± 0.14	BTC
50899.90	1.20 ± 0.21	BTC
50900.74	1.54 ± 0.10	BTC
50900.75	1.32 ± 0.10	BTC
50904.77	1.36 ± 0.11	BTC
50904.78	1.20 ± 0.11	BTC
50904.79	1.42 ± 0.13	BTC
50904.80	1.30 ± 0.09	BTC
50904.81	1.34 ± 0.11	BTC
50912.10	0.79 ± 0.03	HSTPC
50923.12	0.41 ± 0.02	HSTPC
50933.21	0.22 ± 0.02	HSTPC
50947.12	0.12 ± 0.01	HSTPC
50961.90	0.12 ± 0.01	HSTPC
51258.01	-0.15 ± 0.11	WIYN
51279.82	0.07 ± 0.08	BTC
51279.85	-0.05 ± 0.10	BTC
51280.69	-0.02 ± 0.07	BTC
51280.70	0.03 ± 0.06	BTC

a: Zeropoint: 22.779

Table 25: SN 1998ba-I

Julian Day -2,400,000	Flux[a]	Telescope
50907.82	3.18 ± 1.99	WIYN
50907.83	3.96 ± 1.75	WIYN
50907.84	6.80 ± 1.81	WIYN
50907.85	6.04 ± 2.36	WIYN
50912.11	5.74 ± 0.22	HSTPC
50923.13	3.95 ± 0.21	HSTPC
50933.22	2.81 ± 0.12	HSTPC
50947.13	1.57 ± 0.10	HSTPC
50961.92	1.37 ± 0.10	HSTPC
51279.83	-1.51 ± 1.00	BTC
51279.84	0.88 ± 1.09	BTC
51280.69	-1.04 ± 0.83	BTC
51280.71	0.66 ± 0.72	BTC
51280.72	-0.06 ± 0.68	BTC
51280.73	0.13 ± 0.68	BTC

a: Zeropoint: 24.477

Table 26: SN 1998be-R

Julian Day -2,400,000	Flux[a]	Telescope
50490.86	0.49 ± 0.55	BTC
50490.87	-0.39 ± 0.54	BTC
50513.83	-0.02 ± 0.52	BTC
50513.84	0.15 ± 0.54	BTC
50514.83	0.53 ± 0.60	BTC
50514.86	-0.51 ± 0.53	BTC
50517.88	0.33 ± 0.70	BTC
50517.90	-0.26 ± 0.71	BTC
50517.90	0.69 ± 0.81	BTC
50518.86	0.22 ± 0.62	BTC
50518.87	0.57 ± 0.66	BTC
50872.74	-0.75 ± 0.91	BTC
50872.89	1.36 ± 0.93	BTC
50873.87	0.63 ± 0.53	BTC
50895.78	4.22 ± 0.70	BTC
50895.84	5.34 ± 0.88	BTC
50899.75	7.13 ± 0.79	BTC
50899.82	6.98 ± 0.91	BTC
50900.76	4.64 ± 0.65	BTC
50904.73	6.58 ± 0.65	BTC
50904.74	6.90 ± 0.67	BTC
50904.75	6.31 ± 0.72	BTC
50904.75	7.32 ± 0.73	BTC
50904.76	8.29 ± 0.76	BTC
50904.86	7.95 ± 0.89	BTC
50912.23	5.73 ± 0.25	HSTPC
50923.19	2.11 ± 0.18	HSTPC
50932.74	2.04 ± 0.89	WIYN
50932.77	1.38 ± 0.93	WIYN
50934.08	0.73 ± 0.12	HSTPC
50949.00	0.76 ± 0.13	HSTPC
50962.17	0.21 ± 0.13	HSTPC
51279.68	-0.16 ± 0.67	BTC
51279.71	0.31 ± 0.68	BTC
51279.75	0.21 ± 0.73	BTC
51279.77	-0.30 ± 0.79	BTC

a: Zeropoint: 25.350

Table 27: SN 1998be-I

Julian Day -2,400,000	Flux[a]	Telescope
50514.85	-0.21 ± 0.83	BTC
50514.87	-1.02 ± 0.78	BTC
50518.84	2.00 ± 0.90	BTC
50518.85	1.47 ± 0.86	BTC
50518.85	0.31 ± 0.82	BTC
50912.25	3.66 ± 0.18	HSTPC
50923.20	2.19 ± 0.17	HSTPC
50932.80	2.35 ± 1.10	WIYN
50932.85	2.26 ± 0.92	WIYN
50934.09	1.13 ± 0.09	HSTPC
50949.01	0.80 ± 0.08	HSTPC
50962.18	0.37 ± 0.08	HSTPC
51279.69	0.81 ± 0.89	BTC
51279.70	0.49 ± 0.87	BTC
51279.72	1.51 ± 0.73	BTC
51279.73	-0.02 ± 0.71	BTC
51279.76	0.62 ± 0.83	BTC
51279.77	0.58 ± 0.85	BTC
51280.64	-0.87 ± 0.82	BTC
51280.64	0.36 ± 0.84	BTC
51280.65	0.12 ± 0.73	BTC
51280.66	-0.13 ± 0.78	BTC
51280.67	1.24 ± 0.76	BTC
51280.68	-0.62 ± 0.76	BTC

a: Zeropoint: 24.384

Table 28: SN 1998bi-R

Julian Day -2,400,000	Flux[a]	Telescope
50138.79	-1.04 ± 0.91	CTIO
50138.82	0.85 ± 0.86	CTIO
50168.80	-0.68 ± 0.66	CTIO
50490.86	0.40 ± 0.49	BTC
50490.87	-0.09 ± 0.48	BTC
50513.83	0.26 ± 0.51	BTC
50513.84	-0.10 ± 0.53	BTC
50514.83	-1.06 ± 0.58	BTC
50514.86	-0.05 ± 0.50	BTC
50517.88	0.13 ± 0.65	BTC
50517.89	-0.11 ± 0.60	BTC
50517.89	0.93 ± 0.60	BTC
50517.90	-0.29 ± 0.68	BTC
50517.90	-0.35 ± 0.74	BTC
50872.89	0.52 ± 0.81	BTC
50873.87	0.60 ± 0.51	BTC
50895.78	3.15 ± 0.63	BTC
50895.84	3.11 ± 0.79	BTC
50899.75	4.93 ± 0.65	BTC
50899.82	4.28 ± 0.70	BTC
50900.76	4.44 ± 0.55	BTC
50904.73	6.10 ± 0.61	BTC
50904.75	5.30 ± 0.61	BTC
50904.75	5.38 ± 0.64	BTC
50904.76	6.21 ± 0.66	BTC
50904.86	5.27 ± 0.77	BTC
50910.15	5.27 ± 0.20	HSTPC
50922.18	3.75 ± 0.18	HSTPC
51279.71	0.94 ± 0.73	BTC
51279.74	0.63 ± 0.67	BTC
51279.75	-1.14 ± 0.68	BTC
51279.77	0.47 ± 0.76	BTC

a: Zeropoint: 25.213

Table 29: SN 1998bi-I

Julian Day -2,400,000	Flux[a]	Telescope
50910.16	2.07 ± 0.06	HSTPC
50922.20	1.83 ± 0.06	HSTPC
50931.99	1.25 ± 0.04	HSTPC
50946.38	0.54 ± 0.03	HSTPC
50966.88	0.20 ± 0.02	HSTPC

a: Zeropoint: 23.685

Table 30: SN 2000fr-R

Julian Day -2,400,000	Flux[a]	Telescope
51671.77	1.02 ± 0.07	KECK
51671.77	1.05 ± 0.07	KECK
51671.78	1.06 ± 0.07	KECK
51671.78	0.99 ± 0.07	KECK
51679.98	1.66 ± 0.04	HSTPC
51692.91	1.43 ± 0.03	HSTPC
51706.26	0.73 ± 0.02	HSTPC
51718.04	0.39 ± 0.01	HSTPC
51733.86	0.16 ± 0.01	HSTPC
52014.72	-0.01 ± 0.07	NTT
52014.73	-0.08 ± 0.07	NTT
52014.74	0.04 ± 0.08	NTT
52014.75	-0.04 ± 0.06	NTT
52014.76	-0.04 ± 0.07	NTT
52014.77	-0.08 ± 0.10	NTT
52014.78	-0.07 ± 0.09	NTT
52014.79	-0.04 ± 0.10	NTT
52014.80	-0.16 ± 0.14	NTT
52376.98	0.01 ± 0.04	CFHT
52376.99	-0.00 ± 0.03	CFHT
52377.04	0.01 ± 0.04	CFHT
52377.05	-0.02 ± 0.04	CFHT
52382.01	0.03 ± 0.05	CFHT
52384.98	-0.00 ± 0.09	CFHT
52386.85	-0.14 ± 0.10	CFHT

a: Zeropoint: 22.998

Table 31: SN 2000fr-I

Julian Day -2,400,000	Flux[a]	Telescope
51641.99	0.03 ± 0.04	CFHT
51664.95	0.40 ± 0.05	CFHT
51664.99	0.40 ± 0.06	CFHT
51672.86	1.14 ± 0.02	HSTPC
51679.97	1.59 ± 0.03	HSTPC
51692.91	1.46 ± 0.03	HSTPC
51706.20	1.02 ± 0.03	HSTPC
51717.98	0.66 ± 0.02	HSTPC
51733.79	0.40 ± 0.02	HSTPC
51997.93	0.05 ± 0.06	CFHT
51997.94	0.01 ± 0.06	CFHT
51997.99	0.19 ± 0.05	CFHT
51998.00	0.03 ± 0.06	CFHT
51998.01	0.08 ± 0.06	CFHT
52376.96	0.04 ± 0.06	CFHT
52376.97	-0.06 ± 0.06	CFHT
52377.00	0.13 ± 0.06	CFHT
52377.00	-0.09 ± 0.06	CFHT
52377.01	-0.01 ± 0.06	CFHT
52377.03	0.01 ± 0.07	CFHT

a: Zeropoint: 22.805

REFERENCES

Aguirre, A., 1999a, ApJ, 512, L19

Aguirre, A., 1999b, ApJ, 525, 583

Aguirre, A., & Zoltan, H., 2000, ApJ, 532, 28

Alcock, C. *et al.*, 2000, ApJ, 542, 281

Aldering, G., Knop, R., & Nugent, P., 2000, AJ, 119, 2110

Allen, A. W., Schmidt, R. W., & Fabian, A. C., 2002, MNRAS, 334, L11

Amanullah, R., Mörtsell, E., & Goobar, A, 2003, A&A397, 819

Appenzeller, I., *et al.*, 1998, ESO Messenger, 94, 1

Bahcall, N. A., Ostriker, J. P., Perlmutter, S., & Steinhardt, P. J., 1999, Science, 284, 1481

Bahcall, N. A., *et al.*, 2003, ApJ, 585, 182

Benitez, N., Riess, A., Nugent, P., Dickinson, M., Chornock, R., & Filippenko, A. V., 2002, ApJ, 577, L1

Bergström, L., Goliath, M., Goobar, A., & Mörtsell, E., 2000, A&A, 358, 13

Blakeslee *et al.*, 2003, ApJ, in press; astro-ph/0302402

Branch, D., & van den Bergh, S., 1993, AJ, 105, 2231

Branch, D., Romanishin, W., & Baron, E., 1996, ApJ, 465, 73

Bennett, C. L., *et al.*, 2003, submitted to ApJ, astro-ph/0302207

Bessell, M. S., 1990, PASP, 102, 1181

Cardelli, J. A., Clayton, G. C., & Mathis, J., S., 1989, ApJ, 345, 245

Coil, A. L. 2000, *et al.*, ApJ, 544, L111

Csáki, C., Kaloper, N., & Terning, J., 2002, Phys. Rev. Lett., 88, 61302

Dalal, N., Holz, D. E., Chen, X., & Frieman, J. A. 2003, ApJ, 585, L11

Dolphin, 2000, PASP, 112, 1397

Dolphin, 2003, http://www.stsci.edu/hst/HST_overview/ documents/calworkshop/workshop2002/ CW2002_Papers/CW02_dolphin

Efstathiou, G., *et al.*, 2002, MNRAS, 330, L29

Falco, E. E., *et al.*, 1999, ApJ, 523, 617

Frieman, J. A., Comments Astrophys., 18, 323

Fruchter, A., 2000, private communication

Garnavich, P. M., *et al.*, 1998a, ApJ, 493, L53

Garnavich, P. M., *et al.*, 1998b, ApJ, 509, 74

Goldhaber G., *et al.*, 2001, ApJ, 558, 359

Goobar, A., Mörtsell, E., Amanullah, R., Goliath, M., Bergström, L., & Dahlén, T., 2002, A&A, 392, 757

Goobar, A., Bergström, L., & Mörtsell E., 2002, A&A, 384, 1

Hamuy, M., Phillips, M. M., Maza, J., Wischnjewsky, M., Uomoto, A., Landolt, A. U., & Khatwani, R., 1992, AJ, 102, 208

Hamuy, M., *et al.*, 1996a, AJ, 112, 2408 (H96)

Hamuy, M., Phillips, M. M., Suntzeff, N. B., Schommer, R. A., Maza, J., & Aviles, R., 1996b, AJ, 112, 2391

Hamuy, M., Trager, S. C., Pinto, P. A., Phillips, M. M., Schommer, R. A., Ivanov, V., & Suntzeff, N. B., 2000, AJ, 120, 1479

Hamuy, M., Trager, S. C., Pinto, P. A., Phillips, M. M., Schommer, R. A., Ivanov, V., & Suntzeff, N. B. 2001, AJ, 122, 3506 erratum

Hatano, K., Branch, D., & Deaton, J., 1998, ApJ, 502, 177

Hawkins, E., *et al.*, 2002, submitted to MNRAS, astro-ph/0212375

Henry, R. B. C., & Worthey, G., 1999, PASP, 111, 919

Hoeflich, P., Wheeler, J. C., & Thielmann, F. K., 1998, ApJ, 495, 617

Holz, D. E. 1998, ApJ, 506, L1

Holz, D. E. 2001, ApJ, 556, L71

Holtzman, J. A., Burrows, C. J., Casertano, S., Hester, J. J., Traugher, J. T., Watson, A. M. and Worthey, G., 1995, PASP, 107, 1065

Howell, D. A. 2001, ApJ, 554, L193

Ivanov, V. D., Hamuy, M., & Pinto, P. A., 2000, ApJ, 542, 588

Jaffe, A. H., *et al.*, 2001, Phys. Rev. Lett., 86, 3475

James, F., & Roos, M., 1975, Compt. Phys. Comm. 10, 343

Jha, 2002, PhD thesis, Harvard University

Kantowski, R. 1998, ApJ, 507, 483

Kim, A., Goobar, A., & Perlmutter, S., 1996, PASP, 108, 190

Kim, A., Linder, E., Miquel, & Mostek, 2003, MNRAS, submitted, astro-ph/0304509

Kobayashi, C., Tsujimoto, T., Nomoto, K., Hachisu, I., & Kato, M., 1998, ApJ, 503, L155

Krist, J., & Hook, R., "The Tiny Tim Users Guide", available from STScI

Landolt, A. U., 1992, AJ, 104, 340

Leibundgut B., 2001, ARA&A, 39, 67

Lentz, E. J., Baron, E., Branch, D., Hauschildt, P. H., & Nugent, P. E., 2000, ApJ, 530, 966

Lewis, G. F., & Ibata, R. A., 2001, MNRAS, 324, L25

Li, W., Filippenko, A. V., & Riess, A. G. 2001, ApJ, 546, 719

Linder, E. V. & Jenkins, A., 2003, submitted to MNRAS, astro-ph/0305286

Lira, P., *et al.*, 1998, AJ, 115, 234

Malmquist, K. G., 1924, Medd. Lund Astron. Obs. Ser. II, 32, 64

Malmquist, K. G., 1936, Stockholm Observatory Medd., no. 26

Metcalf, R. B. & Silk, J. 1999, ApJ, 519, L1

Metcalf, R. B. 1999, MNRAS, 305, 746

Minty, E. M., Heavens, A. F., & Hawkins, M. R. S. 2002, MNRAS, 330, 378

Mörtsell, E., Gunnarsson, C., & Goobar, A., 2001, ApJ, 561, 106

Mörtsell, E., Bergström, L., & Goobar, A., 2002, Phys. Rev. D, 66, 047702

Mörtsell, E., & Goobar, A., 2003, Journal of Cosmology and Astroparticle Physics, 04, 003

Nobili, S., Goobar, A., Knop, R., & Nugent, P., 2003, A&A, 404, 901

Nomoto, K., Nakamura, T., & Kobayashi, C. 1999, Ap&SS, 265, 37

Nugent, P., Phillips, M., Baron, E., Branch, D., & Hauschildt, P., 1995, ApJ, 455, L147

Nugent P., Kim, A., & Perlmutter, S., 2002, PASP, 114, 803

O'Donnell, J. E., 1994, ApJ, 422, 158

Oguri, M., Suto, Y., & Turner, E. L. 2003, ApJ, 583, 584

Oke, J. B., *et al.*, 1995, PASP, 107, 375

Perlmutter, S., *et al.*, 1995, ApJ, 440, L41

Perlmutter, S., *et al.*, 1997, ApJ, 483, 565

Perlmutter *et al.*, 1998, Nature, 391, 51

Perlmutter *et al.*, 1999, ApJ, 517, 586 (P99)

Perlmutter S. & Schmidt B., 2003, in "Supernovae & Gamma Ray Bursts", ed. Weiler, K. (Springer); astro-ph/0303428

Phillips, M. M., 1993, ApJ, 413, L105

Phillips, M. M., Lira, P., Suntzeff, N. B., Schommer, R., A., Hamuy, M., & Maza, J., 1999, AJ, 118, 1766

Pskovski, 1969, Sov. Astr., 12, 750

Richmond *et al.*, 1995, AJ, 109, 2121

Riess, A. G., *et al.*, 1998, AJ, 116, 1009

Riess, A. G., *et al.*, 1999, AJ, 117, 707 (R99)

Riess, A. G., Filippenko, A. V., Li, W., & Schmidt, B. P. 1999, AJ, 118, 2668

Riess, A. G., *et al.*, 2000, ApJ, 536, 62

Riess, A. G., *et al.*, 2001, ApJ, 560, 49

Rowan-Robinson, M., 2002, MNRAS, 332, 352

Ruiz-Lapuente, P., 2003, in "3K, SNs, Clusters: Hunting the Cosmological Parameters", ed. Barbosa et al. (Kluwer Acad. Publ.); astro-ph/0304108

Schlegel, D. J., Finkbeiner, D. P., & Davis, M., 1998, ApJ, 500, 525

Schmidt, B. P., *et al.*, 1998, ApJ, 507, 46

Seljak, U. & Holz, D. E. 1999, A&A, 351, L10

Spergel, *et al.*, 2003, submitted to ApJ, astro-ph/0302209

Sullivan, M., *et al.*, 2003, MNRAS, 340, 1057

Suntzeff, N. B., *et al.*, 1999, AJ, 117, 1175

Tonry, J., *et al.*, 2003, ApJ, in press, astro-ph/0305008

Turner, M., 2001, PASP, 113, 653

Verde, L., *et al.*, 2002, MNRAS, 335, 432

Wambsganss, J., Cen, R., Xu, G., & Ostriker, J. P. 1997, ApJ, 475, L81

Wang, L., Hoeflich, P., & Wheeler, J. C., 1997, ApJ, 483, L29

Wang, Y., Holz, D. E., & Munshi, D. 2002, ApJ, 572, L15

Wang, L., Goldhaber, G., Aldering, G., & Perlmutter, S. 2003, ApJ, in press; astro-ph/0302341

Wells, L. A., *et al.*, 1994, AJ, 108,2233

Whitmore, B., Heyer, I., & Casertano, S., 1999, PASP, 111, 1559

Wu, H., Yan, H. J., & Zou, Z. L., 1995, A&A, 294, L9